THE UNIVERSITY
of EDINBURGH

Load Balancing in Hybrid LiFi and RF Networks

Yunlu Wang

A thesis submitted for the degree of Doctor of Philosophy.
The University of Edinburgh.
January 2018

Abstract

The increasing number of mobile devices challenges the current radio frequency (RF) networks. The conventional RF spectrum for wireless communications is saturating, motivating to develop other unexplored frequency bands. Light Fidelity (LiFi) which uses more than 300 THz of the visible light spectrum for high-speed wireless communications, is considered a promising complementary technology to its RF counterpart. LiFi enables daily lighting infrastructures, i.e. light emitting diode (LED) lamps to realise data transmission, and maintains the lighting functionality at the same time. Since LiFi mainly relies on line-of-sight (LoS) transmission, users in indoor environments may experience blockages which significantly affects users' quality of service (QoS). Therefore, hybrid LiFi and RF networks (HLRNs) where LiFi supports high data rate transmission and RF offers reliable connectivity, can provide a potential solution to future indoor wireless communications.

In HLRNs, efficient load balancing (LB) schemes are critical in improving the traffic performance and network utilisation. In this thesis, the optimisation-based scheme (OBS) and the evolutionary game theory (EGT) based scheme (EGTBS) are proposed for load balancing in HLRNs. Specifically, in OBS, two algorithms, the joint optimisation algorithm (JOA) and the separate optimisation algorithm (SOA) are proposed. Analysis and simulation results show that JOA can achieve the optimal performance in terms of user data rate while requiring high computational complexity. SOA reduces the computational complexity but achieves low user data rates. EGTBS is able to achieve a better performance/complexity trade-off than OBS and other conventional load balancing schemes. In addition, the effects of handover, blockages, orientation of LiFi receivers, and user data rate requirement on the throughput of HLRNs are investigated. Moreover, the packet latency in HLRNs is also studied in this thesis. The notion of LiFi service ratio is introduced, defined as the proportion of users served by LiFi in HLRNs. The optimal LiFi service ratio to minimise system delay is mathematically derived and a low-complexity packet flow assignment scheme based on this optimum ratio is proposed. Simulation results show that the theoretical optimum of the LiFi service ratio is very close to the practical solution. Also, the proposed packet flow assignment scheme can reduce at most 90% of packet delay compared to the conventional load balancing schemes at reduced computational complexity.

Lay Summary

Due to the exponentially increasing demand for mobile data traffic, the current indoor radio frequency (RF) systems tend to be overloaded. A potential solution is the hybrid network that integrates different wireless technologies to improve the network capacity. Light fidelity (LiFi), which uses existing light emitting diode (LED) lighting infrastructures for high speed wireless communications, has been considered to form a new tier within the future indoor hybrid networks. One major advantage of such a hybrid network is that LiFi and RF signals do not interfere with each other since they use an entirely different part of the electromagnetic spectrum. LiFi can be regarded as nanometre wave (nmWave) wireless communication extending current millimetre wave (mmWave) wireless technologies. Compared with RF systems, LiFi can potentially provide a much higher level of signal-to-noise ratio (SNR). Also, LiFi can use a huge and unregulated bandwidth resource of up to 300 THz, 600,000 times larger than the 500 MHz WiGig (wireless gigabit alliance) channel in the industrial, scientific and medical (ISM) band.

In indoor environments, a single LiFi cell covers a few square meters due to propagation characteristics of light such as high path loss and low multipath reflections. Hence, multiple light sources are required to cover a large room, leading to a high spatial spectral efficiency in LiFi systems. In spite of the dense deployment of access points (APs), LiFi may not provide a uniform coverage in terms of data rate performance mainly due to inter-cell interference (ICI) and blockages. Therefore, a hybrid LiFi/RF network (HLRN) is proposed to mitigate the spatial fluctuation of data rate offering a system throughput greater than that of stand alone LiFi or RF networks. In this thesis, the load balancing (LB) in HLRNs is studied, which mainly consists of AP assignment, resource allocation and handover. At first, the joint optimisation algorithm (JOA) for LB is proposed, which uses convex optimisation method to jointly optimise all of the elements in LB. Following that, the evolutionary game theory (EGT) based scheme is proposed, which is able to achieve a better performance/complexity trade-off than JOA and other benchmark algorithms. At last, the cross-layer load balancing for HLRNs is studied. A delay-minimisation packet flow assignment scheme is proposed. This scheme is able to reduce 90% of packet delay comparing to the state-of-the-art schemes.

Declaration of originality

I hereby declare that the research recorded in this thesis and the thesis itself was composed and originated entirely by myself in the Department of Electronics and Electrical Engineering at The University of Edinburgh.

Yunlu Wang

Edinburgh, Scotland, UK

Jan. 2018

Acknowledgements

Firstly, I would like to offer my sincerest gratitude to my mother, Xiangxia Fu, without her continuous support and encouragement I never would have been able to finish my Ph.D courses.

I would give a special thank you to my wife, Jie Zhang. Words cannot describe how lucky I am to have her in my life. She has selflessly given more to me than I ever could have asked for. I love you, and look forward to our lifelong journey.

I would like to sincerely appreciate my supervisor Prof. Harald Haas, who has led me into the world of LiFi. With his guidance and support, I have gained so much knowledge in the cutting-edge technologies. Thanks very much to his patience and encouragement throughout my Ph.D. study.

Last but not least, I would like to thank my friends and all guys in Institute of Digital Communications (IDCom) who have helped and encouraged me during my academic experience in Edinburgh. The time shared with them is the most precious memory in my life.

Contents

List of figures

List of tables

Acronyms and abbreviations

4G	4th generation mobile network
5G	5th generation mobile network
ACO-OFDM	Asymmetrically clipped optical orthogonal frequency division multiplexing
AP	Access point
APA	Access point assignment
AWGN	Additive white Gaussian noise
CCI	co-channel interference
CDF	Cumulative distribution function
CDMA	Code division multiple access
CIR	Channel impulse response
CSMA	Carrier sense multiple access
CSI	Channel state information
CU	Central unit
DC	Direct current
DCO-OFDM	Direct current biased optical orthogonal frequency division multiplexing
DD	Direct detection
EE	Evolutionary equilibrium
EGT	Evolutionary game theory
EPF	Enhanced proportional fairness
FDD	Frequency division duplex
FDMA	Frequency-division multiple access
FL	Fuzzy logic
FoV	Field of view
HD	High definition
HetNet	Heterogeneous network
HLRN	Hybrid LiFi and RF network
ICI	Inter-cell interference
IFFT	Inverse fast Fourier transform
IM	Intensity modulation

IoT	Internet of Things
IR	Infra-red
ISM	Industrial, scientific and medical
JOA	Joint optimisation algorithm
LB	Load balancing
LED	Light emitting diode
LiFi	Light fidelity
LoS	Line of sight
LTE	Long Term Evolution
MAC	Media access control
MCS	Modulation and coding scheme
MDP	Markov decision process
MF	Max-min fairness
MVR	Maximal vertical ROA
NE	Nash equilibrium
NLoS	Non-line-of-sight
OFDMA	Orthogonal frequency division multiple access
OOK	On-off keying
PAM	Pulse amplitude modulation
PD	Photo diode
PF	Proportional fairness
PLR	Packet loss rate
PPM	Pulse position modulation
QAM	Quadrature amplitude modulation
QoS	Quality of service
RA	Resource allocation
RAA	Random access algorithm
RB	Resource block
RF	Radio frequency
ROA	Receiving orientation angle
RU	Resource unit
SE	Spectral efficiency
SINR	Signal-to-interference-plus-noise ratio

SNR	Signal-to-noise ratio
SOA	Separate optimisation algorithm
TAA	Threshold-based access algorithm
TDD	Time division duplex
TDMA	Time division multiple access
TIA	Transimpedance amplifier
TTI	Transmission time interval
VLC	Visible light communication
VoIP	Voice over Internet protocol
WDM	Wavelength division multiplexing
WiFi	Wireless fidelity

Nomenclature

A_p	Physical area of the receiver photo-diode
A_r	Area of the indoor scenario surface;
B_L	Baseband bandwidth in LiFi systems
B_R	Bandwidth in RF systems
$\mathcal{C}_\mathcal{L}$	Set of LiFi APs
$\mathcal{C}_\mathcal{R}$	Set of RF APs
$D_{\mu,\alpha}$	LiFi link data rate with blocking considered
D_{CU}	Average delay of packets in the CU buffer
D_{AP}	Average delay of packets in the AP buffer
f_c	Cut-off frequency of the diffuse optical channel
f_0	Cut-off frequency of the LiFi front-end filtering effect
$g(\theta)$	Concentrator gain in LiFi channel
$g_{\mu,\alpha}$	Binary number representing whether user μ is served by AP α
h_w	Height of the room
$h(t)$	Impulse response of LiFi channel
$h_{me}(t)$	Impulse response of reflective LiFi channel
$h_{fe}(t)$	Impulse response caused by LiFi front-end filtering effect
$H(f)$	Frequency response of LiFi channel
$H_{me}(f)$	Frequency response of reflective LiFi channel
$H_{fe}(f)$	Frequency response caused by LiFi front-end filtering effect
$H_{\mu,\alpha}$	Frequency response of LiFi channel between user μ and AP α
l_μ	Allocatable LiFi AP for user μ in FL-based LB scheme
L_{ave}	Average length of a packet
$L(d)$	Large scale fading loss in decibels at the separation distance, d for RF channels
$k_{\mu,m}$	Number of RUs allocated to user μ on subcarrier m
$k_{\mu,\alpha}$	Proportion of resources allocated to user μ from AP α
K_m	Number of LiFi OFDM subcarriers
M_e	Number of effective subcarriers in DCO-OFDM systems
M_α	Number of users in set $\mathcal{U}_\alpha$

N_{B} — Numbers of blockages

N_{ap} — Numbers of all APs in HLRNs

N_l — Number of LiFi access points

N_r — Number of RF access points

N_s — Number of states considered in dynamic hybrid LiFi/RF networks

N_α — Number of users served by AP α

N_{L} — Single-side band noise spectrum in LiFi systems

P_{max} — Maximum output optical power

P_{min} — Minimum output optical power

P_{opt} — Range of output optical power

P_{R} — Transmit power on each subcarrier in RF systems

$r_{\mu,m}$ — The data rate achieved by user μ on subcarrier m in LiFi systems

$r_{\mu,\alpha}$ — Link data rate between user μ and AP α with handover considered

R_b — The processing data rate of the CU buffer

S — Area of the simulation scenario

$S_{\mu,\alpha}$ — User satisfaction of user μ served by AP α

$\mathcal{S}_\mu$ — Strategy set for user μ in the EGT-based LB scheme

$t_{a,ap}$ — Arrival time of a packet at the AP buffer

$t_{a,cu}$ — Arrival time of a packet at the CU buffer

$t_{a,user}$ — Arrival time of a packet at the user

t_{ij} — Handover time from AP i to AP j

T_p — Interval of two neighbouring states

$T_s(\theta)$ — Gain of the optical filter in LiFi channel

$\mathcal{Y}_\mu$ — Set of allocatable APs for user μ in the FL-based LB scheme

z — Horizontal distance from a LiFi AP to the optical receiver

$z_{\mu,\alpha}$ — Horizontal distance from LiFi AP α to the optical receiver μ

α — Access point

β — fairness coefficient

ε_p — Amplification gain in LiFi systems

λ — Average user data rate (or packet) requirement

λ_μ — Data rate requirement for user μ

κ — Optical to electric conversion efficiency at the LiFi receivers

ζ_{ij} — Mean of handover overhead from AP i to AP j

ρ	Reflectivity of the walls
θ	Angle of incidence to the PDs
$\theta_{1/2}$	Half-intensity radiation angle
θ_{PD}	Maximal vertical orientation angle of LiFi receivers
ϕ	Angle of irradiation
Φ_0	Outage probability of user QoS
$\psi_\beta(x)$	β-proportional fairness utility function
Θ_F	Half angle of the receiver FoV
μ	User in HLRNs
χ	Refractive index in LiFi channel
$\gamma_{\mu,\alpha}$	Link data rate between user μ and AP α without handover considered
$\Gamma_{\mu,\alpha}(f)$	RF channel gain between user μ and RF AP α in the frequency domain
$\tau_{p,ap}$	Packet processing time by the AP
$\tau_{p,cu}$	Packet processing time by the CU
$\tau_{q,ap}$	Packet queueing time in the AP buffer
$\tau_{q,cu}$	Packet queueing time in the CU buffer
$\pi_{\mu,\alpha}$	Payoff of user μ served by AP α in the EGT-based LB scheme
η	Average handover efficiency
η_b	Blockage density
η_{LoS}	LoS LiFi channel gain
η_{ij}	Handover efficiency from AP i to AP j
σ^2	Variance of the additive white Gaussian noise (AWGN)
$\mathcal{U}$	Set of users
$\mathcal{U}_\alpha$	Set of users that are served by AP α

Chapter 1
Introduction

1.1 Motivation

It is forecast that the number of Internet-connected mobile terminals all over the world will be close to 50 billions by 2020 [1–3]. The variety of multimedia and cloud-based services operated on those terminals, such as watching online high-definition (HD) streams, voice over Internet phone (VoIP) and cloud storage consume enormous data capacity. It has been reported that by 2020, nearly 44 zettabyes (4.4×10^{22} bytes) of data will be generated and particularly, a vast amount of them will be generated by machines, i.e. 80 billion Internet-of-Things (IoT) devices [4]. This rapidly growing data traffic generates huge pressure on the currently established radio frequency (RF) communication networks, i.e. the 4th generation (4G) mobile network, Wireless Fidelity (WiFi), Bluetooth etc, and many studies agree that these technologies cannot meet the tremendous growth of data rate requirement [5, 6]. In order to overcome this issue, academia and industry have began to develop the new generation of mobile technology termed as the 5th generation (5G) mobile network [7]. This technology aims to improve the data capacity performance by more than 1000 times compared to the current technologies. An unanimous idea is that unlike conventional RF systems, the higher ranges of the electromagnetic spectrum must be considered in 5G to boost wireless system throughputs. Therefore, the 5G concept will be a combination of various innovative inter-networking schemes rather than based on a single technology.

An emerging perspective in 4G and 5G is the concept of heterogeneous networks (HetNets) which combine macro base stations (BSs), small-cell and pico-cell access points (APs) that operate on different spectra [8–10]. The macro BSs provide ubiquitous coverage while the small-cell and pico-cell APs are able to offer high area data rates for hot spots. In general, a higher-frequency carrier means a potentially larger bandwidth in wireless communications. Light fidelity (LiFi), which works on the 300 THz visible light spectrum - 1000 times larger than the 300 GHz RF spectrum, has been recently considered as one of the promising solutions to increase transmission capacity [11, 12]. The LiFi technology exploits light emitting diodes

(LEDs) that are widely used in homes, offices, buildings and street-lighting systems to provide high speed wireless communications. Unlike visible light communication (VLC) technology which is mainly to establish a point-to-point light-based communication link between two devices - essentially a cable replacement, LiFi in contrast provides a completely wireless networking system, including bi-directional multi-user communications (i.e. point-to-multipoint and multipoint-to-point communications), multiple access and handover. The advantages of LiFi technology include [4, 13]:

i). High spatial data rate: LiFi can potentially use an enormous bandwidth to achieve high data rates. Despite the bandwidth limit of off-the-shelf LEDs, research shows that LiFi is capable of achieving speeds of over 7.36 Gbit/s from a single LED [14]. When using wavelength division multiplexing, LiFi is able to offer data rates of 14 Gbit/s, beyond 6.7 Gbit/s, the throughput of a WiFi AP in IEEE 802.11 ac Standard [15, 16]. Moreover, since most of the optical power lies in the line-of-sight (LoS) channel, a LiFi AP covers a spatially confined cell, referred to as an attocell. The small LiFi attocells ensure that users hardly ever receive severe interference from ambient LiFi APs. Therefore, LiFi networks can achieve a high spatial spectral efficiency by radically harnessing bandwidth reuse [17].

ii). High utility and power efficiency: Light resources can be found everywhere in everyday life from flash-light, to street lamps and lights in hospitals. LiFi enables these light resources to provide illumination as well as high speed communications. This means that first, we do not need to generate new transmitters for LiFi systems, leading to an efficient use of facilities; second, LiFi is able to achieve a significant improvement in energy efficiency [4].

iii). High security: Since light cannot pass through opaque structures, LiFi Internet is available only to the users within a room and cannot be breached by users in other rooms or buildings. Also, compared with WiFi, of which signals can be intercepted by any device within range of the transmitter, LiFi signals are focused and must land directly on the receiver to be intercepted. This prevents other devices from intercepting and decoding the communications in LiFi systems. Communication security is greatly improved using LiFi as it enables users to focus the transfer stream to a very small area.

Despite these advantages, LiFi still has some limitations, such as sensitivity to the LoS blocking and non-uniform spatial distribution of data rates caused by the co-channel interference (CCI) [18]. In order to provide users with a high quality of services (QoS), it is better to use LiFi technology to form an additional layer within the existing RF heterogeneous wireless networks. An advantage of this hybrid LiFi and RF network (HLRN) is that LiFi and RF do not interfere

with each other. This means that the hybrid LiFi/RF network can offer a system throughput greater than that of stand alone LiFi or RF networks. In addition, it has been shown in [18, 19] that the spatial distribution of data rates achieved by LiFi fluctuates due to the inter-cell CCI and blockage. A well designed hybrid LiFi and RF network is able to improve both the average data rate and the outage performance.

In the hybrid LiFi/RF network, users can either be served by a LiFi AP or a RF AP, resulting in numerous kinds of possible AP assignments (APAs) [20]. This indicates that load balancing (LB) in hybrid networks can be a very challenging issue. Simply, system LB contains two aspects: AP assignment and resource allocation (RA) in each cell. In general, the resource can either be time slots in the time division multiple access (TDMA) scheme, or resource units in the orthogonal frequency division multiple access (OFDMA) scheme. When a user is transferred from a LiFi AP to a RF AP, it will increase the load in the respective RF cell. Other users served by this RF AP may have to be transferred to neighbouring RF APs, or have reduced data rates. This may also lead to ping-pong effects which have to be avoided. Thus, an efficient LB technique is necessary in order to improve user data rates and to achieve fairness in the system.

Some research on the system LB for hybrid LiFi/RF networks has been undertaken [21–24]. Rahaim *et al.* pioneered the early research on VLC/RF hybrid network on the topic of system throughput optimisation [21]. An experimental study of a practical hybrid VLC/WiFi system was given in [22]. The authors implemented an asymmetric system comprised of a WiFi uplink and a VLC downlink, which differs from the network structure of a LiFi/RF downlink combination. The majority of subsequent research focused on system load balancing so as to improve the performance of data rate and user fairness [23, 24]. However, most research has not considered the handover overhead. In contrast to the outdoor heterogeneous networks, the cell size of indoor LiFi/RF hybrid networks is very small so that the movement of users may frequently prompt handovers. Mobility scenarios can be classified into horizontal (between different cells of the same network) and vertical (between different types of networks) [25]. In homogeneous networks, horizontal handovers are typically required when the serving access router becomes unavailable due to users' movement. In heterogeneous networks, the need for vertical handovers can be initiated for convenience rather than connectivity reasons (e.g., according to user choice for a particular service). In hybrid LiFi/RF networks, the handover between LiFi attocells is the horizontal handover, and the handover between LiFi and WiFi APs is the vertical handover. During a handover, the signalling information is exchanged between users and the

central unit (CU). This process takes time ranging from around 30 ms to 3000 ms on average, depending on the algorithm used [26–28]. Both steps of APA and RA in system load balancing are under the influence of the handover overhead. In practice, the channel state information (CSI) of LiFi and RF systems is time-varying because of the user movement, and this dynamic process can be divided into many quasi-static periods with a short duration which is referred to as a state. Therefore, the dynamic load balancing can be separated into two sections: static load balancing in each state and handover. A well designed dynamic LB scheme should ensure high user throughput, reduce handover overhead, improve fairness and stability in hybrid LiFi/RF networks. In this work, a comprehensive study of dynamic load balancing aiming at improving user QoS is undertaken. Specifically, user fairness, data rate requirement, and LoS blockage and receiver orientation in LiFi systems are considered. The performance of user data rate and packet latency is analysed.

1.2   Contribution

This thesis focuses on the study of downlink load balancing schemes for hybrid LiFi and RF networks. Specifically, three research objectives are addressed:

1). Optimisation of load balancing with handover considered in hybrid LiFi/RF networks;

2). Improving the performance of user data rate at low computational complexity for system LB in practical hybrid LiFi/RF networks;

3). Optimisation of packet flow assignment to reduce packet latency in hybrid LiFi/RF networks.

Several contributions have been established in relation to these research objectives. With respect to the first research objective, a novel dynamic LB scheme for hybrid LiFi/RF networks is proposed, which contains the handover scheme and the static LB scheme. Specifically, two static LB algorithms that optimise the APA and the RA in each quasi-static state are proposed, termed as joint optimisation algorithm (JOA) and separate optimisation algorithm (SOA) respectively. In this work, the optimality of JOA and the optimal threshold in SOA are analysed. A comparison of data rate performance and computational complexity between these two algorithms is made. In addition, the effect of handover overhead on the user data rate is evaluated. A special case with proportional fairness among user population is discussed. The handover

boundary and the relationship between LiFi throughput and RF throughput are analysed.

Following the second research objective, a practical hybrid LiFi/RF network including the following issues: i). LiFi LoS blockages; ii). receiving orientation angle (ROA) of LiFi; iii). user data rate requirement, is considered. Moreover, in order to achieve a better throughput/complexity trade-off, an evolutionary game theory (EGT) based static LB scheme is proposed. The EGT based LB scheme jointly handle the APA and the RA, and the optimality of this algorithm is analysed in this study. When considering user data rate requirement, conventional fairness schedulers such as max-min fairness and proportional fairness may lead to inefficient use of communication resources. In the proposed EGT based algorithm, an enhanced proportional fairness scheduler for resource allocation is proposed to avoid inefficient use of transmission resources. The performance of user satisfaction for both conventional and proposed fairness schedulers is evaluated by computer simulations. Also, the effects of blockages and the ROA, which are unique channel characteristics of LiFi, are analysed in this work. To the best of the authors knowledge, this is the first time that an investigation on how these two issues affect the system load balancing in hybrid LiFi/RF networks is conducted.

Finally, regarding the third research objective, we build a bridge between the physical and the media access control (MAC) layers for cross-layer transmission design to enhance the performance of users' QoS in hybrid LiFi/RF networks. In this study, a two-tier buffer framework for hybrid LiFi/RF networks is proposed, which contains a CU buffer and one buffer for each AP. Specifically, the arrival packets will be initially queued in the buffer of a central unit (CU). The CU coordinates all of the APs and carries out AP assignment for packet flow. According to the AP assignment results, the packet in the CU buffer will be delivered to the buffers of serving APs, then transmitted to the target users via wireless channels. In this study, the notion of a LiFi service ratio is introduced, referring to the proportion of users that are served by LiFi APs. With the practical distribution of LiFi data rates considered, an analytical solution to the optimum LiFi service ratio is derived. Based on this optimum LiFi service ratio, a novel AP assignment scheme is proposed which is able to minimise the overall system delay. To the best of the authors knowledge, this is the first time a comprehensive investigation has been conducted on the performance of packet latency in hybrid LiFi/RF networks.

1.3 Thesis Layout

The rest of the thesis is organised as follows. In Chapter 2, the communication architecture of hybrid LiFi/RF networks is firstly introduced. Following that, the characteristics of LiFi system components and channel model are provided. The basic concepts on modulation and multiple access schemes in LiFi systems are also introduced in this chapter. Specifically, a low complexity OFDMA scheme in LiFi systems is proposed, and a data rate comparison between OFDMA and TDMA is conducted. In addition, the introduction of channel model and multiple access schemes in the RF system is provided.

In Chapter 3, the optimisation of dynamic load balancing is studied, which needs to address two issues: static LB and handover. Firstly, a handover scheme to reduce the overhead between two neighbouring states is proposed. Using this handover scheme, a proportional fairness based LB scheme is analysed, where the users' behaviour of handover and the relation of throughput between LiFi and RF systems are investigated. In order to maximise the system throughput, the JOA for static LB is proposed with different kinds of fairness considered. Also, the SOA which separately optimises the APA and the RA is proposed. The complexity and data rate performance of JOA and SOA are analysed by simulations.

In Chapter 4, an evolutionary game theory based LB scheme is proposed. In this chapter, a static hybrid LiFi/RF network is considered, and three practical issues, LiFi LoS blockage, orientation angle of LiFi receivers and user data rate requirement are taken into account. Initially, the blockage model in the LiFi system is introduced. After that, the EGT-based LB scheme is proposed in which an enhanced proportional fairness RA scheduler is applied in order to minimise the waste of resources. The performance evaluation on user satisfaction level is provided and the effect of blockage and orientation angle is evaluated. Based on this analysis, conclusions are drawn at the end of this chapter.

In Chapter 5, the optimisation of packet flow assignment for hybrid LiFi/RF networks is investigated. Unlike the LB in the physical layer, the packet latency are taken into account in this study. At first, a two-tier buffer model for hybrid LiFi/RF network is introduced. Based on the queueing theory, an analysis to optimise the packet flow assignment is undertaken. The optimal LiFi service ratio to minimise system delay is mathematically derived and a low-complexity packet flow assignment scheme based on this optimum ratio is proposed. The performance evaluation on packet delay is provided via simulations.

In Chapter 6, the key findings of this thesis are summarised. In addition, the limitations of the research presented in this thesis and future research directions are also discussed.

1.4 Summary

LiFi is a recently proposed technology that combines illumination and high speed wireless communication using LEDs. Since a LiFi AP covers a small area, the spatial distribution of data rates achieved by multi-AP LiFi systems fluctuates due to CCI. Therefore, hybrid LiFi/RF networks are proposed to provide mobile terminals with better user data rate performance. In such hybrid networks, efficient load balancing can be a challenge, of which there are three main issues to address: AP assignment, resource allocation and handover. The research presented in this thesis provides a comprehensive analysis of dynamic load balancing for hybrid LiFi/RF networks. The motivation, the main contributions and the layout of the thesis are presented in this chapter.

Chapter 2

Background and System Model

2.1 Background

The development of visible light communications (VLCs) can be traced back to the late 19th century, when Alexander Graham Bell invented the photo-phone by sending speech signals over modulated sunlight [29]. Inspired by this ground-breaking experiment, the Nakagawa laboratory established the implementation of digital signal transmission by using light emitting diodes (LEDs) in 2001 [30]. Following these pioneering efforts, link-level visible light communication systems achieving hundreds of Mbit/s using state-of-the-art LEDs and photo diodes (PDs) have been presented in [31]. Recently, the current achievable data rate in a VLC link can be towards 100 Gb/s by using wavelength division multiplexing (WDM) in conjunction with off-the-shelf LEDs [15]. In 2011, Haas coined the term light fidelity (LiFi) for VLC at his 2011 TED Global Talk, showing that unlike VLC, LiFi defines a complete small-cell wireless networking system, rather than a point-to-point technique. In 2012, pureLiFi, formerly pureVLC, was founded. This is an original equipment manufacturer (OEM) firm set up to commercialise LiFi products for integration with existing LED-lighting systems.

The development of visible light communication is essentially based on the sophisticated and improving techniques of wireless communications as well as the wide use of LEDs. It is envisioned that LEDs will dominate the illumination market due to their energy-efficiency, color-rendering capability and longevity. When considering wireless communication, LEDs can potentially offer a large modulation bandwidth to achieve high data rates. This modulation bandwidth is much greater than the human eyes fusion rate, which will not affect the illumination function of LEDs. As LiFi is able to realise the dual goal of simultaneous communication and illumination, it is considered as an eco-friendly technology for the next generation of wireless communication networks.

Despite the promise of visible light communication applications, they may not be operated in isolation because of its limited coverage and sensitivity to the line-of-sight (LoS) blocking.

9

Therefore, hybrid LiFi and RF networks (HLRNs) are proposed to provide users with large data capacity and pervasive connectivity [32].

The discussion on how optical networks and RF are complementary technologies began in 1998 [33]. The optical network can provide high throughput performance to users within a confined area while RF networks can offer a much larger coverage at lower data capacity. This heterogeneous nature of LiFi and RF shows that both systems would benefit from their combination. Particularly, the indoor environments such as homes, offices and public areas are the best candidates to implement hybrid LiFi and RF networks. For example, LiFi systems can be deployed to establish discrete high-speed lighting attocells, each covering a number of desks, while the WiFi system can be deployed to cover the entire office. The use of hybrid LiFi/RF networks relies on the growing user demand of seamless connection to the Internet, while achieving high levels of QoS and avoiding network congestions and delays. There are a number of research works that have been done on HLRNs. In [21], authors show that hybrid VLC/RF networks can provide additional aggregate capacity and alleviate contentions on the RF channels. In [21, 23, 34], load balancing for HLRNs is investigated, where the proportional fairness utility function which has been widely used in RF heterogeneous networks is taken into account. In [18], user data rate requirement is considered and the outage performance of users in HLRNs is analysed. In [35], a new protocol for hybrid VLC and RF networks is proposed where VLC is used for downlink transmission and orthogonal frequency division multiple access (OFDMA) based RF network is used for uplink communications. In [36], a hybrid VLC/RF network is implemented, which allows a fast handover between VLC APs. Moreover, the combination of power line communication (PLC) and HLRNs has also been studied. It is shown in [37] that a PLC backhaul system is integrated with HLRNs and user data rate performance is optimised.

In this thesis, we focus on the investigation of load balancing in downlink HLRNs. The rest of this chapter is organised as follows. In Section 2.2, the overall introduction of HLRNs is presented. In Section 2.3, the LiFi system model is introduced, including channel model, optical-OFDM transmission and multiple access technologies. In Section 2.4, the RF channel model and multiple access methods are introduced and the summary is given in Section 2.5.
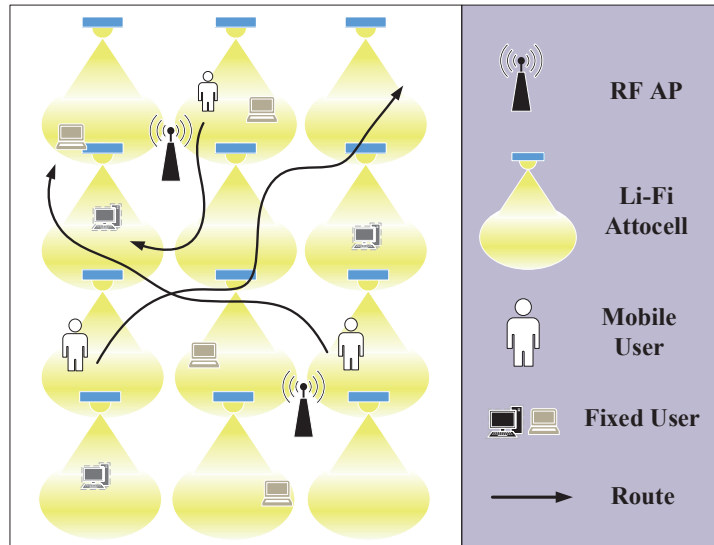
Figure 2.1: *Schematic diagram of the hybrid LiFi/RF network model*

2.2 Hybrid LiFi and RF Network Model

2.2.1 Overall Communication Architecture Description

Referring to Fig. 2.1, a multi-user indoor hybrid LiFi/RF network is considered, where N_l LiFi access points (APs) and N_r RF APs are deployed. In the LiFi system, downlink transmission is realised by using visible light, with uplink communication using infra-red (IR). For the downlink connection, the modulated electrical signals are firstly converted to light signals and then transmitted via a large LED lamp that consists of several low power LEDs. A typical LED is constituted by a semiconductor with a p-n junction. When excited by electrons, LEDs are able to generate incoherent photons by spontaneous radiation [38]. At the receiver side, optical signals will be detected and converted back to the modulated electrical signals by a PD. A PD is a type of optoelectronic semiconductor that is able to produce a photo-current that is proportional to the power of the detected optical electromagnetic wave. For the uplink connection in LiFi systems, each user is equipped with a low-power IR transmitter because of the optical radiation safety and limited power capacity of the mobile users. In order to receive IR signals, the LiFi APs should include a IR detector. Since the IR communication and the visible light communication use different spectra, there is no interference between uplink and downlink in LiFi systems, which can significantly improve the overall system capacity. In the RF system, a RF AP could be a WiFi router or a micro/pico-cell base station. The time division duplex (TDD) or frequency division duplex (FDD) technologies can be used for uplink/downlink transmission

11

[39, 40]. The RF APs are assumed to cover the entire indoor area.

In this study, we mainly focus on the downlink transmission in hybrid LiFi/RF networks. Since the field of view (FoV) of the LEDs is restricted, each LiFi AP covers a confined area which is referred to as an optical attocell. In order to improve the spatial spectral efficiency, all LiFi APs reuse the same modulation bandwidth, and users residing in the cell overlapping areas may experience optical inter-cell interference (ICI), which is treated as additional noise [34]. The ICI and blocking effects in the LiFi system may lead to a fluctuating spatial distribution in terms of LiFi data rates. Therefore, the LiFi network is augmented by a RF network to improve the users' quality of service (QoS). To avoid the ICI in the RF system, each RF AP is allocated a non-overlapping RF spectrum.

2.2.2 Central Unit and Backhaul Connection

In hybrid LiFi/RF networks, all of the LiFi and RF APs are connected to a central unit (CU) through error free inter-connection links, which can be Ethernet cables, optical fibres or a power-line backbone. The CU is responsible for the hybrid network management including AP assignment for users, resource allocation (RA) and handover etc.

Unlike in RF, the LiFi channels do not exhibit significant fading characteristics as the detector size is much larger than the wavelength [41]. They only exhibit shadowing effects so that the LiFi channel between fixed APs and users are not time-varying. In the indoor scenario, moving users are always at a low level of speed and users in the LiFi system do not experience Doppler shift due to using intensity modulation. This means that LiFi channels vary slowly in the dynamic indoor environment. In addition, users served by the RF AP in the indoor scenario can be assumed to experience slow channel fading. Therefore, in the dynamic hybrid LiFi/RF network, the channel state information (CSI) of both LiFi and RF can be considered constant for a short period. It is assumed that the coherent time of LiFi and RF channels are denoted by T_l and T_r, respectively. During the coherent time, the LiFi and RF channels are considered stable. Accordingly, the hybrid LiFi/RF system can be divided into several quasi-static states over time. In each state, the CSI of LiFi and RF channels is fixed and the duration of a quasi-static state is denoted by T_p, which is the minimum between T_l and T_r. The evaluation of the coherent time in both LiFi and RF systems is out of the scope of this work, but it will be considered in our future research. The CU monitors the HLRN continuously in every quasi-static state, where each user is assumed to have a constant data rate requirement. The CU determines the

network load balancing based on the users' CSI at the beginning of each state, which includes AP assignment, handover and resource allocation. Handover occurs when the serving AP of a user changes. During the handover, the overhead will be consumed, leading to a reduction in the user data rate.

2.3 LiFi System Model

In this section, the LiFi system model is introduced. Specifically, the LiFi channel model, modulation and multiple access technology will be explained.

2.3.1 LiFi Channel Model

The downlink LiFi channel model consists of three parts: LoS path loss, multi-path effect in indoor scenarios and the frond-end filtering effect. Due to the limitation of the front-end devices, the LiFi system uses intensity modulation (IM)/direct detection (DD) and baseband bandwidth communication for downlink transmission. The LED and the PD function as a low pass filter [42]. In addition, due to the reflective indoor environment, receivers collect signals from multiple paths. Therefore, the channel impulse response (CIR) of downlink LiFi system can be expressed as [17]:

$$h(t) = (\eta_{\text{LoS}}\delta(t) + h_{\text{me}}(t)) \otimes h_{\text{fe}}(t), \tag{2.1}$$

where η_{LoS} is the LoS channel gain; $\delta(t)$ is the Dirac delta function; $h_{\text{me}}(t)$ is the multi-path CIR and $h_{\text{fe}}(t)$ is the CIR caused by the front-end filtering effect. The corresponding frequency response of LiFi channels can be calculated by using Fourier transform:

$$H(f) = \int_0^{+\infty} (\eta_{\text{LoS}}\delta(t) + h_{\text{me}}(t)) \otimes h_{\text{fe}}(t)e^{-2\pi ft}\mathrm{d}t = (\eta_{\text{LoS}} + H_{\text{me}}(f))H_{\text{fe}}(f). \tag{2.2}$$

2.3.1.1 LoS Channel Gain

According to [43], the LoS channel gain can be written as:

$$\eta_{\text{LoS}} = \begin{cases} \frac{(\dot{m}+1)A_p}{2\pi(z^2+h_w^2)}g(\theta)T_s(\theta)\cos^{\dot{m}}(\phi)\cos(\theta), & \theta \leq \Theta_F \\ 0, & \theta > \Theta_F \end{cases}, \tag{2.3}$$
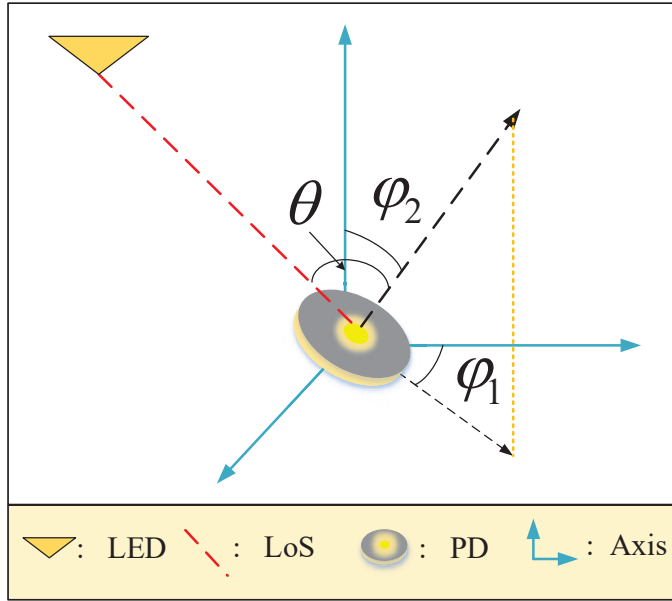
Figure 2.2: *Illustration of the angle of incidence to the PDs*

where $\dot{m}$ is the Lambertian index which is a function of the half-intensity radiation angle $\theta_{1/2}$, expressed as $\dot{m} = -1/\log_2(\cos(\theta_{1/2}))$; A_p is the physical area of the receiver photo-diode; z is the horizontal distance from a LiFi AP to the optical receiver; h_w is the height of the room; ϕ is the angle of irradiation; θ is the angle of incidence to the PDs; Θ_F is the half angle of the receiver FoV; $g(\theta)$ is the concentrator gain; and $T_s(\theta)$ is the gain of the optical filter. The concentrator included at the receiver is to trade FoV for extra signal gain [43], and the concentrator gain can be written as:

$$g(\theta) = \begin{cases} \frac{\chi^2}{\sin^2 \Theta_F}, & 0 \leq \theta \leq \Theta_F \\ 0, & \theta > \Theta_F \end{cases}, \tag{2.4}$$

where χ is the refractive index. The optical filter that is made of glass or plastic is used to remove unwanted signals for PDs. In general, the gain of optical filters is assumed to be 1 with $\theta \leq \Theta_F$.

The PD at each LiFi receiver may have horizontal and vertical tilts, which affect the angle of incidence to the PDs. As shown in Fig. 2.2, in Cartesian coordinates, the direction vector of the PD can be expressed as:

$$\overrightarrow{d_1} = (\cos(\varphi_1)\sin(\varphi_2), \sin(\varphi_1)\sin(\varphi_2), \cos(\varphi_2)), \tag{2.5}$$

where φ_1 is the horizontal orientation angle which follows a uniform distribution between $0°$ and $360°$; and φ_2 is the vertical orientation angle which follows a uniform distribution between 0° and θ_{PD}, where $0° \leq \theta_{\text{PD}} \leq 90°$ is the maximum vertical orientation angle. A PD of $\theta_{\text{PD}} = 0^o$ is perpendicular to the floor. In this case, the angle of incidence to PDs is equal to the angle of irradiation. The distance vector from a user to a LiFi AP is denoted by:

$$\overrightarrow{d_2} = (x_a - x_u, y_a - y_u, z_a - z_u), \tag{2.6}$$

where (x_a, y_a, z_a) and (x_u, y_u, z_u) are the coordinates of the LiFi AP and the user, respectively. The angle of incidence to the PDs can be expressed as:

$$\theta = \arccos < \overrightarrow{d_1}, \overrightarrow{d_2} >, \tag{2.7}$$

where $<, >$ is the inner product operator.

2.3.1.2 Multi-path Component

Referring to [44–47], the characteristics of non-LoS (NLoS) channels in the indoor environment in LiFi systems have been widely studied. It has been show that the NLoS channels are mainly due to diffused reflections caused by human bodies, furniture and other objects, and are difficult to predict and model. In [45–47], ray-tracing technique based approaches are developed to calculate the NLoS channel impulse response caused by internal surface reflections. In [44], according to simulations and measurements, an approximated diffused channel model in the frequency domain for LiFi systems is proposed:

$$H_{\text{me}}(f) = \frac{\rho A_p e^{-j2\pi f \Delta T}}{A_r(1-\rho)(1+j\frac{f}{f_c})}; \tag{2.8}$$

where A_r is the area of the indoor scenario surface; ρ is the reflectivity of the walls; ΔT is the delay between the LoS signal and the onset of the diffuse signals; and $f_c = 1/2\pi\tau$ is the cut-off frequency of the diffuse optical channel with τ denoting the transmission delay of a photon via reflective channels.

15

2.3.1.3 Front-end Filtering Effects

The frequency response of a LED shows a low-path characteristic because of the long carrier lifetime in the device active region and the large capacitance of the LED device [48]. In order to characterise the LED low pass filtering effect, several expressions are used as approximations. In [17], it has been shown that the normalised magnitude response in decibel can be approximated to be inversely proportional to the frequency, which can be expressed as:

$$H_F(f) = \exp(-\frac{f}{v_e f_0}), \tag{2.9}$$

where f_0 is the 3 dB cut-off frequency of the front-end filtering effect; and $v_e = 2.88$ is the fitting coefficient, enabling to achieve $|H_F(f_0)|^2 = -3$ dB.

2.3.2 O-OFDM Based Transmission

In LiFi networks, typical modulation schemes can fall into one of two categories: single carrier modulation and multiple carrier modulation. Due to the increasing data rate requirement, single carrier modulation schemes such as on-off keying (OOK), pulse position modulation (PPM) and pulse amplitude modulation (PAM) start to suffer from unwanted effects, such as non-linear signal distortion at the LED front-end and inter-symbol interference caused by the frequency selectivity in dispersive optical wireless channels [11]. Moreover, multiple carrier modulation is more bandwidth-efficient but less energy-efficient than single carrier modulation. One of the most widely used multiple carrier modulation schemes is orthogonal frequency division multiplexing (OFDM) [49]. When using OFDM, parallel data streams are transmitted via a collection of orthogonal subcarriers. The modulation bandwidth of the modulated signals is smaller than the coherence bandwidth of the optical channel. Each sub-channel can be considered as a flat fading channel. This allows for further adaptive bit and power loading techniques on each subcarrier to enhance system data rate performance.

Due to the complex and bipolar signals generated by the OFDM modulator, the conventional OFDM scheme cannot fit the IM/DD requirement (positive real-valued signals) in LiFi systems [50]. Therefore, two methods to modify the conventional OFDM scheme, direct current biased optical-OFDM (DCO-OFDM) and asymmetrically clipped optical OFDM (ACO-OFDM) are introduced in this section [51, 52].
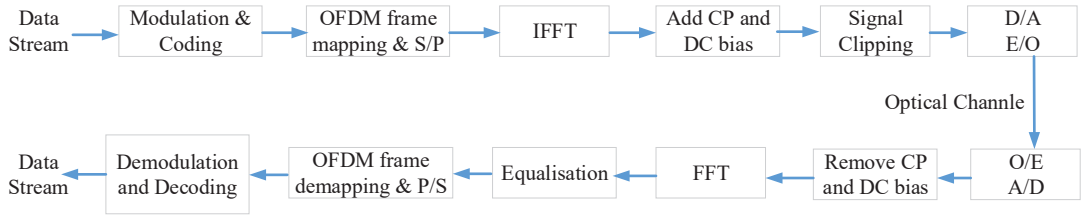
Figure 2.3: *Illustration of key elements in DCO-OFDM systems*

2.3.2.1 DCO-OFDM

The key elements in DCO-OFDM systems are shown in Fig. 2.3. The data stream is firstly coded and modulated to quadrature amplitude modulation (QAM) symbols. After that, the QAM symbols are grouped and converted to a parallel OFDM frame, which can be expressed as:

$$\mathbf{X} = [X(0), X(1), ..., X(K_m - 2), X(K_m - 1)], \tag{2.10}$$

where $X(k)$ is the symbol conveyed on the k-th OFDM subcarrier; and K_m is an even integer denoting the number of OFDM subcarriers. In DCO-OFDM transmission, the Hermitian symmetric operation is required to generate real-valued signals in the time domain [17]. Specifically, the Hermitian symmetry follows:

$$X(0) = X(K_m/2) = 0 \ \text{ and } \ X(K_m - k) = X^*(K_m), \ \ k = 1, 2, ..., \frac{K_m}{2} - 1. \tag{2.11}$$

After the inverse fast Fourier transform (IFFT) operation, the transmission signals in the time domain will be converted to real-valued numbers. In addition, a positive direct current (DC) bias is added to the time domain OFDM signals for unipolar signal generation. In OFDM transmission, the time domain signals have been converted to an approximated Gaussian waveform, which has a very high peak-to-average power ratio. However, the LED lamps operate in the linear region where the output optical power is proportional to the modulated input voltage. This region is termed as the linear working region of the LED. The signals outside this region are clipped before transmission. Assume that the output optical power of the LED falls in a region of $[P_{\min}, P_{\max}]$, where the range of the region is denoted by $P_{\text{opt}} = P_{\max} - P_{\min}$. The optical power of DC bias should satisfy the following condition:

$$P_{\text{DC}} \geq P_{\min} + \frac{P_{\text{opt}}}{2}. \tag{2.12}$$

Moreover, the ratio between the range of output optical power and the electric power of modulation signals without bias is denoted by:

$$\iota = P_{\text{opt}}/\sqrt{P_t}. \tag{2.13}$$

It is shown in [53] that an increase of ι results in a decrease in the probability of LiFi signals outside the LED linear working region. In general, $\iota = 6$ means that approximately 0.3% of the signals are clipped. In this case, the clipping noise can be considered negligible.

Since there is no modulation signal transmitted on the 0-th and $\frac{K_m}{2}$-th subcarriers, a power amplification can be achieved for the modulation signals on the subcarrier $1, 2, ..K_m/2 - 1, K_m/2 + 1, ..K_m$. The amplification gain can be denoted as $\varepsilon_p = \sqrt{K_m/(K_m - 2)}$. Particularly, when K_m is a large number, the amplification gain is approximately 1. The signal-to-noise ratio (SNR) with respect to frequency f in LiFi systems can be written as:

$$\text{SNR}_{\text{LiFi}}(f) = \frac{(\kappa \varepsilon_p P_{\text{opt}} H(f))^2}{\iota^2 N_{\text{L}} B_{\text{L}}}, \tag{2.14}$$

where κ is the optical to electric conversion efficiency at the receivers; $H(f)$ is the LiFi channel gain in the frequency domain; N_{L} is the single side-band noise spectrum; and B_{L} is the baseband bandwidth. In LiFi systems, the receive noise mainly consists of shot noise and thermal noise. Shot noise is due to the particle characteristics of photons [38]. For an incident light with constant power, the number of incoming photons per unit time follows a Poisson distribution. This randomness of arriving photon numbers leads to the shot noise. With a large number of photons, the shot noise can be modelled as an additive white Gaussian noise (AWGN). Thermal noise mainly results from the temperature variation caused by the resistive units in the receiver circuit [38]. In most of the optical receivers, a transimpedance amplifier (TIA) is included to amplify the received signal. The resistance of the TIA is a major source of thermal noise. This noise can also be modelled as an AWGN.

2.3.2.2 ACO-OFDM

Unlike DCO-OFDM, the Hermitian symmetric operation in ACO-OFDM only uses odd subcarriers for data transmission and the even subcarriers are set to zero. In this case, after the IFFT operation, the signals in the time domain can be positive and real-valued. Therefore, a large DC-bias is not required in ACO-OFDM, which can achieve better energy efficiency per-

formance than DCO-OFDM [54]. However, as only the odd subcarriers are used, the spectral efficiency of ACO-OFDM is further halved, compared with DCO-OFDM, resulting in a reduction of data rates. In this thesis, the DCO-OFDM is used for LiFi transmission in order to improve the performance of user data rates.

2.3.3 Multiple Access Technology

In wireless communication networks, a multiple access technology allows several terminals connected to the same multi-point transmission medium to transmit over it and to share its capacity. In the RF networks, conventional multiple access technologies include time division multiple access (TDMA), code division multiple access (CDMA), carrier sense multiple access (CSMA) and OFDMA, etc [55–57]. In particular, OFDMA is considered as an efficient multiple access method which has been widely used in 4G and 5G communication networks [58]. One of the main advantages of OFDMA is the flexibility for resource allocation. In the OFDMA scheme, resources are partitioned in both time and frequency domains. Such time-frequency blocks are known as resource blocks (RBs), and each RB contains a number of resource units (RUs), which are the minimum and indivisible time-frequency slots. It is evident that allocating those RUs to different users is more efficient and flexible than allocating subcarriers or time slots only. Another benefit of OFDMA is the multi-user diversity gain. OFDMA allows users to transmit over different sub-channels, and different users may have different high-quality subchannels. Hence, each user can select their high-quality sub-channels for transmission to achieve an improvement in overall capacity. In this section, the OFDMA technology and the relative resource allocation schemes in LiFi systems will be introduced.

2.3.3.1 Introduction: OFDMA in LiFi systems

In the conventional RF networks, the OFDMA method can substantially enhance the overall system spectral efficiency (SE) by using an adaptive user-to-RU assignment. In recent research on LiFi systems, OFDMA has been also used for RA [59, 60]. However, most of them assume an equal channel gain over the OFDM subcarriers. The LiFi OFDMA systems with practical channel responses have so far not been studied. As shown in Section 2.3.1, the LiFi channel gain in the frequency domain is mainly affected by the characteristics of front-end devices and the multi-path effect. It has been shown that in an open space office scenario, LiFi channels are mainly affected by the front-end filtering effect, functioning as a low-pass filter [17]. This
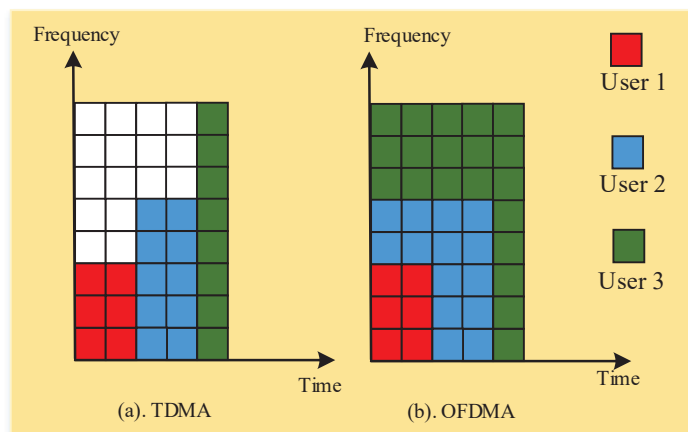
Figure 2.4: *Resource allocation in TDMA and OFDMA schemes.*

results in a decrease in the amplitude of the channel response, with an increase in frequency. The multipath component, however, plays a less important role in LiFi links with a maximum variance of less than 2.5 dB [17]. Therefore, for all users served by a specific LiFi AP, the LiFi channel response over the subcarriers are almost the same, and the channel quality at low frequencies is always better than at high frequencies.

Despite the inconspicuous multi-user diversity, we find that OFDMA can still achieve a higher SE than TDMA in LiFi systems by carefully allocating high-frequency subcarriers to users. It is shown in [17] that the LiFi channel response in the frequency domain is approximately inversely proportional to the frequency. This means that users with high DC SNR are able to use a large modulation bandwidth, while the users with low DC SNR may not be able to transmit signals on high-frequency subcarriers. As shown in Fig. 2.4 (a), in the TDMA scheme, some of the high-frequency RUs, which are coloured white, are not usable due to the low DC SNR of the corresponding users. However, those RUs can be assigned to users with high DC SNR to enhance overall data rates, depicted in Fig. 2.4 (b). In this subsection, two OFDMA-based RA schemes are proposed in order to exploit the multi-user diversity gain in LiFi systems. One is the optimisation-based RA scheme which formulates the RA issue as an optimisation problem. The other is the low-complexity RF scheme which exploits the unique characteristics of LiFi channels for RA to reduce the computational complexity.

In this study, an indoor LiFi network with N_l APs is considered. As shown in Fig. 2.5, the deployment of LiFi APs follows a square lattice topology which models a regular lighting
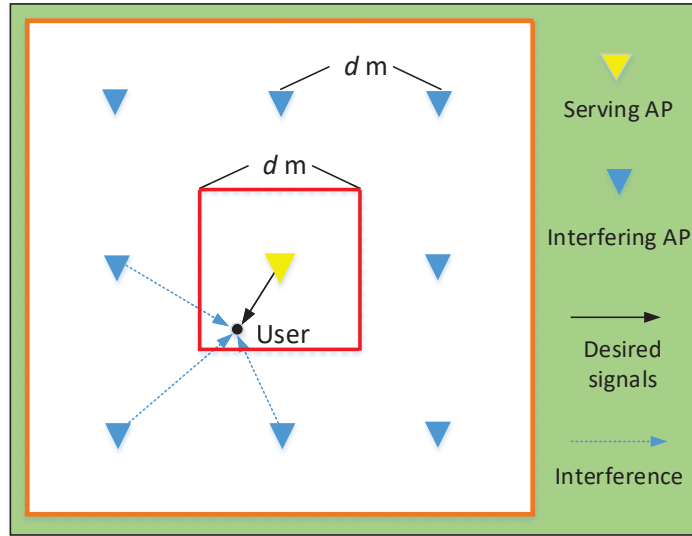
Figure 2.5: *Illustration of LiFi networks for the evaluation of the OFDMA-based RA schemes.*

placement commonly used in large offices and public places. The distance between two neighbouring APs is denoted by d. Each LiFi AP is a large LED lamp consisting of several low power LEDs, and each user has a PD, assumed to be oriented perpendicularly to the floor. In the overlapping areas of LiFi attocells, the ICI exists, which is considered and treated as noise. In addition, DCO-OFDM is used in the LiFi systems. The sequence number of OFDM subcarriers is denoted by $m \in [0, K_m - 1]$, $m \in \mathbb{N}$, where K_m is an even positive integer, denoting the number of OFDM subcarriers. In DCO-OFDM, complex-valued modulated symbols are conveyed on subcarriers from 1 to $K_m/2 - 1$, and subcarriers from $K_m/2 + 1$ to $K_m - 1$ are used to realise their Hermitian conjugate. The signals on the 0-th and $K_m/2$-th subcarriers are set at zero. Hence, the real number constraint can be satisfied after the Fourier transform. The effective subcarriers which can transmit signals in DCO-OFDM transmission are denoted by $\mathcal{M}_e = \{m | m \in [1, K_m/2 - 1], m \in \mathbb{N}\}$, and $M_e = K_m/2 - 1$ is defined as the number of effective subcarriers. Also, the DC bias added to the modulated signals guarantees the output signals to be positive. According to Eq. (2.14), the signal-to-interference-plus-noise ratio (SINR) between user μ and its serving AP α can be written as follows:

$$\text{SINR}_{\mu,\text{LiFi}}(f) = \frac{(\kappa \varepsilon_p P_{\text{opt}} H_{\mu,\alpha}(f))^2}{\iota^2 N_{\text{L}} B_{\text{L}} + \sum_{j \neq \alpha}(\kappa \varepsilon_p P_{\text{opt}} H_{\mu,j}(f))^2}, \tag{2.15}$$

where $H_{\mu,\alpha}(f)$ is the channel gain between user μ and AP α, according to Eq. (2.2); and $H_{\mu,j}(f)$ is the channel gain between user μ and the interfering LiFi AP j. In addition, adaptive

min. SINR [dB]	Modulation	Code rate	SE [bit/s/Hz]
-	-	-	0
1	QPSK	0.44	0.8770
3	QPSK	0.59	1.1758
5	16QAM	0.37	1.4766
8	16QAM	0.48	1.9141
9	16QAM	0.60	2.4063
11	64QAM	0.45	2.7305
12	64QAM	0.55	3.3223
14	64QAM	0.65	3.9023
16	64QAM	0.75	4.5234
18	64QAM	0.85	5.1152
20	64QAM	0.93	5.5547

Table 2.1: *Modulation and Coding Table*

M-QAM is used on different OFDM subcarriers. Note that the frequency of subcarrier m is denoted by f_m and the achievable SE on subcarrier m is denoted by q_m. The relationship between q_m and $\mathrm{SINR}_{\mu,\mathrm{LiFi}}(f_m)$ follows the modulation and coding scheme (MCS) given in Table 2.1 [61]. Specifically, given a $\mathrm{SINR}_{\mu,\mathrm{LiFi}}(f)$, we can firstly find the min. SINR level which is closest to and less than $\mathrm{SINR}_{\mu,\mathrm{LiFi}}(f)$ in Table 2.1. Then, q_m will be the corresponding SE shown in the table. The data rate achieved by user μ on subcarrier m can be expressed as $r_{\mu,m} = 2B_\mathrm{L}q_m/K_m$.

In this study, it is assumed that a RB contains $M_e K$ RUs, where K is the number of subframes in the time domain. Since LiFi channels do not exhibit fading characteristics, the LiFi CSI on each subcarrier can be assumed to be constant in a RB period. In the following subsections, two RA schemes in LiFi OFDMA systems are proposed. In the first scheme, the RA is formulated as an optimisation problem, and an iterative algorithm is proposed to find the optimum. In the second scheme, RUs are allocated to users from high-frequency to low-frequency subcarriers in order to make full use of high-frequency subcarriers. This method can significantly reduce computational complexity as it does not require iterative operations.

2.3.3.2 Optimisation-based RA scheme

In this scheme, a utility function involving the data rates and fairness of users is considered for RA. This is referred to as β-proportional fairness function defined in [61]:

$$\psi_\beta(x) = \begin{cases} \ln(x), & \beta = 1 \\ \dfrac{x^{1-\beta}}{1-\beta}, & \beta > 0, \ \beta \neq 1 \end{cases}, \quad (2.16)$$

where x is the user data rate; and β is the fairness coefficient. This utility function includes several well known fairness concepts. For instance, when $\beta \to +\infty$, a max-min fairness scheduler is realised and when $\beta = 1$, a proportional fairness is achieved. In a LiFi attocell, the resource allocation with the β-proportional fairness function can be formulated as an optimisation problem:

$$\max_{k_{\mu,m}} \sum_{\mu \in \mathcal{U}} \psi_\beta \left(\sum_{m \in \mathcal{M}_e} k_{\mu,m} r_{\mu,m} \right) \quad (2.17)$$

$$\text{s.t.} \quad \sum_{\mu \in \mathcal{U}} k_{\mu,m} = K, \ \ m \in \mathcal{M}_e; \quad (2.18)$$

$$k_{\mu,m} \in [0, K], \ k_{\mu,m} \in \mathbb{N}, \quad (2.19)$$

where $\mathcal{U}$ is the set of all users; and $k_{\mu,m}$ is the number of RUs allocated to user μ on subcarrier m. This is a integer programming problem. In order to simplify this problem, the variable $k_{\mu,m}$ is firstly assumed to be a non-negative real number and the Lagrangian multiplier method can be used to find the optimal solution. The Lagrangian function is given by:

$$F_1(k_{\mu,m}, \omega_m) = \sum_{\mu \in \mathcal{U}} \psi_\beta \left(\sum_{m \in \mathcal{M}_e} k_{\mu,m} r_{\mu,m} \right) + \omega_m \left(K - \sum_{\mu \in \mathcal{U}} k_{\mu,m} \right), \quad (2.20)$$

where ω_m is the Lagrangian multiplier for the m-th constraint in Eq. (2.18). The optimal $k_{\mu,m}$ can be obtained by making the gradient of the Lagrangian function in Eq. (2.20) equal to 0:

$$\frac{\partial F_1(k_{\mu,m}, \omega_m)}{\partial k_{\mu,m}} = \frac{\partial \psi_\beta(\sum_{m \in \mathcal{M}_e} k_{\mu,m} r_{\mu,m})}{\partial k_{\mu,m}} - \omega_m = 0, \quad (2.21)$$

According to Eq. (2.16), we have

$$\frac{\partial \psi_\beta(\sum_{m \in \mathcal{M}_e} k_{\mu,m} \gamma_{\mu,m})}{\partial k_{\mu,m}} = r_{\mu,m} \left(\sum_{m \in \mathcal{M}_e} k_{\mu,m} r_{\mu,m} \right)^{-\beta}. \quad (2.22)$$

Substituting Eq. (2.22) into Eq. (2.21), it gives:

$$k_{\mu,m} = \frac{1}{r_{\mu,m}} \left(\frac{r_{\mu,m}}{\omega_m} \right)^{\frac{1}{\beta}} - \frac{1}{r_{\mu,m}} \sum_{\substack{i \neq m}}^{i \in \mathcal{M}_e} k_{\mu,i} r_{\mu,i}. \tag{2.23}$$

We denote $\omega_m^{-1/\beta}$ by T_m. Combining Eq. (2.23) and the constraints in Eq. (2.18), T_m can be expressed as:

$$T_m = \left(K + \sum_{\mu \in \mathcal{U}} \sum_{\substack{i \neq m}}^{i \in \mathcal{M}_e} \frac{k_{\mu,i} r_{\mu,i}}{r_{\mu,m}} \right) \Big/ \sum_{\mu \in \mathcal{U}} (r_{\mu,m})^{\frac{1}{\beta}-1} . \tag{2.24}$$

Inserting Eq. (2.24) into Eq. (2.23), the number of RUs allocated to user μ on subcarrier m can be expressed as:

$$k_{\mu,m} = r_{\mu,m}^{\frac{1}{\beta}-1} T_m - \frac{1}{r_{\mu,m}} \sum_{\substack{i \neq m}}^{i \in \mathcal{M}_e} k_{\mu,i} r_{\mu,i}. \tag{2.25}$$

It can be seen that $k_{\mu,m}$ is determined by $k_{\mu,i}$, $i \neq m$ and $i \in \mathcal{M}_e$. Without loss of generality, $k_{\mu,m}$ can be written as a function of $k_{\mu,i}$ according to Eq. (2.25):

$$k_{\mu,m} = G(k_{\mu,2}, k_{\mu,3}, ..., k_{\mu,m-1}, k_{\mu,m+1}, ...k_{\mu,M_e}, k_{\mu,M_e+1}), \tag{2.26}$$

and an iterative algorithm is designed to obtain a solution to $k_{\mu,m}$. In each iteration, $k_{\mu,m}$ is updated sequentially from $m = 2$ to $M_e + 1$ by using the latest values of $k_{\mu,i}$ ($i \neq m$). Note that in the t-th iteration, $k_{\mu,m}$ is denoted by $k_{\mu,m}^{(t)}$, where $k_{\mu,m}^{(t)}$ can therefore be expressed as:

$$k_{\mu,m}^{(t)} = G(k_{\mu,2}^{(t)}, k_{\mu,3}^{(t)}, ..., k_{\mu,m-1}^{(t)}, k_{\mu,m+1}^{(t-1)}, ...k_{\mu,M_e}^{(t-1)}, k_{\mu,M_e+1}^{(t-1)}). \tag{2.27}$$

The iterative algorithm to solve the optimisation problem in Eq. (2.17) is summarised in Algorithm. 1. Since $k_{\mu,m}$ must be an integer, the RA result obtained by Algorithm. 1 needs to be rounded to the nearest integer, denoted by $\bar{k}_{\mu,m}$. Also, in order to guarantee the constraints in Eq. (2.18), a fine tuning of $\bar{k}_{\mu,m}$ is required for each subcarrier. It can be seen from Eq. (2.22) that the derivative of the objective function in Eq. (2.17) is positive, which means the objective function is monotonically increasing. If we have $\sum_{\mu \in \mathcal{U}} \bar{k}_{\mu,m} > K$, $\bar{k}_{\mu,m}$ with the smallest derivative should be reduced in order to maximise the objective function, which can be expressed as:

$$\bar{k}_{\mu,m} = \bar{k}_{\mu,m} - \left(\sum_{\mu \in \mathcal{U}} \bar{k}_{\mu,m} - K \right), \quad \mu = \arg\min_j D_{j,m}, j \in \mathcal{U}, \tag{2.28}$$

Algorithm 1 : Optimisation-based RA algorithm for LiFi OFDMA systems

---

1: Initialisation: The objective function in Eq. (2.17) at the t-th iteration is denoted by $O^{(t)}$; $O^{(0)} = 0$; $O^{(-1)} = -\infty$; $k_{\mu,m}^{(0)} = 0$, $m \in \mathcal{M}_e$; $t = 1$; ε is small enough positive number.

2: **while** $|O^{(t-1)} - O^{(t-2)}| < \varepsilon$ **do**

3:    **for** m from 2 to $M_e + 1$ **do**

4:       Calculate $k_{\mu,m}^{(t)}$ for all users according to Eq. (2.25), where

$$k_{\mu,i} = \begin{cases} k_{\mu,i}^{(t)}, & i < m \\ k_{\mu,i}^{(t-1)}, & i > m \end{cases} ; \tag{2.30}$$

5:    **end for**

6:    Calculate $O^{(t)}$ by using $k_{\mu,m}^{(t)}$ for all users according to Eq. (2.17);

7:    $t = t + 1$.

8: **end while**

---

where $D_{j,m}$ is the first-order derivative of the objective function in Eq. (2.17) with respect to $k_{j,m}$. Oppositely, if we have $\sum_{\mu \in \mathcal{U}} \bar{k}_{\mu,m} < K$, $\bar{k}_{\mu,m}$ with the largest derivative should increase, which can be expressed as:

$$\bar{k}_{\mu,m} = \bar{k}_{\mu,m} + \left(K - \sum_{\mu \in \mathcal{U}} \bar{k}_{\mu,m} \right), \quad \mu = \arg \max_j D_{j,m}, j \in \mathcal{U}. \tag{2.29}$$

With $\sum_{\mu \in \mathcal{U}} \bar{k}_{\mu,m} = K$, the fine tuning is not required.

2.3.3.3 Low-complexity RA scheme

As shown in [17], the LiFi channel gain in the frequency domain decreases with an increase in frequency. Therefore, in a LiFi attocell, there are fewer users that can use high-frequency resources than those who can use low-frequency resources. Based on this fact, a low-complexity RA scheme is proposed in which RA is carried out from high-frequency to low-frequency subcarriers. On each subcarrier, the RUs are assigned based on the CSI and the resources obtained by users on the higher-frequency subcarriers. The aggregate data rate achieved by user μ over subcarriers from m to $K_m/2 - 1$ is denoted by:

$$Z_{\mu,m} = \begin{cases} Z_{\mu,m+1} + k_{\mu,m} r_{\mu,m}, & 1 \leq m \leq K_m/2 - 1 \\ 0 \quad , & m = K_m/2 \end{cases} . \tag{2.31}$$

On the m-th subcarrier, the resource allocation using β-proportional fairness function can be formulated as:

$$\max_{k_{\mu,m}} \sum_{\mu \in \mathcal{U}_m} \psi_\beta \left(k_{\mu,m} r_{\mu,m} + Z_{\mu,m+1} \right) \tag{2.32}$$

$$\text{s.t.} \quad \sum_{\mu \in \mathcal{U}_m} k_{\mu,m} = K; \tag{2.33}$$

$$k_{\mu,m} \in [0, K], \ k_{\mu,m} \in \mathbb{N}, \tag{2.34}$$

where $\mathcal{U}_m$ is the set of users whose link data rates on subcarrier m, $r_{\mu,m}$, are greater than zero.

The Lagrangian multiplier method is used to solve the optimisation problem in Eq. (2.32). The Lagrangian function is given by:

$$F_2(k_{\mu,m}, \varrho) = \sum_{\mu \in \mathcal{U}_m} \psi_\beta \left(k_{\mu,m} r_{\mu,m} + Z_{\mu,m+1} \right) + \varrho \left(K - \sum_{\mu \in \mathcal{U}_m} k_{\mu,m} \right), \tag{2.35}$$

where ϱ is the Lagrangian multiplier for the constraint in Eq. (2.33). The optimal $k_{\mu,m}$ can be obtained by making the gradient of the Lagrangian function in Eq. (3.83) equal to 0, which is written as:

$$\frac{\partial F_2(k_{\mu,m}, \varrho)}{\partial k_{\mu,m}} = r_{\mu,m} (k_{\mu,m} r_{\mu,m} + Z_{\mu,m+1})^{-\beta} - \varrho = 0. \tag{2.36}$$

It can be obtained from Eq. (2.36) that:

$$k_{\mu,m} = \frac{1}{r_{\mu,m}} \left(\frac{r_{\mu,m}}{\varrho} \right)^{\frac{1}{\beta}} - \frac{Z_{\mu,m+1}}{r_{\mu,m}}. \tag{2.37}$$

Combining Eq. (2.37) and the constraint in Eq. (2.33), it can be derived that:

$$\varrho^{-\frac{1}{\beta}} = \left(K + \sum_{\mu \in \mathcal{U}_m} \frac{Z_{\mu,m+1}}{r_{\mu,m}} \right) \bigg/ \sum_{\mu \in \mathcal{U}_m} (r_{\mu,m})^{\frac{1}{\beta} - 1}. \tag{2.38}$$

Inserting Eq. (2.38) into Eq. (2.37), the number of RUs allocated to user $\mu \in \mathcal{U}_m$ on subcarrier m can be expressed as:

$$k_{\mu,m} = \frac{r_{\mu,m}^{\frac{1}{\beta} - 1}}{\sum_{\mu \in \mathcal{U}_m} r_{\mu,m}^{\frac{1}{\beta} - 1}} \left(K + \sum_{\mu \in \mathcal{U}_m} \frac{Z_{\mu,m+1}}{r_{\mu,m}} \right) - \frac{Z_{\mu,m+1}}{r_{\mu,m}}. \tag{2.39}$$

Algorithm 2 : Low-complexity RA algorithm for LiFi OFDMA systems

---

1: Initialisation: Calculate the link data rate for user m on subcarrier $m \in \mathcal{M}_e$; $Z_{\mu, M_e+2} = 0$.

2: **for** Subcarrier m from $M_e + 1$ to 2 **do**

3:   Determine the user set $\mathcal{U}_m = \{\mu \mid r_{\mu,m} \neq 0, \mu \in \mathcal{U}\}$;

4:   Calculate $Z_{\mu, m+1}$ for all users;

5:   For user $\mu \in \mathcal{U}_m$, calculate $k_{\mu,m}$ according to Eq. (2.39);

6:   For user $\mu \notin \mathcal{U}_m$, $k_{\mu,m}$ equals to zeros;

7: **end for**
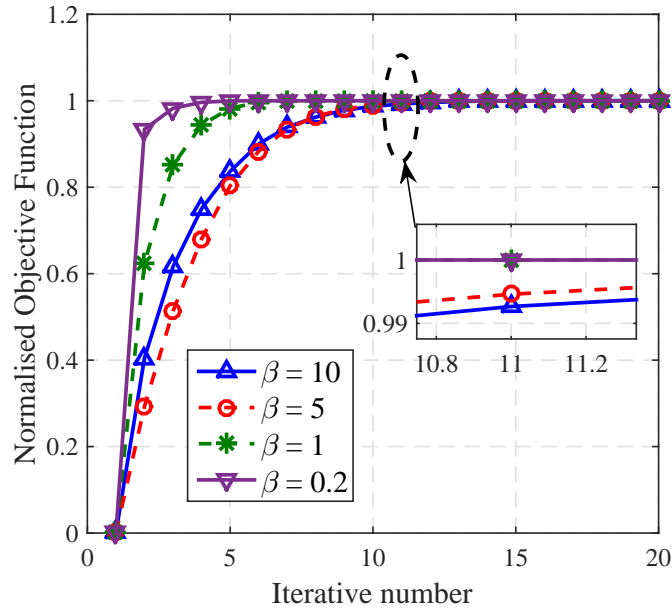
Figure 2.6: *Iterative number in optimisation-based RA scheme in OFDMA systems ($B_L = 250$ MHz).*

It can be seen that $k_{\mu,m}$ in Eq. (2.39) is a closed-form solution, and iterative computation is not required here, leading to a reduced computational complexity. In addition, no RU on subcarrier m will be allocated to users that do not belong to $\mathcal{U}_m$. The low-complexity RA algorithm is summarised in Algorithm. 2. The final RA result can be obtained via an integer conversion and fine tuning of $k_{\mu,m}$, which are the same as those in the optimisation-based RA algorithm.

2.3.3.4   Performance evaluation

As shown in Fig. 2.5, an indoor office space scenario is considered where 9 LiFi APs are deployed in a square lattice topology. Each AP covers a 4 m $\times$ 4 m attocell, with 6 users uniformly distributed in the central attocell, which are served by the central LiFi AP and receive

Name of Parameters	Value
Vertical distance between APs and users, h_w	2 m
Optical power range of each LiFi AP, P_{opt}	18 W
The physical area of a PD, A_p	1 cm^2
Half-intensity radiation angle, $\theta_{1/2}$	60 deg.
Gain of optical filter, $T_s(\theta)$	1.0
Receiver FoV semi-angle, Θ_F	90 deg.
Refractive index, χ	1.5
Optical to electric conversion efficiency, κ	0.53 A/W
Noise power spectral density of LiFi, N_{L}	10^{-19} A^2/Hz
OFDM subcarrier number, K_m	64
Number of subframes in a RU, K	20

Table 2.2: *Simulation parameters for the evaluation of OFDMA-based RA schemes*

interference from neighbouring APs. Simulation parameters are given in Table 4.1. In this study, a RA scheme using β-proportional fairness function in LiFi TDMA systems is considered as a benchmark, where resources are partitioned only in the time domain [61].

The normalised value of the objective function with respect to the iterative number of the optimisation-based RA scheme is shown in Fig. 2.6. It is shown that this algorithm converges after nearly 10 times the iteration, and the iterative number increases with the fairness coefficient β. According to Eq. (2.23) and Eq. (2.39), it can be seen that the computational complexity in each iteration in the optimisation-based RA scheme is almost the same with the low-complexity RA scheme. Since the optimisation-based RA scheme requires nearly 10 times the iteration, it can be concluded that the low-complexity RA scheme is able to achieve a 90% reduction of computational complexity compared to the optimisation-based RA scheme.

In Fig. 2.7 and Fig. 2.8, the average data rate and user fairness index corresponding to β are presented, respectively. The fairness index was introduced in [34]. In the legend, 'Optimal OFDMA' and 'LC OFDMA' represent optimisation-based RA scheme and low complexity RA scheme for OFDMA transmission, respectively. It appears that the RA schemes in the OFDMA system outperform that in the TDMA system on both user data rate and fairness index. This is because the OFDMA scheme can more efficiently utilise the high-frequency RUs than the TDMA scheme. In addition, it is shown that the low-complexity RA scheme achieves throughput performance close to the optimal scheme. Particularly, the largest gap of data rate between the optimal scheme and the low-complexity scheme takes place at around $\beta = 1$, where the low-complexity scheme can achieve better fairness performance than the optimal scheme, as shown
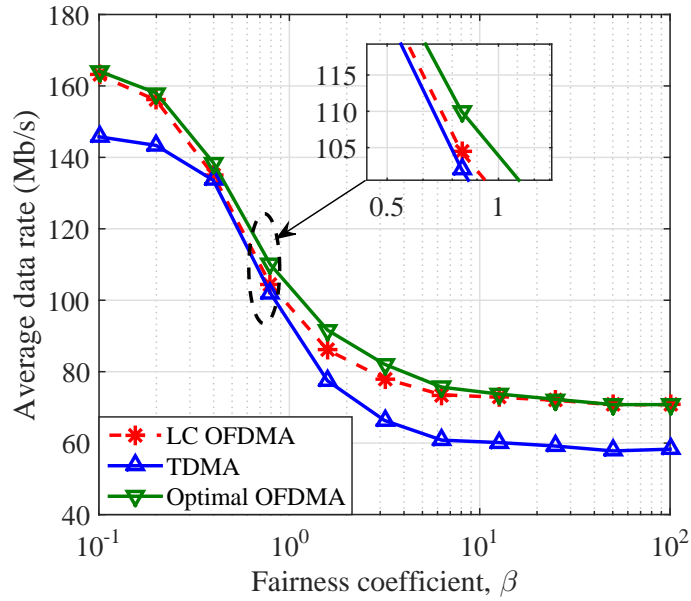
Figure 2.7: *User data rate corresponding to β ($B_L = 280$ MHz for OFDMA-based and TDMA-based RA schemes)*

in Fig. 2.8. This is because the low-complexity RA scheme is based on how much resource users have gained. Users that have obtained more resources on the high-frequency subcarriers will obtain less resources on the low-frequency subcarriers, and this principle improves user fairness.

2.3.3.5 Remarks

In this section, the multi-user diversity gain achieved by OFDMA in LiFi networks is analysed, and the optimisation-based RA scheme and the low-complexity RA scheme for LiFi OFDMA systems are proposed. The performance of these two schemes, in terms of computational complexity, data rate and user fairness, is evaluated and compared to a benchmark RA scheme in the TDMA system. Two conclusions can be drawn based on the simulation results: i) the RA schemes in OFDMA systems outperform those in TDMA systems on both data rate and user fairness because of an efficient use of high-frequency resources; and ii) the low-complexity RA scheme is able to achieve near-optimal performance at a reduction of 90% in computational complexity.
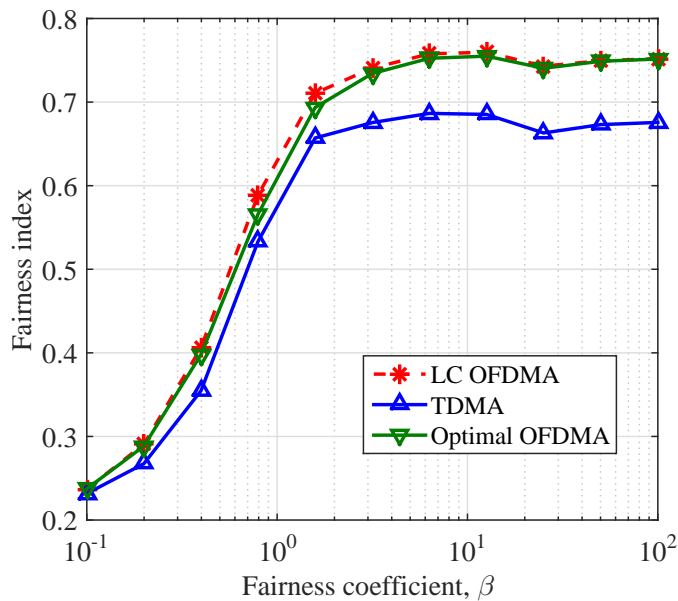
Figure 2.8: *Fairness index corresponding to β ($B_L = 280$ MHz for OFDMA-based and TDMA-based RA schemes)*

2.4 RF System Model

In hybrid LiFi/RF networks, the RF network can achieve ubiquitous coverage which provides the basic data rate requirement. Conventional RF networks for indoor scenarios include pico-cell cellular network and wireless fidelity (WiFi) network. A pico-cell is a small cellular base station typically covering in-building areas such as offices, shopping malls, train stations, stock exchanges, or more recently in-aircraft. Pico-cells are available for most cellular technologies including CDMA, universal mobile telecommunications system (UMTS) and Long term evolution (LTE) from manufacturers including ZTE, Huawei and Airwalk. WiFi is a technology for wireless local area networking with devices based on the IEEE 802.11 standards. WiFi most commonly uses the 2.4 GHz (12 cm) ultra high frequency (UHF) and 5.8 GHz (5 cm) super high frequency (SHF) industrial scientific medical (ISM) radio bands [62]. In general, a WiFi AP has a range of about 20 meters (66 feet) in indoor scenarios. In this study, the RF system is assumed to employ 2.4 GHz spectrum which is suitable for the indoor coverage. The channel model and multiple access technology used in the hybrid LiFi/RF network model are introduced in this section.

2.4.1 RF Channel Model

In the RF system, an omni-directional transmit antenna is employed for the 2.4 GHz RF AP. The OFDM transmission is used and the RF channel gain between user μ and RF AP α on each OFDM subcarrier is given by [16]:

$$\Gamma_{\mu,\alpha}(f) = \sqrt{10^{\frac{-L(d)}{10}}} h_r, \tag{2.40}$$

where f is the central frequency of OFDM subcarriers; h_r is the small scale fading gain which has an independent identical Rayleigh distribution with average power 2.46 dB; and $L(d)$ is the large-scale fading loss in decibels at the separation distance, d, which is given by [16]:

$$L(d) = \begin{cases} L_{\text{FS}}(d) + X_{\text{SF}}, & d < d_{\text{BP}} \\ L_{\text{FS}}(d_{\text{BP}}) + 35 \log_{10}(d/d_{\text{BP}}) + X_{\text{SF}}, & d \geq d_{\text{BP}} \end{cases}, \tag{2.41}$$

where $L_{\text{FS}}(d) = 20 \log_{10}(d) + 20 \log_{10}(f) - 147.5$ (dB) is the free space loss up to a breakpoint distance $d_{\text{BP}} = 10$ m, where f is the carrier frequency; and X_{SF} is the shadowing fading loss due to large scale blockage, which is 3 dB in typical indoor scenarios. It is assumed that the RF APs use different spectra to avoid ICI. The SNR on each subcarrier with central frequency f can be expressed as:

$$\text{SNR}_{\mu,\text{RF}}(f) = \frac{|\Gamma_{\mu,\alpha}(f)|^2 P_{\text{R}}}{\sigma^2}, \tag{2.42}$$

where P_{R} is the transmit power on each subcarrier; σ^2 is the variance of the additive white Gaussian noise (AWGN); and $\Gamma_{\mu,\alpha}(f)$ is the channel gain according to Eq. (2.40).

2.4.2 Multiple Access Technology

In the RF networks, the multiple access technologies include OFDMA, TDMA, CDMA and CSMA, etc. The OFDMA method is widely used in LTE cellular networks, which has been introduced in Section 2.3.3. In WiFi networks, CSMA is the main approach for multiple access in order to avoid ICI [16]. In CSMA transmission, a transmitter attempts to determine whether another transmission is in progress before initiating a transmission using a carrier-sense mechanism. If a carrier is sensed, the transmitter waits for the transmission in progress to end before initiating its own transmission. Using CSMA, multiple nodes may, in turn, send and receive on the same medium. In this study, the RF APs work on different sub-channel, therefore the ICI is avoided and CSMA is not used in this model. Moreover, in order to reduce the complexity,

the OFDM-TDMA method instead of OFDMA is taken into account in RF systems. TDMA allows the AP to communicate with users through different time slots, which can be realised at a reduced complexity [58].

2.5   Summary

In this chapter, the downlink system model for hybrid LiFi/RF networks is introduced. The overall communication architecture is described, and the channel model, OFDM transmission and multiple access technology for LiFi and RF systems are discussed, respectively. Specifically, the LiFi channel mainly contains three components: the LoS path loss, front-end low pass filtering effect. In addition, the DCO-OFDM and ACO-OFDM transmissions are introduced. Since LiFi uses IM/DD and baseband bandwidth communications, the transmit signals should be positive and real. In DCO-OFDM, complex modulated signals are conveyed on the first half of the OFDM subcarriers, and the second half of the subcarriers are used for Hermitian symmetry. After IFFT operation, the signals in the time domain are real-valued. Also, a DC bias is added to signals to guarantee the positivity. In ACO-OFDM, the complex modulated symbols are mapped to the odd subcarriers, and the signals on the other subcarriers are zero. The time-domain signals after IFFT can be positive and real-valued. In Section 2.3, the multiple access technologies for LiFi systems have been introduced, and OFDMA transmission techniques have been discussed. It has been shown that despite the inconspicuous multi-user diversity in LiFi networks, OFDMA can still achieve a higher SE than TDMA by carefully allocating high-frequency subcarriers to users. Two OFDMA-based RA schemes are proposed in order to exploit the multi-user diversity gain in LiFi systems. One is the optimisation-based RA scheme which formulates the RA issue as an optimisation problem. The other is the low-complexity RF scheme which exploits the unique characteristics of LiFi channels for RA to reduce the computational complexity. Simulation results show that by efficiently using high-frequency bandwidth resources, the RA schemes in OFDMA systems outperform those in TDMA systems in terms of both data rate and user fairness. Also, the low-complexity RA scheme is able to achieve near-optimal performance at a reduction of 90% in computational complexity. Finally, the system model for RF networks is introduced. In this study, the 2.4 GHz spectrum band is considered for RF transmission, which is typically appropriate to cover typical in-building areas. In addition, in order to reduce the complexity, the OFDM-TDMA method instead of OFDMA is taken into account in RF systems.

Chapter 3
Dynamic Load Balancing with Handover for HLRNs

3.1 Introduction

The increasing number of multi-media mobile devices and the extensive use of data-demanding mobile applications means that current mobile networks are at their maximum capacity due to the limited availability of the radio frequency (RF) spectrum. The light fidelity (LiFi) technology, which uses 300 THz of licence-free and unused optical spectrum for high-speed wireless communications, has recently been regarded as a solution to this problem [11]. One advantage of LiFi is that it does not cause interference to existing RF communication systems, because it uses an entirely different part of the electromagnetic spectrum [23]. This enables the creation of hybrid networks that combine LiFi with RF systems.

In an indoor situation, a hybrid integration of RF and LiFi is expected to improve both the system throughput and the user's quality of service (QoS) [21]. Since LiFi does not affect the RF coverage and throughput, the total system throughput of a LiFi/RF hybrid network is always greater than that of separate RF or LiFi networks [23]. On the one hand, according to the IEEE 802.11 ad standard, the latest wireless fidelity (WiFi) protocol provided by Wireless Gigabit Alliance (WiGig) enables devices to operate in three centre frequencies (2.4, 5 and 60 GHz), and WiGig can achieve a total data rate up to 6.7 Gb/s [63]. On the other hand, recent research shows that the achievable data rate of a single light emitting diode (LED) can be more than 7.3 Gb/s [14]. A large number of LiFi access points (APs) can be deployed in an indoor scenario and thus a high area spectral efficiency can be achieved with a LiFi network [64], and the total throughput of a LiFi/RF hybrid system can be considerable. Also, a hybrid network can improve the user QoS by ensuring a high throughput at all locations. In general, the RF network can achieve ubiquitous coverage which provides the basic data rate requirement and LiFi can significantly augment the maximum capacity.

In a hybrid LiFi/RF network, fair and efficient load balancing (LB) can be a challenge due to the small size of LiFi attocells. Most of the recent research focuses on the resource allocation (RA)

problem in static systems where users are assumed to be fixed [23, 24]. However, in practical scenarios, some users will be moving. In an indoor scenario, the coverage of a RF AP is beyond a single room whereas each LiFi cell in a LiFi network covers only a few square meters due to the rectilinear propagation of light. However, there are many light sources in a room for illumination purposes and LiFi harnesses significant gains by reusing transmission resources. As a consequence, when assuming user movement, users may experience many handovers between LiFi attocells. During a handover, the signalling information exchange between users and a central unit (CU) is required, resulting from the handover overhead. This overhead must be considered in the design of LB schemes for such hybrid networks.

In this chapter, dynamic load balancing that contains AP assignment, resource allocation and handover is studied. Specifically, optimisation-based dynamic LB schemes and the fuzzy logic (FL) based dynamic LB scheme are proposed. In Section 3.2, a special case for optimisation based LB schemes with proportional fairness is analysed, and the handover boundary and the relationship between LiFi throughput and RF throughput are discussed. In Section 3.3, the optimisation based LB scheme with different user fairness scheduler is proposed. In Section 3.4, the FL based dynamic LB scheme is proposed, where AP assignment, RA and handover are jointly designed. Section 3.5 gives the summary.

3.2 A Special Case: Optimisation based dynamic LB Scheme with Proportional Fairness

Referring to Section 2.1-2.2, a LiFi/RF hybrid downlink is considered. This hybrid network covers an indoor area by N_l LiFi APs and a single RF AP. Each LiFi AP is a large LED lamp which contains many low power LEDs, and each user has a photo detector (PD). It is assumed that all of the PDs are oriented perpendicular to the floor. This means that the angle of irradiation is equal to the angle of incidence. The field of view (FoV) of the LEDs and PDs can be designed so that the transmission can be contained within a certain space. In this hybrid network, the network load balancing should be undertaken in regular quasi-static states. The interval time between two neighbouring states is denoted by T_p. In each state, the load balancing configuration is assumed to be fixed and users receive constant data rates. The natural number t denotes the sequence number of the states. The set of LiFi and RF APs is denoted by $\mathcal{C}_\mathcal{L} = \{\alpha | \ \alpha \in [0, N_l], \alpha \in \mathbb{Z}\}$, where $\alpha = 0$ represents the RF AP and $\alpha \in [1, N_l]$

denotes the LiFi APs. The set of users is denoted by $\mathcal{U}$. A full buffer traffic model is considered so that the maximum achievable data rate can be evaluated for each user at all times.

In this section, the dynamic load balancing algorithm is given and the throughput analysis is carried out. In order to reduce the complexity of theoretical analysis, we only consider the LoS path loss in the LiFi channel model, the multi-path effect and the front-end filtering effect are not taken into account. Therefore, the LiFi channel response in the frequency domain is considered to be flat. The channel model in the LiFi system can be seen in Section 2.3. When considering DCO-OFDM transmission, the LiFi signal-to-interference-plus-noise ratio (SINR) between user μ and AP α can be written as:

$$\mathrm{SINR}_{\mu,\alpha} = \frac{(\kappa \varepsilon_p P_{\mathrm{opt}} H_{\mu,\alpha})^2}{\iota^2 N_{\mathrm{L}} B_{\mathrm{L}} + \sum (\kappa \varepsilon_p P_{\mathrm{opt}} H_{\mu,\mathrm{else}})^2}, \tag{3.1}$$

where κ is the optical to electric conversion efficiency at the receivers; $\varepsilon_p \approx 1$ is power amplification gain; $H_{\mu,\alpha}$ is the channel gain between user μ and AP α, according to Eq. (2.3); and $H_{\mu,\mathrm{else}}$ is the channel gain between user μ and the interfering LiFi AP; N_{L} is the single side-band noise spectrum; and B_{L} is the baseband bandwidth. Since approximately half of the bandwidth can be used for data transmission in DCO-OFDM system, the achievable data rate is expressed as:

$$R_{\mu,\alpha} = B_{\mathrm{L}} \log_2(1 + \mathrm{SINR}_{\mu,\alpha}). \tag{3.2}$$

The WiFi protocol is considered for RF transmission. During the last ten years, the WiFi physical layer protocol has been enhanced, including IEEE 802.11 a/g, 802.11 n and 802.11 ac. According to [16], the current IEEE 802.11 protocol can guarantee a constant maximum throughput for users which are located within 12 m from the transmitter, which is shown in Table. 3.1. In general, the small scale fading in the RF wireless communication systems results in a fluctuation of the data rates. In order to simplify the analysis complexity, the small scale fading of RF channels is not considered in this study. This assumption is also used in [23] which considers the LB problem in hybrid LiFi/WiFi networks. Therefore here, the distance between users and the RF AP is set to be within 12 m, and the WiFi throughput is assumed to be constant and equal to the maximum throughput shown in Table. 3.1, which is denoted by R_0.

Protocol Name	Carrier Frequency (GHz)	Bandwidth (MHz)	Spatial Stream	Throughput
802.11 n	2.4	20	1	120 Mb/s
802.11 n	5	40	1	600 Mb/s
802.11 ac	5	80	4	1 Gb/s
802.11 ac	5	160	4	2.4 Gb/s
802.11 ac	5	160	8	6.7 Gb/s

Table 3.1: *WiFi throughput for hybrid LiFi/WiFi networks*

3.2.1 Handover scheme

Due to the small coverage area of LiFi attocells, the movement of users can prompt handover. When the serving AP of a user is switched in two neighbouring states, a handover occurs. In general, the handover overhead in an indoor scenario is in the order of milliseconds, which is assumed to be lower than the state interval T_p. According to [26], the overhead time can be modelled as a Poisson random process [65], and the probability mass function (PMF) of the overhead is given by:

$$\Pr(t_{ij} = x) = \frac{\zeta_{ij}^x e^{-\zeta_{ij}}}{x!}, \quad x = 0, 1, 2...(\text{ms}) \tag{3.3}$$

where $\zeta_{ij} = \mathbb{E}[t_{ij}]$ is the mean of the handover overhead from AP i to AP j. The overhead incurs a certain decrease in the average data rate of users that experience handover. In this study, the handover efficiency between two adjacent states is defined as:

$$\eta_{ij} = \begin{cases} \left[1 - \dfrac{t_{ij}}{T_p}\right]^+, & i \neq j \\ 1, & i = j \end{cases}, \qquad i, j \in \mathcal{C}_{\mathcal{L}}, \tag{3.4}$$

where t_{ij} is the overhead of AP switch from AP i to AP j; and $[.]^+$ is the maximum operator, $\max(\,.\,, 0)$. In order to implement the proposed load balancing schemes, the handover overhead between any two APs should be estimated in each state. The Kalman filtering approach can be applied for the overhead estimation [76]. Since it is outside the scope of this study, the overhead estimation is omitted here and will be the subject of future research.

Assuming that the natural number n denotes the sequence number of the states, the link data

---

Algorithm 3 Dynamic algorithm executed by the central unit.

1: Initialisation: α'_μ $n \leftarrow 1$;
2: **while** $n \leq N_s$ **do**
3:     **for all** each $\mu \in \mathcal{U}$ **do**
4:         find $\alpha' = \arg_{\alpha \in \mathcal{C}_\mathcal{L}} g_{\mu,\alpha}^{(n-1)} = 1$;
5:         **for all** each $\alpha \in \mathcal{C}_\mathcal{L}$ **do**
6:             Calculate the handover efficiency $\eta_{\alpha'\alpha}$;
7:             Calculate $r_{\mu,\alpha}^{(n)}$ between μ and α;
8:         **end for**
9:     **end for**
10:    Calculate $g_{\mu,\alpha}^{(n)}$ and $k_{\mu,\alpha}^{(n)}$ based on $r_{\mu,\alpha}^{(n)}$ by using load balancing algorithm;
11:    $n \leftarrow n + 1$;
12: **end while**

---

rate between AP α and user μ in state n with handover efficiency can be expressed as:

$$
r_{\mu,\alpha}^{(n)} = \begin{cases} \eta_{\alpha'\alpha} R_0, & \alpha = 0 \\ \eta_{\alpha'\alpha} R_{\mu,\alpha}^{(n)}, & \alpha = 1, 2...N_l \end{cases} , \tag{3.5}
$$

where $R_{\mu,\alpha}^{(n)}$ is the LiFi data rate $R_{\mu,\alpha}$ in state n, according to Eq. (3.2); α' is the AP allocated to user μ in the state $n-1$; $\eta_{\alpha'\alpha}$ is the handover efficiency from AP α' to AP α, according to Eq. (3.4); and R_0 is the WiFi throughput.

In each state, the system load balancing, which consists of the AP assignment and communication resource allocation, is undertaken by the CU. Two variables, $g_{\mu,\alpha}^{(n)}$ and $k_{\mu,\alpha}^{(n)}$, are used to represent the load balancing results in these two aspects respectively. Variable $g_{\mu,\alpha}^{(n)}$ is a binary number which equals 1 when user μ is served by AP α, and equals 0 when α is not the serving AP of this user. Variable $k_{\mu,\alpha}^{(n)}$ is the proportion of the resource that user μ is able to use for communication. The time division multiple access (TDMA) method is applied in each cell, and $k_{\mu,\alpha}^{(n)}$ is considered as the proportion of time resource block allocated to μ. Thus, $k_{\mu,\alpha}^{(n)}$ is a fractional number between 0 and 1 with $\sum_\mu k_{\mu,\alpha}^{(n)} = 1$ for each AP α. The number of states considered in this study is denoted by N_s. The dynamic algorithm executed by the CU is summarised in Algorithm 3. The load balancing algorithm used in each state is given in the next section.

3.2.2 Load Balancing Algorithm in One State

In this section, the load balancing algorithm used in each state is shown, and the superscript (n) is omitted for simplicity. According to Eq. (2.16), a logarithmic utility function with $\beta = 1$ is used, which achieves proportional fairness [24]. By using the logarithmic utility function, the load balancing problem can be formulated as a utility maximisation problem, which can be expressed as:

$$\max_{g_{\mu,\alpha},k_{\mu,\alpha}} \quad \sum_{\mu \in \mathcal{U}} \sum_{\alpha=0}^{N_l} g_{\mu,\alpha} \log(k_{\mu,\alpha} r_{\mu,\alpha}) \tag{3.6}$$

$$\text{s.t.} \quad \sum_{\alpha=0}^{N_l} g_{\mu,\alpha} = 1 \qquad \forall \mu \in \mathcal{U};$$

$$\sum_{\mu \in \mathcal{C}_\mathcal{L}} g_{\mu,\alpha} k_{\mu,\alpha} \leq 1 \qquad \forall \alpha \in \mathcal{C}_\mathcal{L};$$

$$g_{\mu,\alpha} \in \{0,1\}, \quad k_{\mu,\alpha} \in [0,1], \quad \forall \mu \in \mathcal{U}, \forall \alpha \in \mathcal{C}_\mathcal{L};$$

where $r_{\mu,\alpha}$ is the communication link data rate given in Eq. (3.5), which is a positive number. The optimum $k_{\mu,\alpha}$ is shown to be greater than zero in Eq. (3.8) so that $\log(0)$ is avoided.

This is a problem of mixed integer and non-linear programming. A decomposition-based approach can be used to solve the problem by decomposing the original problem into solvable sub-problems according to [66]. Initially, the variable $k_{\mu,\alpha}$ is optimised. With a given $g_{\mu,\alpha}$, the objective function for AP α in Eq. (3.6) can be expressed as:

$$F(k_{\mu,\alpha}) = \sum_{\mu \in \mathcal{U}_\alpha} \log(k_{\mu,\alpha} r_{\mu,\alpha})$$

$$\propto \frac{1}{M_\alpha} \sum_{\mu \in \mathcal{U}_\alpha} \log(k_{\mu,\alpha}) = \log \left[\left(\prod_{\mu \in \mathcal{U}_\alpha} k_{\mu,\alpha} \right)^{\frac{1}{M_\alpha}} \right]$$

$$\leq \log \left(\frac{k_{1,\alpha} + k_{2,\alpha} + ... + k_{M_\alpha,\alpha}}{M_\alpha} \right), \tag{3.7}$$

where $\mathcal{U}_\alpha$ is the set of the users allocated to the AP α; and M_α represents its cardinality. According to the rule of inequality, the maximum in Eq. (3.7) is achieved only when:

$$k_{\mu,\alpha} = \frac{1}{M_\alpha}, \quad \forall \mu \in \mathcal{U}_\alpha. \tag{3.8}$$

According to Eq. (3.8), all of the users allocated to a specific AP share an equal proportion of the time resource. By replacing $k_{\mu,\alpha}$ with M_α, the problem in Eq. (3.6) can be re-written as:

$$\max_{g_{\mu,\alpha}, M_\alpha} \quad \sum_{\mu \in \mathcal{U}} \sum_{\alpha=0}^{N_l} g_{\mu,\alpha} \log \left(\frac{r_{\mu,\alpha}}{M_\alpha} \right) \tag{3.9}$$

$$\text{s.t.} \quad \sum_{\alpha=0}^{N_l} g_{\mu,\alpha} = 1 \qquad \forall \mu \in \mathcal{U}; \tag{3.10}$$

$$\sum_{\mu \in \mathcal{U}} g_{\mu,\alpha} = M_\alpha \qquad \forall \alpha \in \mathcal{C}_\mathcal{L}; \tag{3.11}$$

$$g_{\mu,\alpha} \in \{0,1\}, \quad \forall \mu \in \mathcal{U}, \forall \alpha \in \mathcal{C}_\mathcal{L};$$

The Lagrangian multiplier method is used to solve this problem. The two Lagrangian multipliers ϱ_μ and ω_α correspond to the constraints of Eq. (3.10) and Eq. (3.11), respectively. Therefore the Lagrangian function can be expressed as:

$$L = \sum_{\mu \in \mathcal{U}} \sum_{\alpha=0}^{N_l} g_{\mu,\alpha} \log \left(\frac{r_{\mu,\alpha}}{M_\alpha} \right) + \sum_{\mu \in \mathcal{U}} \varrho_\mu \left(1 - \sum_{\alpha=0}^{N_l} g_{\mu,\alpha} \right)$$
$$+ \sum_{\alpha=0}^{N_l} \omega_\alpha \left(M_\alpha - \sum_{\mu \in \mathcal{U}} g_{\mu,\alpha} \right). \tag{3.12}$$

Due to $\sum_{\mu \in \mathcal{U}} g_{\mu,\alpha} = M_\alpha$, the Lagrangian function can be re-written as:

$$L = L_1(g_{\mu,\alpha}, \ \varrho_\mu, \omega_\alpha) + L_2(M_\alpha, \varrho_\mu, \omega_\alpha), \tag{3.13}$$

where

$$L_1 = \sum_{\mu \in \mathcal{U}} \sum_{\alpha=0}^{N_l} g_{\mu,\alpha} (\log r_{\mu,\alpha} - \varrho_\mu - \omega_\alpha), \tag{3.14}$$

$$L_2 = \sum_{\alpha=0}^{N_l} M_\alpha (\omega_\alpha - \log M_\alpha) + \sum_{\mu \in \mathcal{U}} \varrho_\mu. \tag{3.15}$$

In this case, the problem of Eq. (3.9) can be decomposed into two sub-problems which are to maximise L_1 and L_2 using the proper Lagrangian multipliers.

Firstly, ϱ_μ and ω_α are assumed to be fixed; L_1 can be maximised when the following expression

is achieved:

$$g_{\mu,\alpha}^* = \begin{cases} 1, \alpha = \arg\max_{\alpha \in \mathcal{C}_{\mathcal{L}}} (\log r_{\mu,\alpha} - \varrho_\mu - \omega_\alpha) \\ 0, \qquad\qquad \text{otherwise} \end{cases} . \qquad (3.16)$$

Based on Eq. (3.11) and Eq. (3.16), the number of users allocated to AP α can be obtained, which can be written as:

$$M_{\alpha,1} = \sum_{\mu \in \mathcal{U}} g_{\mu,\alpha}^* \qquad (3.17)$$

In addition, given the Lagrangian multipliers, the maximum L_2 is obtained when the following expression is achieved:

$$\frac{\partial L_2}{\partial M_\alpha} = 0 \implies M_\alpha^* = \exp(\omega_\alpha - 1). \qquad (3.18)$$

Then, a variable $\dot{\delta}$ is introduced to represent the difference between $M_{\alpha,1}$ and M_α^*, which can be expressed as:

$$\dot{\delta} = \sum_{\alpha \in \mathcal{C}_{\mathcal{L}}} |M_{\alpha,1} - M_\alpha^*|. \qquad (3.19)$$

The optimisation problem to maximise the Lagrangian function in Eq. (3.12) is solved iteratively by using the gradient projection method [67], where ϱ_μ and ω_α are updated in the opposite direction to the gradient $\nabla L(\varrho_\mu)$ and $\nabla L(\omega_\alpha)$. The i-th iteration of the gradient projection algorithm can be expressed as:

$$\varrho_\mu(i+1) = \varrho_\mu(i) - \epsilon_1(1 - \sum_{\alpha \in \mathcal{C}_{\mathcal{L}}} g_{\mu,\alpha}^*); \qquad (3.20)$$

$$\omega_\alpha(i+1) = \omega_\alpha(i) - \epsilon_2(M_\alpha^* - \sum_{\mu \in \mathcal{U}} g_{\mu,\alpha}^*), \qquad (3.21)$$

where ϵ_1 and ϵ_2 are the sufficiently small step sizes required for guaranteeing convergence. According to Eq. (3.16), $\sum_{\alpha \in \mathcal{C}_{\mathcal{L}}} g_{\mu,\alpha}^* = 1$ is always satisfied in each iteration, and the expression in Eq. (3.20) is re-written as $\varrho_\mu(i+1) = \varrho_\mu(i)$. Therefore, the Lagrangian multiplier ϱ_μ can be set to 0, and only ω_α should be updated in the iteration. An appropriate threshold $\dot{\delta}_T$ is defined and the variables converge to the optimum when $\dot{\delta} \leq \dot{\delta}_T$ is achieved. The threshold $\dot{\delta}_T$ should be small enough but it does not necessarily have to be a particular value. A smaller value of $\dot{\delta}_T$ will make the convergence slower. The iterative algorithm is shown in Algorithm 4.

Algorithm 4 : Load balancing algorithm in each state.

1: Initialisation: $\varrho_\mu(i) = \omega_\alpha(i) = 0$, $i \leftarrow 1$ and $\dot{\delta} \leftarrow +\infty$;
2: **while** $\dot{\delta} \geq \dot{\delta}_T$ **do**
3:    **for all** each $\mu \in \mathcal{U}$ **do**
4:       $\alpha^* = \arg\max_{\alpha \in \mathcal{C_L}} (\log b_{\mu,\alpha} - \varrho_\mu(i) - \omega_\alpha(i))$;
5:       $g^*_{\mu,\alpha} = \begin{cases} 1, & \alpha = \alpha^* \\ 0, & \text{otherwise} \end{cases}$;
6:    **end for**
7:    Calculate $M_{\alpha,1} = \sum_{\mu \in \mathcal{U}} g^*_{\mu,\alpha}$, $\forall \alpha \in \mathcal{C_L}$;
8:    **for all** each $\alpha \in \mathcal{C_L}$ **do**
9:       $M^*_\alpha = \exp(\omega_\alpha(i) - 1)$;
10:      $\omega_\alpha(i+1) = \omega_\alpha(i) - \epsilon_2(M^*_\alpha - \sum_{\mu \in \mathcal{U}} g^*_{\mu,\alpha})$;
11:    **end for**
12:    Calculate $\dot{\delta} = \sum_{\alpha \in \mathcal{C_L}} |M_{\alpha,1} - M^*_\alpha|$;
13:    $i \leftarrow i + 1$;
14: **end while**
15: Calculate $g_{\mu,\alpha} = g^*_{\mu,\alpha}$ and $k_{\mu,\alpha} = 1/M^*_\alpha$;

3.2.3   Analysis of AP Service Area and System Throughput

In order to gain an understanding of the load balancing in a hybrid network, it is important to study the service area of each AP. In this section, the AP service area is identified with a given WiFi throughput, and the throughput of each LiFi attocell is analysed. Firstly, a special case without optical CCI is considered, which is termed as the 'Non-CCI' case. Following that, a generic case with CCI is considered, which is termed as the 'Optical CCI' case.

3.2.3.1   Non-CCI case

In the non-CCI case, users served by LiFi APs do not receive any optical signals from other LiFi APs. It is assumed that each LiFi AP covers the same size of attocell. In order to eliminate the optical interference, the distance between any two LiFi APs should be greater than the diameter of LiFi attocells.

It is assumed that receivers in HLRNs point upwards. Therefore the angle of irradiation is equal to the angle of incidence for each user and the following expression can be achieved:

$$\cos(\phi) = \cos(\theta) = \frac{h}{\sqrt{z^2_{\mu,\alpha} + h^2_w}}, \tag{3.22}$$

41

where $z_{\mu,\alpha}$ is the horizontal distance between LiFi AP α and user μ; h_w is the height of the room; ϕ is the angle of irradiation; and θ is the angle of incidence. The channel model in (2.3) can be expressed as a function with $z_{\mu,\alpha}$, and the data rate between LiFi AP α and user μ can be written as:

$$\rho_\alpha(z_{\mu,\alpha}) = B \log_2(1 + \text{SNR}(z_{\mu,\alpha})) \geq 0, \tag{3.23}$$

where

$$\text{SNR}(z_{\mu,\alpha}) = \frac{[(\dot{m} + 1)\kappa P_{\text{opt}} A_p g(\theta) T_s(\theta) h_w^{\dot{m}+1}]^2}{4\pi^2 \iota^2 N_{\text{L}} B_{\text{L}}} (z_{\mu,\alpha}^2 + h_w^2)^{-\dot{m}-3}. \tag{3.24}$$

It can be seen that $\rho_\alpha(z_{\mu,\alpha})$ is a monotonic decreasing function with respect to $z_{\mu,\alpha}$.

Lemma 1. *It is assumed that users are optimally allocated to APs by using the proposed load balancing scheme in Algorithm 4. For any LiFi AP α, it can be obtained that:*

$$z_{i,\alpha} \leq z_{j,\alpha}, \quad \forall i \in \mathcal{U}_\alpha, j \notin \mathcal{U}_\alpha, \tag{3.25}$$

where $\mathcal{U}_\alpha$ is the set of users allocated to LiFi AP α.

Proof. Firstly, when user j is served by a different LiFi AP from AP α, this user should reside in the corresponding LiFi attocell. Since the LiFi attocells are not overlapping, the inequality $z_{i,\alpha} \leq z_{j,\alpha}$ is satisfied.

When user j is served by the WiFi AP, the method of proof by contradiction is applied to prove this lemma. It is assumed that the optimal load balancing is achieved by using the proposed scheme, and the inequality below is achieved:

$$z_{i,\alpha} > z_{j,\alpha}, \quad \forall i \in \mathcal{U}_\alpha, j \notin \mathcal{U}_\alpha, \tag{3.26}$$

where user i is served by LiFi AP α and user j is served by the WiFi AP. The objective function in Eq. (3.9) can be written as:

$$F_1 = \log\left(\frac{\rho_\alpha(z_{i,\alpha})}{M_\alpha}\right) + \log\left(\frac{R_0}{M_0}\right) + \sum_{\mu \in U - \{i,j\}} \sum_{y=0}^{N_l} g_{\mu,y} \log\left(\frac{\rho_y(z_{\mu,y})}{M_y}\right), \tag{3.27}$$

where M_α and M_0 are the number of users served by LiFi AP α and the WiFi AP, respectively. Now, the APs allocated to user i and j are exchanged. The values of M_α and M_0 stay the same,

and the objective function can be re-written as:

$$F_2 = \log\left(\frac{R_0}{M_0}\right) + \log\left(\frac{\rho_\alpha(z_{j,\alpha})}{M_\alpha}\right) + \sum_{\mu \in U-\{i,j\}} \sum_{y=0}^{N_l} g_{\mu,y} \log\left(\frac{\rho_y(z_{\mu,y})}{M_y}\right). \quad (3.28)$$

Due to the monotonic decrease of $\rho_\alpha(z_{\mu,\alpha})$, it can be obtained that:

$$\rho_\alpha(z_{i,\alpha}) < \rho_\alpha(z_{j,\alpha}). \quad (3.29)$$

As a consequence, $F_2 > F_1$ is achieved. This means that the AP allocation for user i and j is not optimal, leading to a contradiction. The assumption in Eq. (3.26) must be false and the lemma is proved. □

Lemma 1 indicates that users served by LiFi AP α are closer to this AP than the users served by other APs. The service area of a LiFi AP in the non-CCI case is a circular region, and handover only occurs when users go through the boundary of the circular regions. In this study, the boundary is termed as the 'handover circle', and the centre of the handover circle is the location of a LiFi AP. Users that are outside all of the handover circles are served by the WiFi AP.

The radius of the handover circles is analysed as follows. It is assumed that users are uniformly distributed in the entire scenario. The area of the scenario is denoted by Y; the density of users is denoted by ε; the radius of the attocell covered by LiFi AP α is denoted by Z_α; the radius of the handover circle of LiFi AP α is denoted by ν_α; and the average handover efficiency is denoted by $\bar{\eta}$, where $\bar{\eta} = \mathbb{E}[\eta_{ij}]$ and η_{ij} is given in Eq. (3.4). The number of users served by each AP can be written as:

$$M_\alpha(\nu_\alpha) = \begin{cases} \varepsilon Y - \sum_{\alpha=1}^{\alpha=N_l} \varepsilon \pi \nu_\alpha^2, & \alpha = 0 \\ \sum_{\alpha=1}^{\alpha=N_l} \varepsilon \pi \nu_h^2, & \alpha = 1, 2...N_l \end{cases}, \quad (3.30)$$

where

$$Y > \sum_{\alpha=1}^{\alpha=N_l} \pi \nu_\alpha^2, \ 0 < \nu_\alpha \leq Z_\alpha, \quad (3.31)$$

because all of the LiFi attocells are inside the considered scenario. According to the proposed load balancing scheme, the radius of handover circles can be calculated by solving the optimi-

sation problem in Eq. (3.9), which can be written as:

$$\max_{\nu_\alpha} \quad G_1(\nu_\alpha) + G_2(\nu_\alpha) \tag{3.32}$$

$$s.t. \quad 0 < \nu_\alpha \leq Z_\alpha \tag{3.33}$$

where

$$G_1(\nu_\alpha) = \left(\varepsilon Y - \sum_{\alpha=1}^{\alpha=N_l} \varepsilon \pi \nu_\alpha^2 \right) \log \left(\frac{\bar{\eta} R_0}{\varepsilon Y - \sum_{\alpha=1}^{\alpha=N_l} \varepsilon \pi \nu_\alpha^2} \right), \tag{3.34}$$

$$G_2(\nu_\alpha) = 2\pi\varepsilon \sum_{\alpha=1}^{\alpha=N_l} \int_0^{\nu_\alpha} \log \left(\frac{\bar{\eta} \rho_\alpha(x)}{\varepsilon \pi \nu_\alpha^2} \right) x \, dx. \tag{3.35}$$

Specifically, $G_1(\nu_\alpha)$ represents the WiFi part ($\alpha = 0$) in the objective function shown in Eq. (3.6) and $G_2(\nu_\alpha)$ represents the LiFi part ($\alpha = 1, 2, ..., N_l$).

The first order derivatives of $G_1(\nu_\alpha)$ and $G_2(\nu_\alpha)$ can be expressed as:

$$\frac{\partial G_1}{\partial \nu_\alpha} = -2\pi\varepsilon\nu_\alpha \left[\log \left(\frac{\bar{\eta} R_0}{\varepsilon Y - \sum_{\alpha=1}^{\alpha=N_l} \varepsilon \pi \nu_\alpha^2} \right) - 1 \right], \tag{3.36}$$

$$\frac{\partial G_2}{\partial \nu_\alpha} = 2\pi\varepsilon\nu_\alpha \left[\log \left(\frac{\bar{\eta} \rho_\alpha(\nu_\alpha)}{\varepsilon \pi \nu_\alpha^2} \right) - 1 \right]. \tag{3.37}$$

The derivative of the objective function in Eq. (3.32) can therefore be expressed as:

$$\frac{\partial(G_1 + G_2)}{\partial \nu_\alpha} = 2\pi\varepsilon\nu_\alpha \log \left(\frac{\rho_\alpha(\nu_\alpha)(Y - \sum_{\alpha=1}^{\alpha=N_l} \pi \nu_\alpha^2)}{\pi \nu_\alpha^2 R_0} \right). \tag{3.38}$$

Due to $\nu_\alpha > 0$, $\frac{\partial(G_1 + G_2)}{\partial \nu_\alpha}$ can be equal to 0 only when

$$\hat{\nu}_\alpha = F^{-1}(1) > 0, \tag{3.39}$$

where F^{-1} is the inverse function of $F(\nu_\alpha)$, which is

$$F(\nu_\alpha) = \frac{\rho_\alpha(\nu_\alpha)(Y - \sum_{\alpha=1}^{\alpha=N_l} \pi \nu_\alpha^2)}{\pi \nu_\alpha^2 R_0}, \tag{3.40}$$

where $F(\nu_\alpha) > 0$ with $0 < \nu_\alpha \leq Z_\alpha$ due to the conditions in Eq. (3.23) and Eq. (3.31). It can be seen that the function $F(\nu_\alpha)$ is monotonically decreasing with respect to ν_α.

When $0 < \hat{\nu}_\alpha \leq Z_\alpha$ is satisfied, it can be obtained that:

$$\frac{\partial^2(G_1 + G_2)}{\partial \nu_\alpha^2}\bigg|_{\nu_\alpha=\hat{\nu}_\alpha}$$
$$= 2\pi\varepsilon\left[\log(F(\hat{\nu}_\alpha)) + \frac{\hat{\nu}_\alpha}{F(\hat{\nu}_\alpha)}\left.\frac{\partial F(\nu_\alpha)}{\partial \nu_\alpha}\right|_{\nu_\alpha=\hat{\nu}_\alpha}\right] < 0, \tag{3.41}$$

where $\frac{\partial F(\nu_\alpha)}{\partial \nu_\alpha} < 0$ due to monotonic decrease property. As a consequence, $\hat{\nu}_\alpha$ is the optimum for the problem in Eq. (3.32). When $\hat{\nu}_\alpha > Z_\alpha$, since $F(\nu_\alpha)$ is monotonically decreasing, the optimum ν_α equals to Z_α. The radius of handover circles can be expressed as:

$$\nu_\alpha^* = \begin{cases} Z_\alpha, & \hat{\nu}_\alpha > Z_\alpha \\ \hat{\nu}_\alpha, & \hat{\nu}_\alpha \leq Z_\alpha \end{cases}. \tag{3.42}$$

The sum throughput achieved by AP α can be written as:

$$R_{\text{sum},\alpha} = \begin{cases} R_0, & \alpha = 0; \\ \frac{2}{(\nu_\alpha^*)^2}\int_0^{\nu_\alpha^*}\rho_\alpha(x)x\,\mathrm{d}x, & \alpha = 1, 2...N_l \end{cases}. \tag{3.43}$$

According to Eq. (3.23) and Eq. (3.40), the LiFi APs with the same transmit power and modulation bandwidth have the same radius of the handover circles and throughput.

Since all of the users served by an AP share the equal time resource, the resource proportion can be expressed as:

$$k_{\mu,\alpha} = \begin{cases} \frac{1}{\varepsilon(Y-\sum_{\alpha=1}^{\alpha=N_l}\pi(\nu_\alpha^*)^2)}, & \alpha = 0; \\ \frac{1}{\varepsilon\pi(\nu_\alpha^*)^2}, & \alpha = 1, 2...N_l \end{cases}. \tag{3.44}$$

According to Eq. (3.40) and Eq. (3.42), it can be obtained that:

$$F(\nu_\alpha^*) \geq 1 \tag{3.45}$$

$$\Longleftrightarrow \quad \frac{\rho_\alpha(\nu_\alpha^*)}{\varepsilon\pi(\nu_\alpha^*)^2} \geq \frac{R_0}{\varepsilon(Y - \sum_{\alpha=1}^{\alpha=N_l}\pi(\nu_\alpha^*)^2)} \tag{3.46}$$

$$\Longleftrightarrow \quad \frac{\rho_\alpha(\nu_\alpha^*)}{k_{\mu,\alpha}} \geq \frac{R_0}{k_{\mu,0}}, \quad \alpha = 1, 2...N_l \tag{3.47}$$

where the equality in Eq. (3.47) is achieved when $\hat{\nu}_\alpha \leq Z_\alpha$. This inequality indicates that the users served by LiFi APs achieve data rates higher than or equal to those served by the WiFi

AP.

In addition, since $\rho_\alpha(\nu_\alpha)$ is monotonically decreasing, the LiFi throughput increases with a reduction of the radius of handover circles. According to Eq. (3.40), an increase of WiFi throughput results in a decrease of ν_α^*, thus leading to an improvement of LiFi throughput. This means that the WiFi throughput has a significant effect on the LiFi throughput in the hybrid network even though they work on different ranges of the electromagnetic spectrum.

3.2.3.2   Optical CCI case

In this case, the LiFi attocells overlap with each other, and the optical CCI is considered. When LiFi APs are positioned very closely, the achievable spectral efficiency in the LiFi systems would be significantly affected by the CCI. In order to avoid a high level of CCI, the distance between LiFi APs is set to be greater than the radius of an attocell. In the case that the distance is less than or equal to the radius, the technology fractional frequency reuse (FFR) [68] and spatial division multiple access (SDMA) [69] can be used to mitigate the strong interference, which is outside the scope of this study and is not discussed here.

It can be seen from Lemma 1 that users served by LiFi APs must reside in the handover circles. Thus, when a handover circle does not overlap with other attocells, users allocated to the corresponding LiFi AP do not experience optical CCI, as shown in Fig. 3.1(a). In this case, the condition Eq. (3.25) in Lemma 1 is satisfied in this LiFi attocell. However, when a handover circle overlaps with other LiFi attocells, shown in Fig. 3.1(b), some of the users served by this LiFi AP would be affected by optical CCI.

In the case of optical CCI, the communication link data rate between LiFi AP α and user μ can be expressed as:

$$\rho_\alpha(\text{SINR}_{\mu,\alpha}) = B_\text{L} \log_2(1 + \text{SINR}(z_{\mu,\alpha})), \tag{3.48}$$

where $\text{SINR}_{\mu,\alpha}$ is given in Eq. (3.55). In general, when a user experiences interference from more than one LiFi AP, the achievable SINR performance would be less than 0 dB, as shown in [70]. In this case, the LiFi link data rate is much lower than that of WiFi. Accordingly, users in such multi-overlap areas are assumed to have no LiFi access, and this section mainly focuses on the load balancing analysis for the overlap areas of two LiFi attocells.

Lemma 2. *For each LiFi AP α,*

$$SINR_{i,\alpha} \geq SINR_{j,\alpha}, \quad \forall i \in \mathcal{U}_\alpha, j \notin \mathcal{U}_\alpha, \tag{3.49}$$

where $\mathcal{U}_\alpha$ is the set of users allocated to LiFi AP α.

Proof. Initially, if j is allocated to the WiFi AP, this lemma is proved by using the method shown in the proof of Lemma 1.

Then, the case that user j is served by another LiFi AP α' is considered, and the method of proof by contradiction is applied to prove this lemma. It is assumed that:

$$\text{SINR}_{i,\alpha} < \text{SINR}_{j,\alpha}, \quad \forall i \in \mathcal{U}_\alpha, j \in \mathcal{U}_{\alpha'}, \tag{3.50}$$

where $\mathcal{U}_{\alpha'}$ is the set of the users allocated to LiFi AP α'. According to the assumption in Eq. (3.50), the expression $\text{SINR}_{j,\alpha'} < \text{SINR}_{i,\alpha'}$ is achieved. Particularly, if user i or j is outside the overlap area and cannot be served by one of the APs between α and α', the corresponding SINR is 0.

The objective function in Eq. (3.9) can be written as:

$$F_3 = \log\left(\frac{\rho_\alpha(\text{SINR}_{i,\alpha})}{M_\alpha}\right) + \log\left(\frac{\rho_\alpha(\text{SINR}_{j,\alpha'})}{M_{\alpha'}}\right)$$
$$+ \sum_{\mu \in \mathcal{U}-\{i,j\}} \sum_{y=0}^{N_l} g_{\mu,y} \log\left(\frac{\rho_y(\text{SINR}_{\mu,y})}{M_y}\right), \tag{3.51}$$

where M_α and $M_{\alpha'}$ represent the number of users served by LiFi AP α and α', respectively.

Now, the allocated APs of user i and j are exchanged. The values of M_α and $M_{\alpha'}$ stay the same. In this way, the objective function can be written as:

$$F_4 = \log\left(\frac{\rho_\alpha(\text{SINR}_{j,\alpha})}{M_\alpha}\right) + \log\left(\frac{\rho_\alpha(\text{SINR}_{i,\alpha'})}{M_{\alpha'}}\right)$$
$$+ \sum_{\mu \in \mathcal{U}-\{i,j\}} \sum_{y=0}^{N_l} g_{\mu,y} \log\left(\frac{\rho_y(\text{SINR}_{\mu,y})}{M_y}\right). \tag{3.52}$$

According to Eq. (3.50), it can be derived that $F_4 > F_3$. This means that the allocation of APs
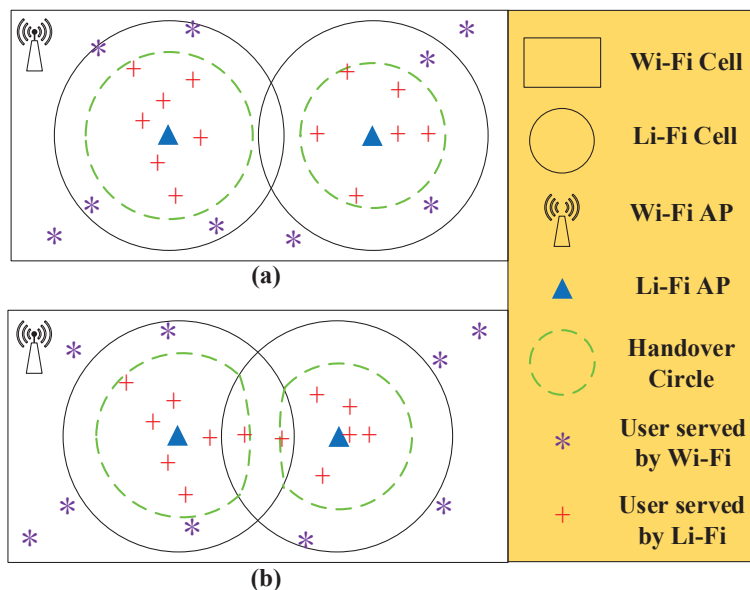
Figure 3.1: *Handover Circle Illustration*

for these two users in this assumption is not optimal, leading to a contradiction. Consequently, the assumption in the proof must be false so that this lemma is proved.

$\square$

According to Lemma 2, all of the users served by a LiFi AP achieve higher SINR than that of other users. The distribution of $\text{SINR}_{\mu,\alpha}$ is closely related to the distance between the user and the serving AP, and between the user and the interfering AP. In general, a high $\text{SINR}_{\mu,\alpha}$ is achieved when a user is close to the serving AP and far away from the interference AP. The boundary of the service area of LiFi APs is shown in Fig. 3.1(b). However, the specific shape of the LiFi service area in the optical CCI case is significantly affected by the layout of the LiFi APs. The analysis of the deployment optimisation of LiFi APs is outside the scope of this study. Hence the numerical estimation is used to analyse the service areas of LiFi APs and the LiFi system throughput, and this is given in Section 3.2.4.

3.2.3.3 Limitation of the WiFi model

In the practical scenario, the WiFi throughput cannot be uniformly distributed in space due to small scale fading. In this hybrid network, due to the fluctuating CSI of moving users, the network load balancing procedure is undertaken in each state. If the coherence time of
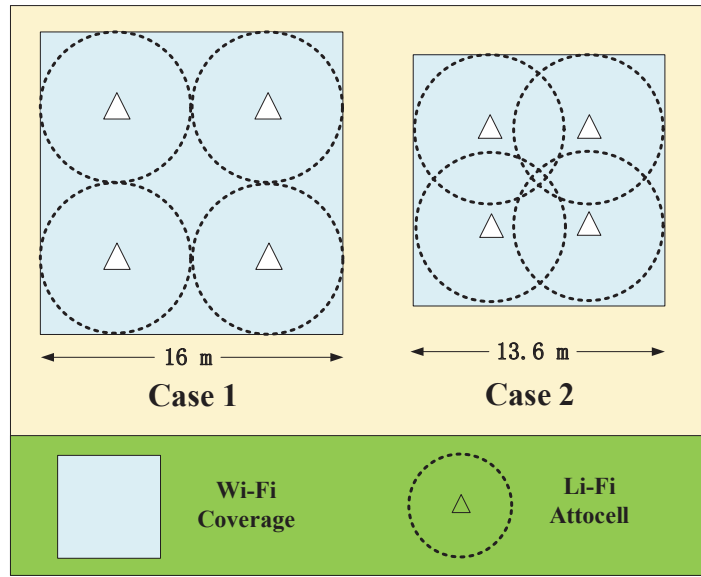
Figure 3.2: *Simulation Scenario*

the channel in WiFi is larger than the duration of the state, T_p, the system would be stable. Otherwise, the average CSI of users in each state can be used for load balancing in order to guarantee the stability of the system. Therefore, in each state, users would achieve different WiFi throughputs R_0 in Eq. (3.5) based on their CSI, and the proposed load balancing scheme can still be effective in this practical scenario. In fact, the data rate performance in both LiFi and WiFi stand-alone network fluctuates in space. By using the proposed scheme, each user is allocated to a better AP between the best LiFi AP and the WiFi AP in terms of data rates, and thus the hybrid network can achieve the diversity gain of two-tier networks. When the WiFi throughput is constant, users inside the handover circles are served by LiFi APs. This is because LiFi offers higher data rate for these users than WiFi. When considering the spatial fluctuation of WiFi throughput, the boundary of the handover circle would be irregularly fluctuating instead of strictly circular shape. Also, if some users inside the handover circles achieve better CSI with WiFi than with LiFi, they would be allocated to the WiFi AP. Therefore, the serving area of LiFi APs cannot be a connected region in the practical LiFi/WiFi hybrid network. In this study, in order to reduce the analysis complexity of the system throughput, a constant WiFi throughput in space is considered. In future research, the load balancing problem with a more practical WiFi model will be studied.

Name of Parameters	Value
Radius of a LiFi cell	4 m
Height of the room	2.3 m
Electric power to optical power conversion, ι	6
Optical power range of each LiFi AP, P_{opt}	20 W
Baseband bandwidth for LED lamp, B_{L}	20 MHz
Physical area of a PD, A_p	1 cm^2
Half-intensity radiation angle, $\theta_{1/2}$	60 deg.
Gain of optical filter, $T_s(\theta)$	1.0
Receiver FoV semi-angle, Θ_F	60 deg.
Refractive index, χ	1.5
Optical to electric conversion efficiency, κ	0.53 A/W
Noise power spectral density, N_{L}	10^{-19} A^2/Hz
Resource allocation interval of central unit, T_p	500 ms

Table 3.2: *Simulation parameters for hybrid LiFi/WiFi networks*

3.2.4   Performance Evaluation

3.2.4.1   Simulation setup

In the simulation, the hybrid network constituted by a WiFi AP and four LiFi APs is considered. The radius of each LiFi attocell is 4 m, and all of the optical attocells reuse the same modulation bandwidth. According to the analysis in Section 3.2.3, two different LiFi AP deployments are considered in the simulation, the non-CCI case and the optical CCI case. In the non-CCI case, the size of the indoor scenario is 16 m × 16 m, shown in Fig. 3.2 (Case 1). The distance between any two neighbouring LiFi APs is 8 m and there is no optical CCI. In the optical CCI case, the size of the indoor scenario is 13.6 m × 13.6 m, shown in Fig. 3.2 (Case 2). The distance between any two neighbouring LiFi APs is 5.6 m, and users in the overlapping areas experience optical CCI. The user density is set to be 0.2 person/m^2 in these two scenarios, which follows the normal user density in indoor office scenarios. Users are uniformly distributed and moving randomly in the considered scenario, and the random way point model is applied [71]. Specifically, each user selects a random destination in the scenario and moves towards the destination with a random speed between 0 and 1 metre per second. After reaching the

destination, a new destination is selected and the user keeps moving. The average handover efficiency is defined as $\eta = \mathbb{E}[\eta_{ij}]$, where η_{ij} is according to Eq. (3.4). The WiFi throughput used in the simulation is based on Table. 3.1. The other parameters are summarised in Table 3.2, which are based on the published research [23, 70, 72].

3.2.4.2 Study of LiFi service areas

In order to study the LiFi service area, a static system is considered where all of the users are fixed. In the non-CCI case, according to the analysis in Section 3.2.3.1, users served by a LiFi AP must reside in the corresponding handover circle. As shown in Fig. 3.3, users served by 4 LiFi APs and the WiFi AP are marked with different signs. There are clear boundaries between the service areas of different APs, and all of the users served by LiFi APs are located inside the region with a circular shape. Since each LiFi AP uses the same configuration for wireless communications, their handover circles have the same radius. In Fig. 3.4, the simulated and theoretical results of the radius of the handover circle are shown. It can be seen that the simulation results closely match the theoretical results. When the WiFi throughput increases, the radius of the handover region decreases because the WiFi AP provides a larger capacity to serve more users. Since the users closer to LiFi APs can achieve higher data rates, the sum-throughput of LiFi increases when the LiFi serving area decreases.

In the optical CCI case, the service areas of the 4 LiFi APs and the WiFi AP with optical CCI is shown in Fig. 3.5 and Fig. 3.6, and the WiFi throughputs are 120 Mb/s and 1 Gb/s, respectively. It can be seen that the service area of each LiFi AP is a connected region but does not have a circular shape. Similar to the non-CCI case, the serving areas of LiFi APs decrease with an increase of WiFi throughput. Due to optical CCI, users in the overlap area of LiFi attocells are more likely to select the WiFi AP when the WiFi throughput increases. As shown in Fig. 3.6, all of the users in the overlap area are served by WiFi when WiFi throughput reaches 1 Gb/s.

3.2.4.3 Study of user data rates

In Fig. 3.7, the relationship between the LiFi throughput and the WiFi throughput is shown. In the non-CCI case, the theoretical LiFi throughput corresponding to the WiFi throughput is evaluated, which matches the simulation results very well. In the optical CCI case, the performance of LiFi throughput is lower than that of the non-CCI case. The difference decreases with
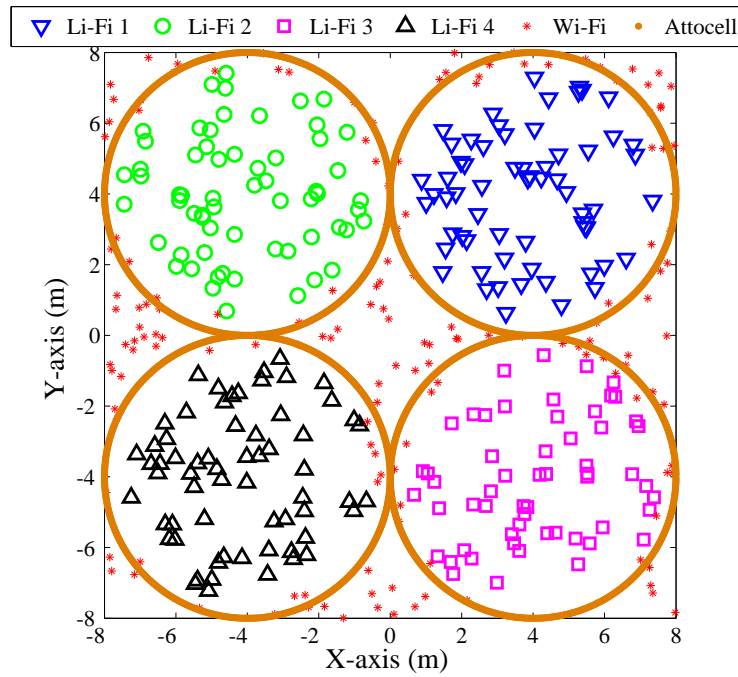
Figure 3.3: *Simulated location of users served by different AP in non-CCI case. (WiFi sum-throughput 120 Mb/s)*
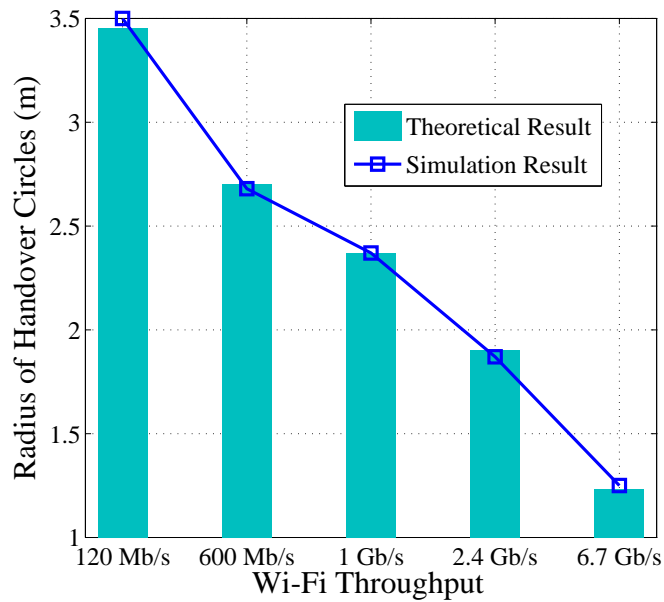
Figure 3.4: *The analysed and simulated radius of handover circles in non-CCI case.*
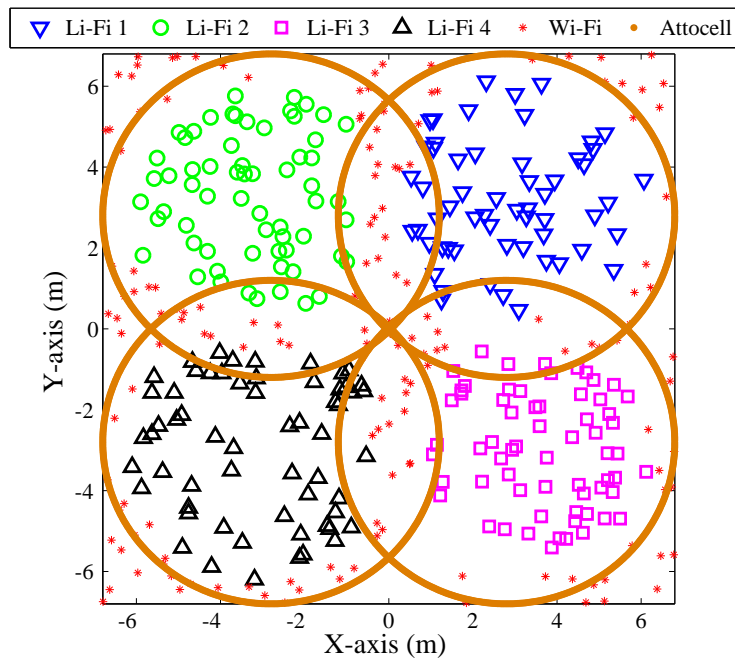
Figure 3.5: *Simulated location of users served by different AP in optical CCI case. (WiFi sum-throughput 120 Mb/s)*
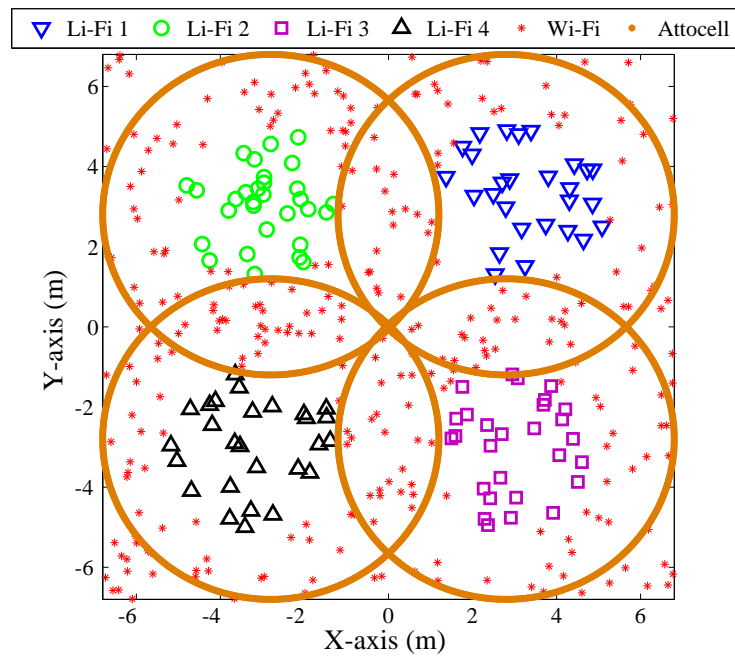
Figure 3.6: *Simulated location of users served by different AP in optical CCI case. (WiFi sum-throughput 1 Gb/s)*

an increase of WiFi throughput. This is because in the optical CCI case the overlap area between the serving region of each LiFi AP and the attocells of other interfering LiFi APs becomes smaller when the WiFi throughput increases. Thus, the optical CCI case tends to the non-CCI case if WiFi throughput is large enough.

The data rate performance of each user is evaluated and shown in Fig. 3.8. According to the analysis in Section 3.2.2, all of the users served by a specific AP share an equal time resource. Thus users served by the WiFi AP achieve an equal data rate due to the spatially uniform distribution of WiFi throughput. The data rate ratio $R_{\text{LiFi}}/R_{\text{WiFi}}$ is used to evaluate the data rate performance of users, where R_{LiFi} represents the data rate of users served by LiFi APs, and R_{WiFi} is the data rate of users served by the WiFi AP. It is shown that the ratio in both non-CCI and optical CCI case is larger than 1. This indicates that users served by LiFi APs always achieve higher data rates than those served by the WiFi AP, which means that the LiFi APs can offer a very good quality of service in the hybrid network. The range of the ratio decreases with an increase of WiFi throughput in both the non-CCI and the optical CCI case. Also, the non-CCI case outperforms the optical CCI case with different WiFi throughputs because of the effect of interference.

3.2.4.4   Study of handover locations

In this subsection, the handover location of moving users in the hybrid network is studied. In the non-CCI case, the handover occurs only between a LiFi AP and the WiFi AP. The distance between the handover location and the LiFi AP is used to represent the handover location information. In the optical CCI case, as well as the handover between LiFi and WiFi, handover also occurs between two LiFi APs. In this situation, the distance between the handover location and the previous serving LiFi AP is used for evaluation.

The CDF of the distance which represents the handover location information in the non-CCI case is given in Fig. 3.9. An interesting result is that when $\eta < 1$, the values of the distance are mainly in two different ranges. This is because the handover overhead results in a handover location offset from the handover circles. For example, if there is no handover overhead, the handover from LiFi to WiFi occurs immediately when users move outside the handover circles. However, with $\eta < 1$, the WiFi data rate is not high enough to prompt a handover due to the loss caused by potential handover. Hence, the handover does not occur on the boundary of handover circles. When users move further away from the LiFi AP, the decrease of LiFi data rates finally
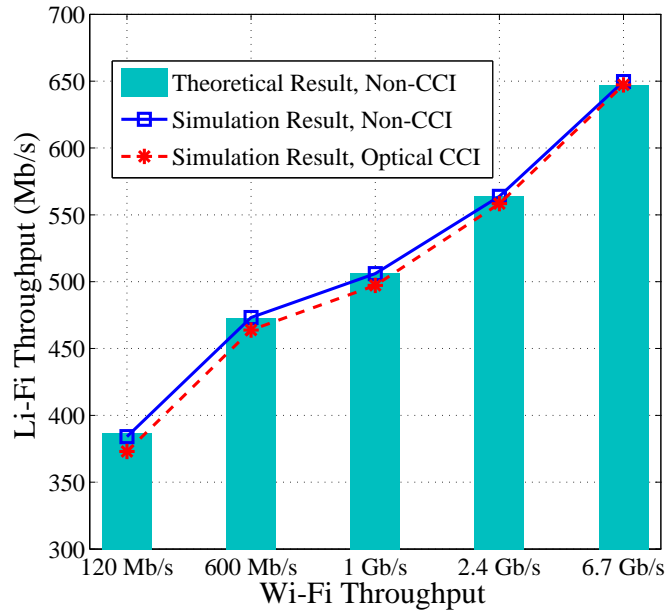
Figure 3.7: *Evaluation of LiFi throughput with different setup of WiFi throughputs in non-CCI and optical CCI cases. ($\eta = 1$)*

results in handover. Due to the handover overhead, the distance of handover from a LiFi AP to the WiFi AP is larger than the radius of handover circle. Similarly, when the handover is from the WiFi AP to a LiFi AP, the distance is less than the radius of handover circles. In addition, a smaller handover efficiency leads to a larger offset. The simulation results also indicate that when the WiFi throughput increases, the handover location becomes closer to the LiFi AP. This is because the radius of the handover circle decreases.

In the optical CCI case, a handover can occur in both non-overlap areas and overlap areas between LiFi attocells. As shown in Fig. 3.10, the values of the distance are still mainly in two different ranges with $\eta < 1$, but around 70% of these values lie in the lower range. This is because the LiFi serving regions in the optical CCI case are in an irregular shape, and the LiFi AP is closer to the boundary of service regions in the overlap area than that in the non-overlap area. Also, similar to the non-CCI case, the distance between handover locations and LiFi APs decreases with an increase of the WiFi throughput.
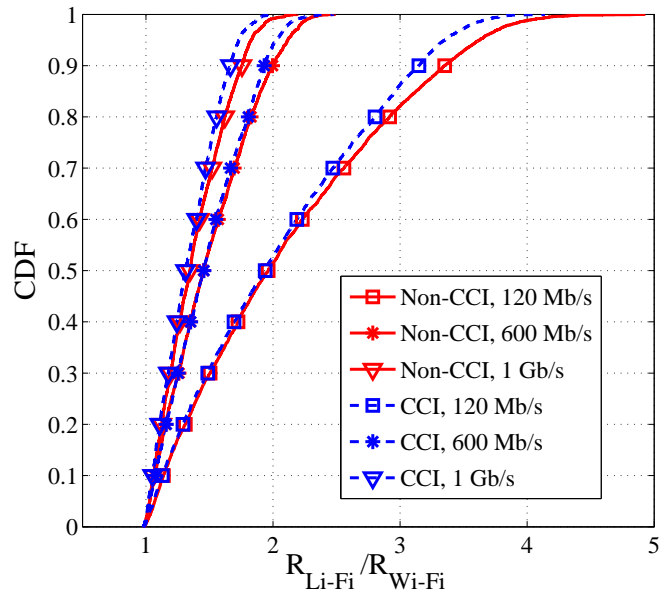
Figure 3.8: *CDF of the user data ratio R_{LiFi}/R_{WiFi} in non-CCI and optical CCI case. The user density is set to be 0.2 person/m², which is normal in the indoor office scenario. ($\eta = 1$)*
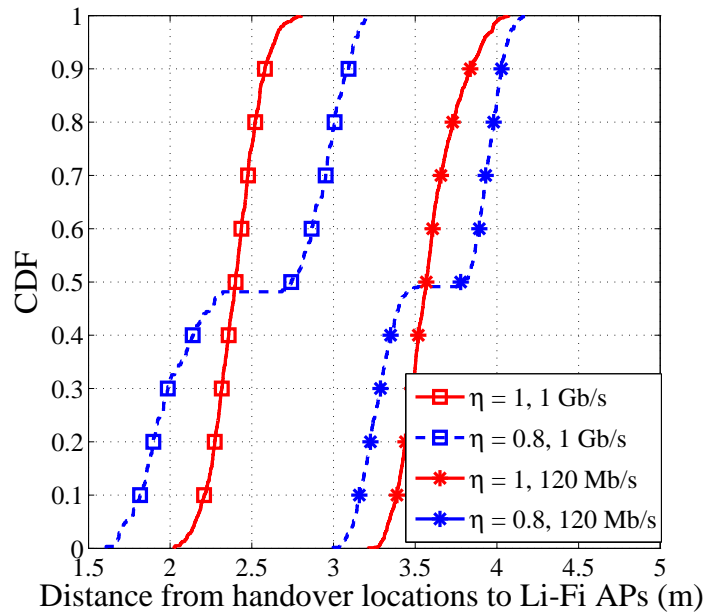
Figure 3.9: *CDF of the distance between the LiFi APs and the handover location in non-CCI case.*
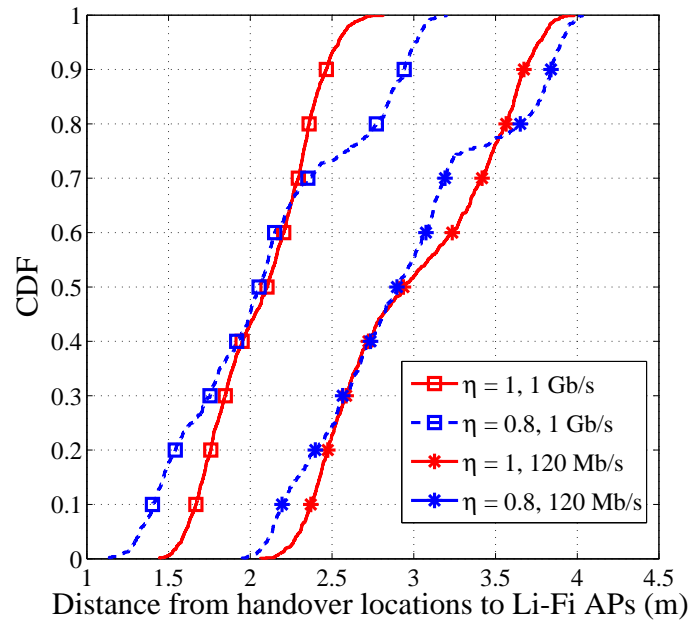
Figure 3.10: *CDF of the distance between the LiFi APs and the handover location in optical CCI case.*
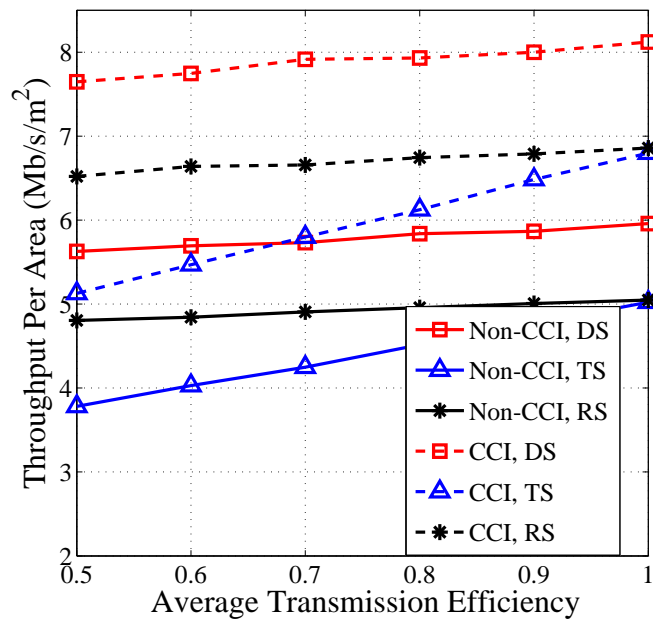
Figure 3.11: *Spatial throughput in non-CCI case and optical CCI case. (WiFi throughput 1 Gb/s)*

3.2.4.5   Proposed scheme vs. other load balancing schemes

In this subsection, the system throughput of a hybrid LiFi/WiFi network is studied. In order to fairly compare the non-CCI case and the optical CCI case, the spatial throughput (throughput per area) is used for evaluation, and is defined as:

$$\text{Spatial Throughput} = \frac{\text{System Throughput}}{\text{Area of Indoor Scenario}}. \tag{3.53}$$

The spatial throughput reflects the performance of user data rate with a given user density, which can be expressed as:

$$\text{Average user data rate} = \frac{\text{Spatial Throughput}}{\text{User density}}. \tag{3.54}$$

The spatial throughputs in both the non-CCI and the optical CCI cases are evaluated and shown in Fig. 3.11. In the legend, the proposed dynamic load balancing scheme is termed as 'DS', and two other load balancing schemes are considered, termed as 'TS' and 'RS' respectively. In 'TS', a threshold is used to determine whether a user is allocated to the best LiFi AP or the WiFi AP [72]. In 'RS', users randomly select the AP between the best LiFi AP and the WiFi AP. In both schemes, users served by the same AP share an equal proportion of time resource, and the handover overhead is considered. As shown in Fig. 3.11, the spatial throughput in the optical CCI case is higher than that of the non-CCI case. This indicates that with the same user density, each user in the optical CCI case can achieve a higher data rate despite the interference, resulting from a large reuse of the communication bandwidth. The spatial throughput decreases with the handover efficiency due to the effect of overhead. The proposed load balancing scheme always outperforms 'TS' and 'RS' with any value of η. The difference is more than 1 Mb/s/m^2. This is because the AP assignment and time resource allocation in 'DS' are jointly designed, which are formulated as an optimisation problem shown in Eq. (3.6), while they are separately designed in 'TS' and 'RS', which are undertaken in sequence [72].

In addition to the indoor LiFi/WiFi scenario, the proposed dynamic load balancing scheme can also be used in hybrid RF small cell networks which combine femto-cells and pico-cells [73]. The pico-cells have a coverage distance of less than 100 meters while the coverage distance of a femto-cell is less than 30 meters. Therefore, handover may occur frequently in these scenarios, and the proposed scheme can offer an efficient and stable load balancing for the femto/pico

hybrid networks.

3.2.5 Discussion

In this section, a dynamic load balancing scheme in a LiFi/WiFi hybrid network is proposed, where the handover overhead is considered. By analysing the service areas of the LiFi APs, the throughput performance of the hybrid system is theoretically studied. Also, the effects of the handover overhead on handover locations and user throughput are simulated and discussed. Three conclusions are made based on the analytical and simulation results: i) the service coverage of LiFi APs are connected regions, which are generally smaller than the entire LiFi attocells. Specifically, these areas are circular in the non-CCI case, but non-circular in the optical CCI case; ii) the WiFi and LiFi throughput in the hybrid network are related despite the independent spectrum transmission. The LiFi throughput can be improved by increasing the WiFi throughput. In addition, the achievable data rates of the users served by LiFi APs are higher than or equal to that of users allocated to the WiFi AP; iii) a handover occurs only when users move across the boundaries of the LiFi service areas. The handover overhead can lead to a handover location offset due to the transmission loss considered in the proposed load balancing scheme.

3.3 Optimisation based dynamic LB Scheme

As known, an efficient load balancing scheme for hybrid networks can improve system throughput and user QoS. In this section, a comprehensive study of dynamic load balancing aiming at improving user data rates is undertaken, where a variety of fairness schemes and user QoS requirements are taken into account. Specifically, two specific algorithms that optimise the AP assignment (APA) and the RA in each quasi-static state are proposed, termed as joint optimisation algorithm (JOA) and separate optimisation algorithm (SOA) respectively. In this work, the optimality of JOA and the optimal threshold in SOA are analysed. Also, a comparison of data rate performance and computational complexity between these two algorithms is made. Moreover, a unified data rate requirement of users is considered as a QoS metric and user outage probability is introduced. In this study, an optimisation problem that maximises the achievable user QoS with a certain outage probability is formulated and solved by numerical simulations. The maximal user QoS in the dynamic hybrid system is evaluated for both JOA and SOA.

3.3.1 System model

In this section, a multi-user indoor hybrid LiFi/RF network is considered, where N_l LiFi APs and N_r RF APs are deployed. The PDs on each LiFi receivers are assumed to be oriented perpendicular to the floor. This means that the angle of irradiance is equal to the angle of incidence in the LoS optical channel. The system setup of hybrid LiFi/RF network follows the model presented in Section 2.1-2.2. The CU monitors the system continuously in every quasi-static state, where the load distribution is assumed to be fixed and users receive a constant data rate. The handover scheme considered in this study is shown in Section 3.2.1. In addition, TDMA is used in both LiFi and RF systems. The set of users is denoted by $\mathcal{U}$; the number of the users is denoted by N_u; the set of optical attocells is denoted by $\mathcal{C}_\mathcal{L} = \{l | l \in [1, N_l], l \in \mathbb{N}\}$; and $\mathcal{C}_\mathcal{R} = \{r | r \in [1, N_r], r \in \mathbb{N}\}$ is the set of RF cells.

Referring to the LiFi channel model in Section 2.3.1, the signal-to-interference-plus-noise ratio (SINR) for user μ connected to AP α can be written as follows:

$$\text{SINR}_{\mu,\alpha}(f) = \frac{(\kappa\varepsilon_p P_{\text{opt}} H_{\mu,\alpha}(f))^2}{\iota^2 N_\text{L} B_\text{L} + \sum(\kappa\varepsilon_p P_{\text{opt}} H_{\mu,\text{else}}(f))^2}, \tag{3.55}$$

where f is the central frequency of OFDM subcarrier; κ is the optical to electric conversion efficiency at the receivers; $\varepsilon_p \approx 1$ is power amplification gain; N_L is the noise power spectral density in the LiFi link; B_L is the baseband modulation bandwidth for each LiFi AP; $H_{\mu,\alpha}(f)$ is the channel gain in the frequency domain between user μ and LiFi AP; and $H_{\mu,\text{else}}(f)$ is the channel gain between user μ and the interfering LiFi APs, according to Eq. (2.3).

In the RF system, the channel model has been shown in Section 2.4. Since there is no CCI in the RF system, the SINR is equivalent to SNR on each sub-carrier, which can be expressed as follows:

$$\text{SNR}_{\mu,\alpha}(f) = \frac{|\Gamma_{\mu,\alpha}(f)|^2 \Delta P_\text{R}}{N_\text{R} \Delta B_\text{R}}, \tag{3.56}$$

where $\Gamma_{\mu,\alpha}(f)$ is the RF channel gain, according to Eq. (2.40); ΔB_R is the modulation bandwidth of each sub-carrier; ΔP_R is the transmit power allocated to each sub-carrier; and N_R is the noise power spectral density in RF link. It is assumed that the transmit power is allocated equally to each sub-carrier. Thus, it is obtained that $\Delta P_\text{R}/\Delta B_\text{R} = P_\text{R}/B_\text{R}$, where P_R and B_R are the total transmit power and modulation bandwidth for a RF AP.

In order to improve the spectrum efficiency, adaptive bit loading is employed over the OFDM

sub-carriers [53]. Note that the frequency of subcarrier m is denoted by f_m and the achievable SE on subcarrier m is denoted by q_m. The relationship between q_m and $\text{SINR}_{\mu,\alpha}(f_m)$ (or $\text{SNR}_{\mu,\alpha}(f_m)$) follows the MCS given in Table 2.1. Specifically, given a user SINR or SNR, we can firstly find the min. SINR level which is closest to and less than the user SINR (SNR) in Table 2.1. Then, q_m will be the corresponding SE shown in the table. The link communication data rate of LiFi and RF between user μ and AP α are denoted as $Z_{\mu,\alpha}$ and $\Upsilon_{\mu,\alpha}$, respectively. When considering the handover scheme in Algorithm. 3, the link data rate between AP α and user μ in state n with handover considered can be expressed as follows:

$$r_{\mu,\alpha}^{(n)} = \begin{cases} \eta_{\alpha'\alpha} Z_{\mu,\alpha}^{(n)}, & \alpha \in \mathcal{C}_{\mathcal{L}} \\ \eta_{\alpha'\alpha} \Upsilon_{\mu,\alpha}^{(n)}, & \alpha \in \mathcal{C}_{\mathcal{R}} \end{cases}, \tag{3.57}$$

where α' is the AP allocated to user μ in the state $n-1$; $\eta_{\alpha'\alpha}$ is the handover efficiency between state $n-1$ and state n according to Eq. (3.4); and $Z_{\mu,\alpha}^{(n)}$ and $\Upsilon_{\mu,\alpha}^{(n)}$ are the data rates of the LiFi link and the RF link in state n, respectively. The value of $r_{\mu,\alpha}^{(n)}$ between user μ and AP α is calculated by the CU in each state.

Two variables $g_{\mu,\alpha}^{(n)}$ and $k_{\mu,\alpha}^{(n)}$ are introduced to model the load balancing in state n. The variable $g_{\mu,\alpha}^{(n)}$ is a binary number which equals 1 when user μ is connected to AP α, otherwise it is 0. The variable $k_{\mu,\alpha}^{(n)}$ is a fractional number between 0 and 1, which represents the proportion of time resources allocated to user μ by AP α in state n.

3.3.2 Joint Optimisation Algorithm (JOA)

In this section, the JOA that jointly optimises the AP assignment and the time resource allocation in each state is proposed. At first, the joint optimisation problem is formulated and an iterative algorithm for the problem is given. After that, the convergence and optimality of the proposed algorithm are analysed. Since the network load balancing of a specific state is studied, the superscript (n) in parameters $g_{\mu,\alpha}^{(n)}$, $k_{\mu,\alpha}^{(n)}$ and $r_{\mu,\alpha}^{(n)}$ is omitted to enhance clarity.

3.3.2.1   Problem Formulation and Iterative Algorithm

As shown in Section 3.2.2, the β-proportional fairness function that considers both sum-rate and user fairness is employed. This utility function is repeated and expressed as:

$$\psi_\beta(x) = \begin{cases} \log(x), & \beta = 1 \\ \dfrac{x^{1-\beta}}{1-\beta}, & \beta \geq 0, \ \beta \neq 1 \end{cases}, \tag{3.58}$$

where x is the achievable data rate; and β is the fairness coefficient. The utility function in Eq. (3.58) includes several well known fairness concepts [74]. Specifically, when $\beta = 1$, a proportional fairness is achieved, where users served by a specific AP share an equal proportion of time resource; and when $\beta \to \infty$, a max-min fair scheduler is realised. Particularly, when $\beta = 0$, a linear utility function is obtained which achieves a maximal system throughput. In this case, each AP only serves the user of the best CSI whereas the other users have zero data rates, which finally leads to an ineffective load balancing solution. Thus, the situation of $\beta = 0$ is beyond the scope of this study.

Using the utility function in Eq. (3.58), the joint optimisation of the APA and the RA can be formulated as follows:

$$\max_{g_{\mu,\alpha}, k_{\mu,\alpha}} \sum_{\mu \in \mathcal{U}} \sum_{\alpha \in \mathcal{C}_\mathcal{L} \cup \mathcal{C}_\mathcal{R}} g_{\mu,\alpha} \psi_\beta(k_{\mu,\alpha} r_{\mu,\alpha}) \tag{3.59}$$

$$s.t. \ \sum_{\mu \in \mathcal{U}} g_{\mu,\alpha} k_{\mu,\alpha} \leq 1 \quad \forall \alpha \in \mathcal{C}_\mathcal{L} \cup \mathcal{C}_\mathcal{R}; \tag{3.60}$$

$$\sum_{\alpha \in \mathcal{C}_\mathcal{L} \cup \mathcal{C}_\mathcal{R}} g_{\mu,\alpha} = 1 \quad \forall \mu \in \mathcal{U};$$

$$g_{\mu,\alpha} \in \{0,1\}, \ k_{\mu,\alpha} \in [0,1], \quad \forall \mu \in \mathcal{U}, \forall \alpha \in \mathcal{C}_\mathcal{L} \cup \mathcal{C}_\mathcal{R},$$

where $r_{\mu,\alpha}$ is the communication link data rate given in Eq. (3.57), which is a positive number. The optimum $k_{\mu,\alpha}$ is shown to be greater than zero in Eq. (3.72) so that $\log(0)$ is avoided.

This optimisation problem in Eq. (3.59) is a mixed integer non-linear programming (MINLP) problem which is mathematically intractable because it involves both binary variables and real-valued positive variables. In order to simplify this problem, the binary variable $g_{\mu,\alpha}$ is assumed to be a fractional number between 0 and 1.

Lemma 3. *The original problem in Eq. (3.59) is able to be converted into a concave optimisa-*

tion problem using the fractional variable $g_{\mu,\alpha}$.

Proof. It is assumed that $g_{\mu,\alpha}$ is a fractional number. The objective function in Eq. 3.13) is denoted as $F(g_{\mu,\alpha}, k_{\mu,\alpha})$, and its Hessian matrix can be written as follows:

$$
\mathcal{H}(F) = \begin{bmatrix} \frac{\partial^2 F}{\partial g_{\mu,\alpha}^2} & \frac{\partial^2 F}{\partial g_{\mu,\alpha} \partial k_{\mu,\alpha}} \\ \frac{\partial^2 F}{\partial k_{\mu,\alpha} \partial g_{\mu,\alpha}} & \frac{\partial^2 F}{\partial k_{\mu,\alpha}^2} \end{bmatrix}, \tag{3.61}
$$

where

$$
\frac{\partial^2 F}{\partial g_{\mu,\alpha}^2} = 0; \tag{3.62}
$$

$$
\frac{\partial^2 F}{\partial k_{\mu,\alpha}^2} = -\beta \frac{r_{\mu,\alpha}^2}{(k_{\mu,\alpha} r_{\mu,\alpha})^{\beta+1}} \leq 0. \tag{3.63}
$$

Since all of the principle minors of the Hessian matrix are non-positive, the objective function is concave with respect to the variables, $g_{\mu,\alpha}$ and $k_{\mu,\alpha}$.

$\square$

The Lagrangian Multiplier method can therefore be used to solve this optimisation problem [24]. The Lagrangian function is expressed as follows:

$$
L(g_{\mu,\alpha}, k_{\mu,\alpha}, \omega_\alpha) = \sum_{\mu \in \mathcal{U}} \sum_{\alpha \in \mathcal{C}_\mathcal{L} \cup \mathcal{C}_\mathcal{R}} g_{\mu,\alpha} [\psi_\beta(k_{\mu,\alpha} r_{\mu,\alpha})
$$
$$
- \omega_\alpha k_{\mu,\alpha}] + \sum_{\alpha \in \mathcal{C}_\mathcal{L} \cup \mathcal{C}_\mathcal{R}} \omega_\alpha, \tag{3.64}
$$

where $g_{\mu,\alpha} \in [0,1]$, $k_{\mu,\alpha} \in [0,1]$ and $\sum_{\alpha \in \mathcal{C}_\mathcal{L} \cup \mathcal{C}_\mathcal{R}} g_{\mu,\alpha} = 1$. The Lagrangian multiplier ω_α corresponds to the α-th constraints in Eq. (3.11). The optimum of $g_{\mu,\alpha}$ and $k_{\mu,\alpha}$ can be obtained by solving the problem:

$$
\min_{\omega_\alpha} \max_{g_{\mu,\alpha}, k_{\mu,\alpha}} L(g_{\mu,\alpha}, k_{\mu,\alpha}, \omega_\alpha). \tag{3.65}
$$

In this study, the problem in Eq. (3.65) is solved by a distributed algorithm via Lagrangian decomposition [75]. According to the Lagrangian function in Eq. (3.64), a dual objective

function in terms of user μ is defined as:

$$\Omega_\mu(g_{\mu,\alpha}, k_{\mu,\alpha}) = \sum_{\alpha \in \mathcal{C}_\mathcal{L} \cup \mathcal{C}_\mathcal{R}} g_{\mu,\alpha}[\psi_\beta(k_{\mu,\alpha} r_{\mu,\alpha}) - \omega_\alpha k_{\mu,\alpha}]. \tag{3.66}$$

The problem in Eq. (3.65) is separated into two steps of optimisation. In the first step, the dual objective function is optimised, and this sub-problem can be formulated as follows:

$$\{g_{\mu,\alpha}^*, k_{\mu,\alpha}^*\} = \arg \max_{g_{\mu,\alpha}, k_{\mu,\alpha} \in [0,1]} \Omega_\mu(g_{\mu,\alpha}, k_{\mu,\alpha}). \tag{3.67}$$

It can be seen that the function $\Omega_\mu(g_{\mu,\alpha}, k_{\mu,\alpha})$ is concave with respect to the variables $g_{\mu,\alpha}$ and $k_{\mu,\alpha}$. The partial derivatives of Ω_μ with $g_{\mu,\alpha}$ and $k_{\mu,\alpha}$ are:

$$\frac{\partial \Omega_\mu}{\partial g_{\mu,\alpha}} = \psi_\beta(k_{\mu,\alpha} r_{\mu,\alpha}) - \omega_\alpha k_{\mu,\alpha}, \tag{3.68}$$

$$\frac{\partial \Omega_\mu}{\partial k_{\mu,\alpha}} = g_{\mu,\alpha} \left[\frac{\partial \psi_\beta(k_{\mu,\alpha} r_{\mu,\alpha})}{\partial k_{\mu,\alpha}} - \omega_\alpha \right], \tag{3.69}$$

where $\psi_\beta(.)$ is given in Eq. (3.58) and its derivative with respect to $k_{\mu,\alpha}$ is:

$$\frac{\partial \psi_\beta(k_{\mu,\alpha} r_{\mu,\alpha})}{\partial k_{\mu,\alpha}} = \frac{r_{\mu,\alpha}}{(k_{\mu,\alpha} r_{\mu,\alpha})^\beta}. \tag{3.70}$$

In conjunction with Eq. (3.70), it can be shown that Eq. (3.69) monotonically decreases as $k_{\mu,\alpha}$ increases. Also, due to the strict positivity of $k_{\mu,\alpha}, r_{\mu,\alpha}$ and β it can be derived that:

$$\lim_{k_{\mu,\alpha} \to 0^+} \frac{r_{\mu,\alpha}}{(k_{\mu,\alpha} r_{\mu,\alpha})^\beta} = +\infty. \tag{3.71}$$

Since ω_α is finite and $g_{\mu,\alpha}$ is non-negative, it can be seen that the condition, $\frac{\partial \Omega_\mu}{\partial k_{\mu,\alpha}}|_{k_{\mu,\alpha}=0} \geq 0$ is satisfied. Thus, the optimum $k_{\mu,\alpha}$ can be calculated by:

$$k_{\mu,\alpha}^* = \begin{cases} 1, & \frac{\partial \Omega_\mu}{\partial k_{\mu,\alpha}}|_{k_{\mu,\alpha}=1} \geq 0 \\ \frac{1}{r_{\mu,\alpha}} \left(\frac{r_{\mu,\alpha}}{\omega_\alpha} \right)^{\frac{1}{\beta}}, & \frac{\partial \Omega_\mu}{\partial k_{\mu,\alpha}}|_{k_{\mu,\alpha}=1} < 0 \end{cases}. \tag{3.72}$$

With $k_{\mu,\alpha}^*$, the optimum $g_{\mu,\alpha}$ is expressed as follows:

$$g_{\mu,\alpha}^* = \begin{cases} 1, & \alpha = \arg \max_{\alpha' \in \mathcal{C}_\mathcal{L} \cup \mathcal{C}_\mathcal{R}} \frac{\partial \Omega_\mu(k_{\mu,\alpha'}^*)}{\partial g_{\mu,\alpha'}} \\ 0, & \text{Otherwise} \end{cases}. \tag{3.73}$$

Algorithm 5 : JOA in each state.

1: Initialisation: $\omega_\alpha(t)$, ε_ω and ε; $t \leftarrow 0$, $L(t+1) \rightarrow \infty$, $L(t) = 0$.

2: **while** $|L(t+1) - L(t)| > \varepsilon$ **do**

3:     **for all** each user $\mu \in \mathcal{U}$ and each AP $\alpha \in \mathcal{C}_\mathcal{L} \cup \mathcal{C}_\mathcal{R}$ **do**

4:         The CU calculates $k^*_{\mu,\alpha}$ according to Eq. (3.72).

5:         The CU calculates $g^*_{\mu,\alpha}$ according to Eq. (3.73).

6:     **end for**

7:     The CU broadcasts $g^*_{\mu,\alpha}$ and $k^*_{\mu,\alpha}$ to all of the users and APs.

8:     **for all** each AP $\alpha \in \mathcal{C}_\mathcal{L} \cup \mathcal{C}_\mathcal{R}$ **do**

9:         AP α updates the Lagrangian multiplier ω_α by using $g^*_{\mu,\alpha}$ and $k^*_{\mu,\alpha}$, according to Eq. (3.76).

10:         AP α broadcasts the updated ω_α.

11:     **end for**

12:     The CU calculates the objective function $L(t)$ by using $g^*_{\mu,\alpha}$, $k^*_{\mu,\alpha}$ and ω_α, according to Eq. (3.64).

13:     $t \leftarrow t + 1$;

14: **end while**

15: Output: $g^*_{\mu,\alpha}$ and $k^*_{\mu,\alpha}$;

In the second step, the dual optimum $\{g^*_{\mu,\alpha}, k^*_{\mu,\alpha}\}$ is introduced to the optimisation problem in Eq. (3.65), and this problem can be converted to:

$$\min_{\omega_\alpha} \ L(\Omega_\mu(g^*_{\mu,\alpha}, k^*_{\mu,\alpha}), \omega_\alpha), \tag{3.74}$$

where

$$L(\Omega_\mu(g^*_{\mu,\alpha}, k^*_{\mu,\alpha}), \omega_\alpha) = \sum_{\mu \in \mathcal{U}} \Omega_\mu(g^*_{\mu,\alpha}, k^*_{\mu,\alpha}) + \sum_{\alpha \in \mathcal{C}_\mathcal{L} \cup \mathcal{C}_\mathcal{R}} \omega_\alpha. \tag{3.75}$$

The objective function in Eq. (3.74) is concave and differentiable. Thus it can be solved by using the gradient projection method [67]. The update of ω_α is expressed as follows:

$$\omega_\alpha(t+1) = \left[\omega_\alpha(t) - \varepsilon_\omega \left(1 - \sum_{\mu \in \mathcal{U}} g^*_{\mu,\alpha} k^*_{\mu,\alpha} \right) \right]^+, \tag{3.76}$$

where ε_ω is the step size taken in the direction of the negative gradient of ω_α.

Based on the analysis above, the JOA can be regarded as a distributed iterative algorithm summarised in Algorithm 5, where $L(t)$ is the objective function in Eq. (3.65) in the t-th iteration; and ε is a threshold which is used to determine whether the algorithm converges.

3.3.2.2 Convergence analysis of JOA

According to Algorithm 5, JOA converges after the difference between the objective functions in two neighbouring iterations is small enough. In particular, we assume $\varepsilon = |L(t+1)|/50$ in the algorithm. According to Eq. (3.76), the step size ε_ω can significantly affect the speed of convergence. In general, a larger value of ε_ω can result in a faster convergence. However, when ε_ω is set to be very large, the algorithm becomes unstable so that the objective function tends to oscillate and the convergence cannot be guaranteed. In order to facilitate both the speed and the stability of the convergence, an adaptive step size is considered and designed as follows:

$$\varepsilon_\omega \leftarrow \varepsilon_\omega d^{\frac{t}{2}}, \quad (0 < d < 1) \tag{3.77}$$

where t is the number of iterations and d is a bias weight. This step size decreases with t, which enables more efficient iterations. Moreover, the step size, ε_ω approaches zero when t is large, and its gradient is affected by d. It is possible that ε_ω tends to zero before the algorithm converges. Hence, d should be well designed. In this study, it is set to be between 0.8 and 0.9. The simulations confirm that this range is a suitable choice for the simulation scenario considered in this section.

Since the threshold, ε in JOA cannot be zero, the optimum $k_{\mu,\alpha}^*$ gained in JOA may not strictly satisfy the constraint in Eq. (3.60). In order to avoid the situation $\sum_{\mu \in \mathcal{U}} g_{\mu,\alpha}^* k_{\mu,\alpha}^* > 1$, the optimum $k_{\mu,\alpha}^*$ achieved by Algorithm 5 should be normalised, which can mathematically be expressed as follows:

$$\bar{k}_{\mu,\alpha} = \frac{k_{\mu,\alpha}^*}{\sum_{\mu \in \mathcal{U}} g_{\mu,\alpha}^* k_{\mu,\alpha}^*}, \quad \forall \alpha \in \mathcal{C}_\mathcal{L} \cup \mathcal{C}_\mathcal{R}, \tag{3.78}$$

where $g_{\mu,\alpha}^*$ is the optimum of the variable $g_{\mu,\alpha}$ obtained by using JOA. The normalised resource proportion $\bar{k}_{\mu,\alpha}$ strictly satisfies the constraint in Eq. (3.60). The load balancing results achieved by JOA can be denoted as follows:

$$\begin{cases} g_{\mu,\alpha}^{(\text{JOA})} & = g_{\mu,\alpha}^*; \\ k_{\mu,\alpha}^{(\text{JOA})} & = \bar{k}_{\mu,\alpha}. \end{cases} \tag{3.79}$$

3.3.2.3 Optimality analysis

Due to the dual decomposition method used in JOA, it is difficult to discover whether the results attained in Eq. (3.79) after convergence are the global optima or not. Since a closed-form solution of the original optimisation problem is mathematically intractable, an exhaustive search is used to find the global optimum.

With the assumption of N_u users and $N_l + N_r$ APs in this network, there are $(N_l + N_r)^{N_u}$ possibilities of AP allocation. Note that the AP assignments are denoted as $\mathbf{g}^{(i)}$, $i = 1, 2...(N_l + N_r)^{N_u}$. When a certain $\mathbf{g}^{(i)}$ is considered, the joint optimisation problem in Eq. (3.59) can be transformed as follows:

$$\max_{k_{\mu,\alpha}^{(i)}} \quad \sum_{\alpha \in \mathcal{C}_\mathcal{L} \cup \mathcal{C}_\mathcal{R}} \sum_{\mu \in \mathcal{U}_\alpha} \psi_\beta(k_{\mu,\alpha}^{(i)} r_{\mu,\alpha}), \tag{3.80}$$

where $\mathcal{U}_\alpha$ is the set of users allocated to AP α. According to Eq. (3.80), the optimisation of $k_{\mu,\alpha}$ can be undertaken independently in each cell, which is expressed as follows:

$$\max_{k_{\mu,\alpha}^{(i)}} \quad \sum_{\mu \in \mathcal{U}_\alpha} \psi_\beta(k_{\mu,\alpha}^{(i)} r_{\mu,\alpha}), \tag{3.81}$$

$$s.t. \quad \sum_{\mu \in \mathcal{U}_\alpha} k_{\mu,\alpha}^{(i)} \leq 1, \tag{3.82}$$

The Lagrangian multiplier method is used to solve this problem. The Lagrangian function is given by:

$$F(k_{\mu,\alpha}^{(i)}, \omega) = \sum_{\mu \in \mathcal{U}_\alpha} \psi_\beta(k_{\mu,\alpha}^{(i)} r_{\mu,\alpha}) + \omega \left(1 - \sum_{\mu \in \mathcal{U}_\alpha} k_{\mu,\alpha}^{(i)} \right), \tag{3.83}$$

where ω is the Lagrangian multiplier for the constraint in Eq. (3.82). The optimum $k_{\mu,\alpha}^{(i)}$ can be found by making the gradient of the Lagrangian function in Eq. (3.83) equal to 0, which is written as follows:

$$\frac{\partial F(k_{\mu,\alpha}^{(i)}, \omega)}{\partial k_{\mu,\alpha}^{(i)}} = \frac{r_{\mu,\alpha}}{(k_{\mu,\alpha}^{(i)} r_{\mu,\alpha})^\beta} - \omega = 0, \; \mu \in \mathcal{U}_\alpha. \tag{3.84}$$
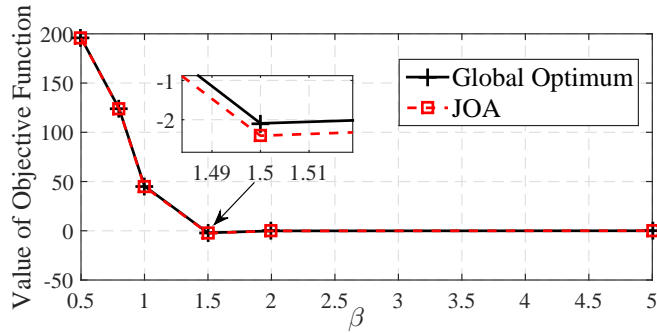
Figure 3.12: *Comparison of optimums between global optimisation and JOA (1000 independent and identical simulations are considered.)*

It can be derived from Eq. (3.84) that:

$$k_{\mu,\alpha}^{(i)} = \frac{r_{\mu,\alpha}^{\frac{1}{\beta}-1}}{\omega^{\frac{1}{\beta}}}. \tag{3.85}$$

According to Eq. (4.12) and Eq. (3.82), it can be found that:

$$\omega^{\frac{1}{\beta}} = \sum_{\mu \in \mathcal{U}_\alpha} r_{\mu,\alpha}^{\frac{1}{\beta}-1}. \tag{3.86}$$

Combining Eq. (4.12) and Eq. (4.13), the optimum $k_{\mu,\alpha}^{(i)}$ can be expressed as follows:

$$k_{\mu,\alpha}^{(i)} = \frac{r_{\mu,\alpha}^{\frac{1}{\beta}-1}}{\sum_{i \in \mathcal{U}_\alpha} r_{i,\alpha}^{\frac{1}{\beta}-1}} \qquad (\beta > 0). \tag{3.87}$$

Given a certain AP allocation $\mathbf{g}^{(i)}$, it is possible to compute the objective function in Eq. (3.80) based on the RA result in Eq. (3.87). Subsequently, the global optimum of the original joint optimisation problem can be determined using an exhaustive search. A comparison between the JOA and the global optimum is shown in Fig. 4.2. It can be seen that the JOA technique approaches the optimal solution very closely. Also, the gap between the JOA result and the global optimum diminishes with an increase in β. Therefore, it can be concluded that the JOA attains the performance of the global optimal solution to the original optimisation problem in Eq. (3.59).

3.3.3 Separate Optimisation Algorithm (SOA)

In this section, the SOA that separately optimises the AP assignment and the time resource allocation in each state is proposed. As before, the superscript n is omitted in parameters $g_{\mu,\alpha}^{(n)}$, $k_{\mu,\alpha}^{(n)}$ and $r_{\mu,\alpha}^{(n)}$ for clarification.

3.3.3.1 AP assignment in SOA

In order to make use of the high spatial spectrum efficiency of LiFi, the APA step in SOA can be realised as follows: users achieving LiFi data rates higher than a certain threshold, denoted by γ, are served by LiFi APs; and the others of data rates falling below the threshold via LiFi links would be assigned to the RF APs. Moreover, the criterion of maximal effective throughput is applied for the APA step. In terms of user μ, the LiFi AP offering the maximal link data rate involving handover is expressed as follows:

$$\tau_{1,\mu} = \arg\max_{j \in \mathcal{C}_\mathcal{L}} r_{\mu,j}, \tag{3.88}$$

where $r_{\mu,j}$ is the LiFi data rate according to Eq. (3.57). Assuming that the time resource is equally shared by users in each cell, the potential LiFi data rate of user μ can be written as follows:

$$\dot{\lambda}_\mu = r_{\mu,\tau_{1,\mu}}/M_{\tau_{1,\mu}}, \tag{3.89}$$

where $M_{\tau_{1,\mu}}$ is the number of users served by LiFi AP $\tau_{1,\mu}$.

According to the principle of APA step, users following $\dot{\lambda}_\mu < \gamma$ should be allocated to RF APs. The RF AP assigned to user μ can be written as follows:

$$\tau_{2,\mu} = \arg\max_{j \in \mathcal{C}_\mathcal{R}} r_{\mu,j}, \quad \dot{\lambda}_\mu < \gamma. \tag{3.90}$$

Based on Eq. (3.88) (3.90), the APA result of SOA is expressed as follows:

$$g_{\mu,\alpha}^{(\text{SOA})} = \begin{cases} 1, & \alpha = \begin{cases} \tau_{1,\mu}, & \dot{\lambda}_\mu \geq \gamma \\ \tau_{2,\mu}, & \dot{\lambda}_\mu < \gamma \end{cases} \\ 0, & \text{Otherwise} \end{cases}. \tag{3.91}$$

Algorithm 6 SOA in each state.

1: Initialisation: $r_{\mu,\alpha}$ and γ.

2: **for all** user μ **do**

3:     The CU calculates $\tau_{1,\mu}$ according to Eq. (3.88).

4:     The CU calculates the optical data rate $\dot{\lambda}_\mu$ according to Eq. (3.89);

5:     **if** $\dot{\lambda}_\mu \geq \gamma$ **then**

6:         User μ is allocated to LiFi AP $\tau_{1,\mu}$.

7:     **else**

8:         User μ is allocated to RF AP $\tau_{2,\mu}$, according to Eq. (3.90).

9:     **end if**

10: **end for**

11: **for all** AP α **do**

12:     Each AP determines the resource allocation for its serving users, according to Eq. (3.92).

13: **end for**

3.3.3.2 Resource allocation in SOA

In the RA step, each AP allocates the time resources to the connected users independently. Similar to JOA, the generalised utility function in Eq. (3.58) that considers both sum-rate and user fairness is used so that the RA can be formulated as a utility maximisation problem as expressed in Eq. (3.80). According to Eq. (3.87), the RA result of SOA consequently can be written as follows:

$$k_{\mu,\alpha}^{(\text{SOA})} = \frac{r_{\mu,\alpha}^{\frac{1}{\beta}-1}}{\sum_{i \in \mathcal{U}_\alpha} r_{i,\alpha}^{\frac{1}{\beta}-1}} \quad (\beta > 0). \tag{3.92}$$

Based on Eq. (3.91) and Eq. (3.92), the SOA can be summarised in Algorithm 6. In SOA, an optimal threshold is very crucial to enhance the system performance. It appears that a low threshold leads to overloaded LiFi attocells as well as an insufficient utilisation of RF resources whereas a high threshold leads to the inverse effect. In order to obtain an appropriate threshold, the characteristics of the LiFi and RF link data rates should be considered. These are closely related to the hybrid network topology and user distribution. Consequently, deriving a general closed-form solution of the optimal threshold in SOA is excessively complex to attain. In this study, therefore, a numerical simulation approach is used to find the best threshold.

3.3.4 QoS Enhancement in JOA and SOA

In the two previous subsections, two load balancing algorithms, JOA and SOA, are proposed. The user data rate in state n for both JOA and SOA can be written as follows:

$$R_\mu^{(n)} = \sum_{\alpha \in \mathcal{C}_\mathcal{L} \cup \mathcal{C}_\mathcal{R}} g_{\mu,\alpha}^{(n)} k_{\mu,\alpha}^{(n)} r_{\mu,\alpha}^{(n)}, \tag{3.93}$$

where $g_{\mu,\alpha}^{(n)}$ is given in Eq. (3.79) and Eq. (3.91) for JOA and SOA, respectively; and $k_{\mu,\alpha}^{(n)}$ is given in Eq. (3.79) and Eq. (3.92) for JOA and SOA, respectively. According to Eq. (3.93), the data rate of users that are using JOA can be expressed as a function of the fairness coefficient β, denoted by $R_{\mu,\text{JOA}}^{(n)}(\beta)$. Similarly, the data rate of users that are using SOA can be written as a function of the threshold γ and the fairness coefficient β, denoted by $R_{\mu,\text{SOA}}^{(n)}(\gamma, \beta)$. In JOA and SOA, the user data rate can be significantly affected by β. An increase in β results in a decrease in the system sum-rate, but it enables an improvement of the user fairness. Moreover, when employing SOA, the data rates are also affected by the threshold γ. The optimum threshold can contribute to an efficient utilisation of the multiple APs for users, which enables the system load to be well balanced.

In this study, it is assumed that all of the users have the same data rate request. The QoS is defined as the maximal achievable data rate of users given an outage probability. The QoS is denoted by Γ_0. The outage probability of the user QoS is defined as follows:

$$\Phi_0 = \Pr(\ R_\mu^{(n)} < \Gamma_0\ ). \tag{3.94}$$

This probability can be calculated by Monte Carlo simulations, which is expressed as follows:

$$\Phi_0 = \frac{\sum_n \text{Number of Users with } R_\mu^{(n)} < \Gamma_0}{\sum_n \text{Number of Total Users}} \tag{3.95}$$

In general, the design specifications of communication systems include a per user rate outage probability constraint. Let this outage probability constraint be denoted as Φ. The problem of maximising the QoS in JOA under the outage probability constraint can be formulated as
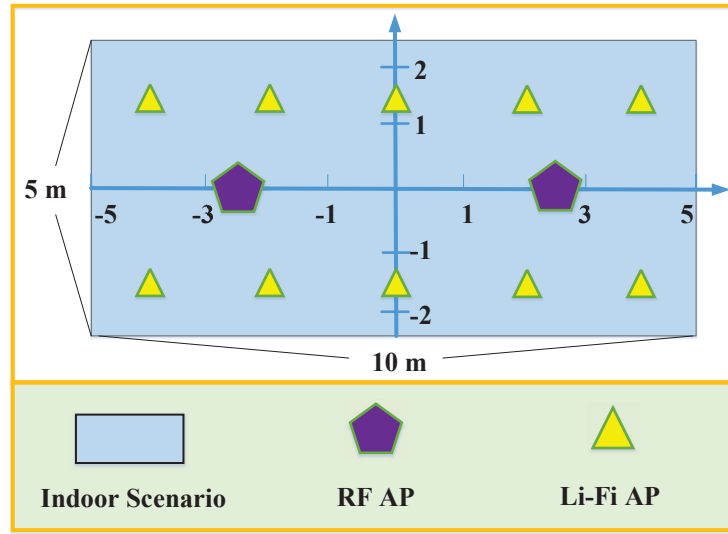
Figure 3.13: *Simulation scenario for optimisation-based LB schemes in HLRNs*

follows:

$$\Gamma_{\text{JOA}} = \max_{\beta} \ \Gamma_0, \tag{3.96}$$

$$s.t. \quad \text{Pr}(\ R^{(n)}_{\mu,\text{JOA}}(\beta) < \Gamma_0 \ ) \leq \Phi, \tag{3.97}$$

and the problem formulation in SOA becomes:

$$\Gamma_{\text{SOA}} = \max_{\beta, \ \gamma} \ \Gamma_0, \tag{3.98}$$

$$s.t. \quad \text{Pr}(\ R^{(n)}_{\mu,\text{SOA}}(\beta, \gamma) < \Gamma_0 \ ) \leq \Phi, \tag{3.99}$$

where $R^{(n)}_{\mu,\text{JOA}}(\beta)$ and $R^{(n)}_{\mu,\text{SOA}}(\beta, \gamma)$ can be calculated according to Eq. (3.93). Since the analytical investigation of the problems in Eq. (3.96) and Eq. (3.98) is challenging, numerical simulations are used to find the optimum values for β and γ, respectively.

72

Name of Parameters	Value
Vertical distance between APs and users, h_w	2 m
The range of the optical power per LiFi AP, P_{opt}	18 W
Baseband modulation bandwidth for LED lamp, B_{L}	30 MHz
The physical area of a PD, A_p	1 cm^2
Half-intensity radiation angle, $\theta_{1/2}$	30 deg.
Gain of optical filter, $T_s(\theta)$	1.0
Receiver FoV semi-angle, Θ_F	90 deg.
Refractive index, χ	1.5
Optical to electric conversion efficiency, κ	0.53 A/W
Transmitted power for each RF AP, P_{R}	10 dBm
Modulation bandwidth for each RF AP, B_{R}	10 MHz
Noise power spectral density in LiFi, N_{L}	-190 dBm/MHz
Noise power spectral density in RF, N_{R}	-75 dBm/MHz
Resource allocation interval of central unit, T_p	200 ms

Table 3.3: *Simulation parameters for optimisation-based LB schemes in HLRNs*

3.3.5   Performance Evaluation and Discussion

3.3.5.1   Simulation setup

As shown in Fig. 3.13, a 10 m $\times$ 5 m indoor office space is considered, which is equipped with 10 LiFi APs and 2 RF APs. It is assumed that the number of users in the simulation scenario is 30. All of the users move randomly in the indoor area, where the random way point model is applied [71]. The user speed is between 0 and 1 m/s. The average handover efficiency is defined as $\eta = \mathbb{E}[\eta_{ij}]$, where η_{ij} is defined in Eq. (3.4). The other parameters are given in Table 3.3, which is based on published research [18, 24, 34, 44, 70]. In the simulation, the outage probability is calculated based on 2000 realisations. We focus on the outage probability ranging between 0 and 0.2, and disregard the values from 0.2 to 1 since they are not practical.

In Section 3.3.5.2, the computational complexity of JOA and SOA is analysed. In Section 3.3.5.3, the effects of β and γ on JOA and SOA are studied, and the optimum values of β and γ to maximise the QoS are obtained. In Section 3.3.5.4, the effect of handover efficiency η on
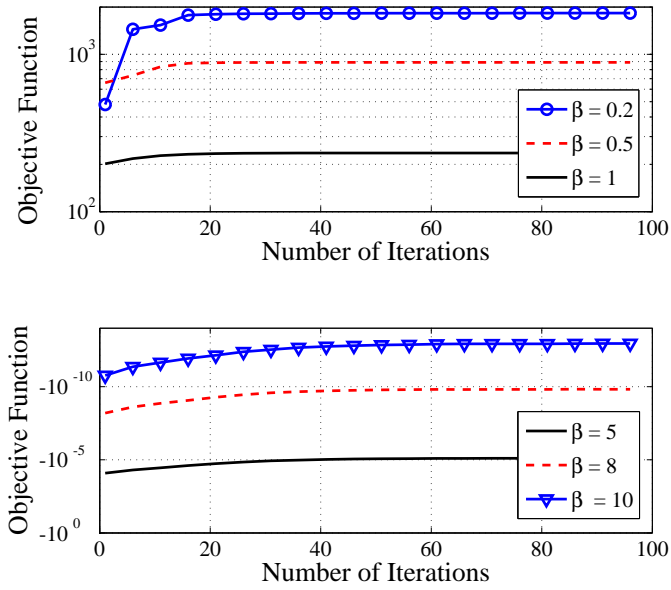
Figure 3.14: *The number of iterations with different fairness coefficient β*

Algorithm	Addition	Multiplication	Exponentiation
JOA	$O(N_u N_{\mathrm{ap}} I)$	$O(N_u N_{\mathrm{ap}} I)$	$O(N_u N_{\mathrm{ap}} I)$
SOA	$O(N_u N_{\mathrm{ap}})$	$O(N_u)$	$O(N_u)$

Table 3.4: *Computation Complexity between JOA and SOA ($N_{ap} = N_l + N_r$)*

network load balancing are investigated, and the performance of the maximum achievable QoS (MAQ) in JOA and SOA is compared with that of conventional load balancing schemes.

3.3.5.2 Evaluation of computational complexity

In JOA, $g_{\mu,\alpha}^{(\mathrm{JOA})}$ and $k_{\mu,\alpha}^{(\mathrm{JOA})}$ can be obtained after several iterations, and the required number of the iterations is denoted by I. In Fig. 3.14, the objective function in Eq. (3.65) with respect to the number of iterations is shown. It can be seen that I increases with the fairness coefficient β. This signifies that when β tends to be infinite, JOA is not feasible due to the prohibitive complexity required. In order to avoid a large number of iterations, the values for β in the range $0 < \beta < 10$ is only considered for JOA in this study.

In SOA, $g_{\mu,\alpha}^{(\mathrm{SOA})}$ and $k_{\mu,\alpha}^{(\mathrm{SOA})}$ can be calculated without iterations. The number of additions, multiplications and exponential operations in both JOA and SOA are summarised in Table. 4.2,

where $N_{ap} = N_l + N_r$, is the number of the APs. As shown, the number of the three types of computations in JOA are all greater than those in SOA. With the configuration $N_u = 30$, $N_{ap} = 12$ and $I = 40$, the average numbers of the three operations are evaluated in Matlab. The simulation shows that the number of additions in JOA is 66 times greater than that in SOA; the number of multiplications in JOA is 1445 times greater than that in SOA; and the number of exponentiation in JOA is 1440 times greater than that in SOA. The gap between the computational complexity of JOA and SOA increases as the parameters, N_u, N_{ap} and I increase. Therefore, it can be concluded that SOA achieves much lower computational complexity than JOA.

3.3.5.3 Effects of β and γ on JOA and SOA

In this subsection, the maximum QoS achieved by the proposed schemes is analysed and the effects of β and γ on JOA and SOA are evaluated. The handover efficiency, η is set to be 1, which means the handover overhead is neglected in this case.

a) JOA Case: Fig. 3.15 shows that the QoS for JOA is a function of the outage probability. It can be seen that Γ_0 increases as β increases from 0.5 to 2, but reduces when β increases up to 5. This is because a higher β means better user fairness is achieved, resulting in an increase of Γ_0. However, in order to improve the fairness performance, some time resource should be allocated to the users with poor channel gains, and this leads to a decrease in the user data rates. Thus, when β is set to be very large, Γ_0 in the hybrid network would be low. The simulation results show that the maximum QoS in JOA is achieved at $\beta = 2$ for $0.02 \leq \Phi \leq 0.2$, and $\beta = 5$ can achieve the maximum QoS for the range of $0 \leq \Phi < 0.02$.

b) SOA Case: The QoS performance for SOA is affected by both the threshold, γ and the fairness coefficient, β. Fig. 3.16 shows the QoS Γ_0 performance corresponding to β and γ with $\Phi = 0.1$. As shown, Γ_0 always increases with β for any threshold. Also, Fig. 3.17 shows that Γ_0 increases with β when the outage probability constraint is between 0 and 0.2. It can be concluded that for given Φ and γ, QoS performance always improves as β increases. This means that the optimum fairness coefficient β tends to be positive infinite, where the max-min fairness is achieved. According to Eq. (3.92), the time resource proportion to achieve the

maximum QoS in SOA can be written as follows:

$$k_{\mu,\alpha}^{(\text{SOA})} = \frac{r_{\mu,\alpha}^{-1}}{\sum_{i\in\mathcal{U}_\alpha} r_{i,\alpha}^{-1}}. \tag{3.100}$$

The time resource allocation in SOA is undertaken independently for each AP. Thus, β here represents the fairness of the users in each cell, and not in the entire system.

Fig. 3.18 shows the QoS of users with respect to γ and Φ, where β approaches infinity. It can be seen that Γ_0 is a concave function of γ for a specific, Φ. This is because a large threshold results in a large number of users allocated to RF APs, and thus the user data rates in the RF cells would be low. On the other hand, for a small value of γ, the number of users served by LiFi increases so that a low data rate performance of LiFi is achieved. It can be seen that the optimal γ decreases as Φ increases. Specifically, the optimum γ is 9 Mb/s at $\Phi = 1\%$; and it decreases to 3 Mb/s at $\Phi = 15\%$. With the optimum γ and $\beta \to +\infty$, the maximum QoS in SOA can be achieved.
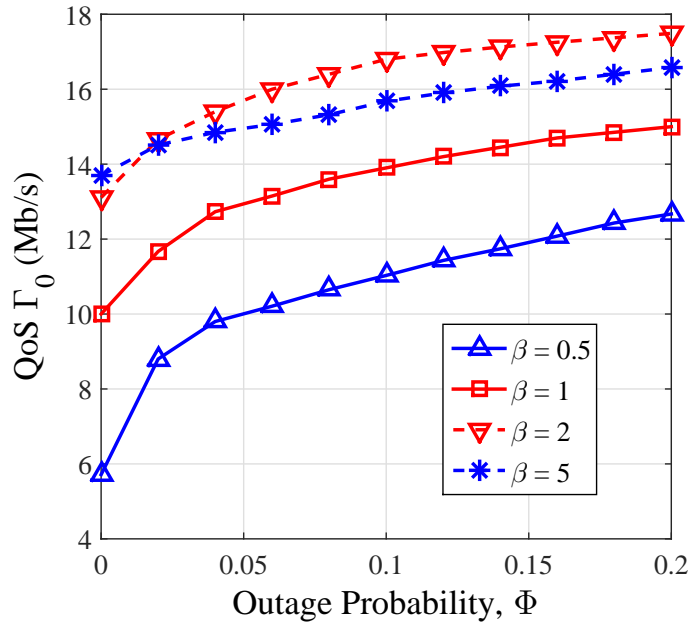
Figure 3.15: *QoS Γ_0 with outage probability constraints in JOA ($\eta = 1$)*
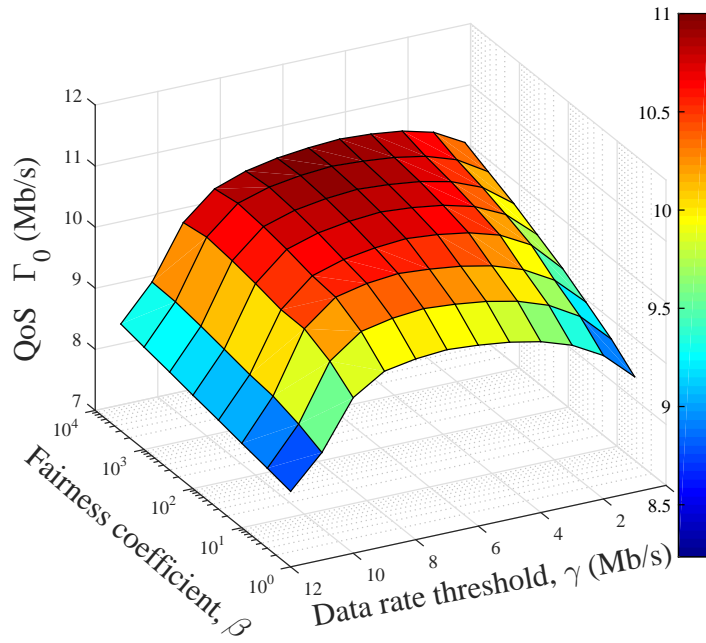
Figure 3.16: *QoS Γ_0 with respect to β and threshold γ in SOA ($\Phi = 0.1$, $\eta = 1$).*
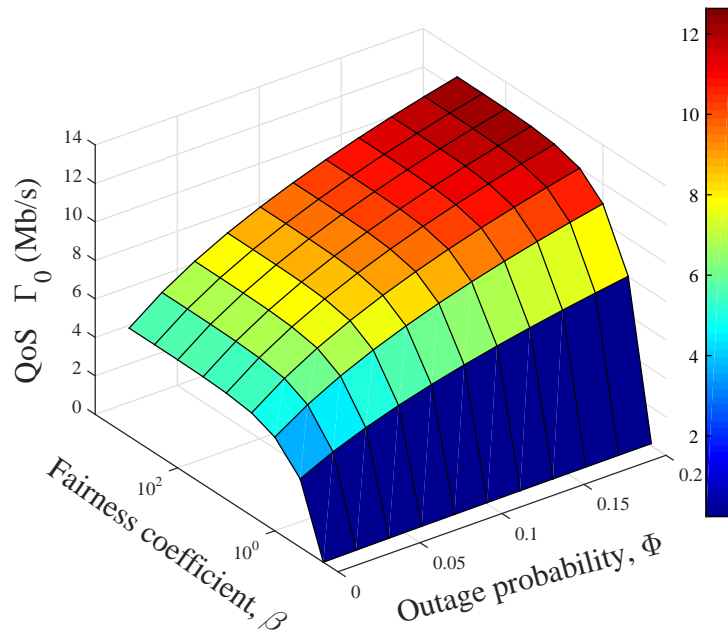
Figure 3.17: *QoS Γ_0 with respect to β and Φ in SOA (γ is optimised, $\eta = 1$)*
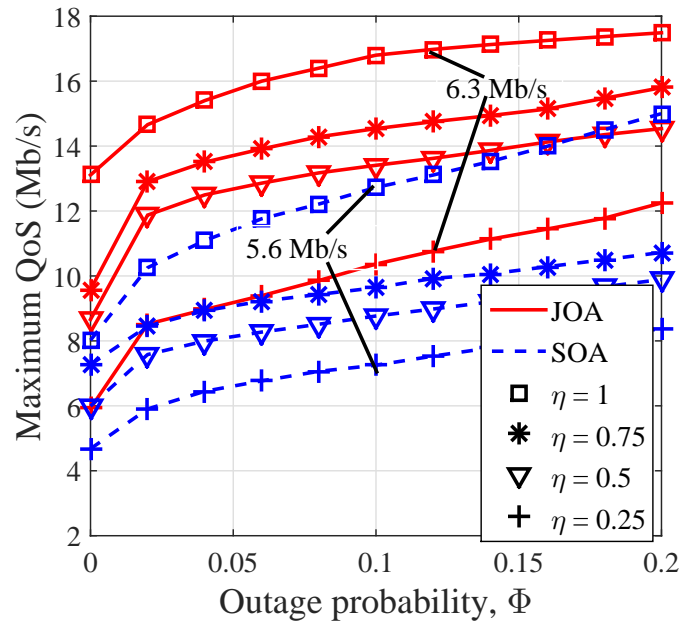
Figure 3.19: *The maximum QoS corresponding to Φ with different values of η by using JOA and SOA*
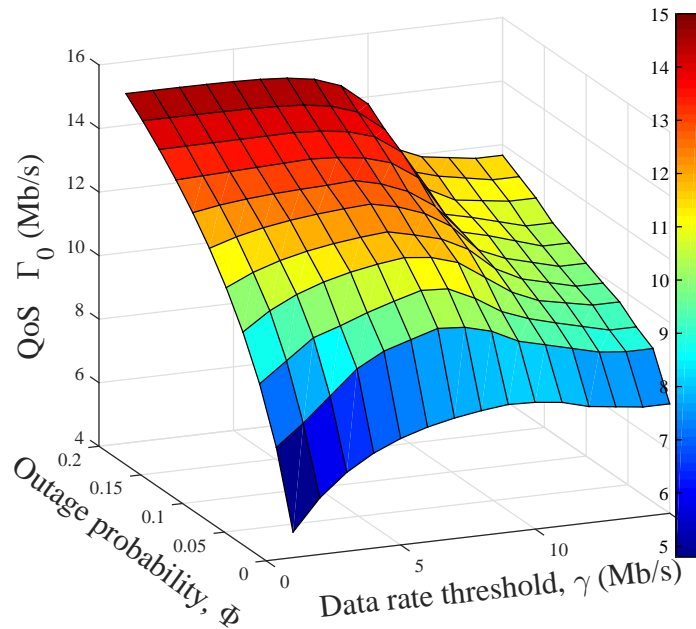
Figure 3.18: *QoS Γ_0 with respect to γ and Φ in SOA ($\beta \to +\infty$, $\eta = 1$)*

3.3.5.4 Effect of η on load balancing

The effect of handover efficiency η on JOA and SOA is evaluated and presented in Fig. 3.19. The maximum QoS of JOA and SOA with $\Phi = 0.1$ are 16.8 Mb/s and 12.8 Mb/s, respectively. This means that 90% of the users can approximately achieve 1.3 times higher data rate in JOA than in SOA. In both algorithms, the maximum QoS decreases along with η, and a large η results in a steep reduction. The simulation results show that when η increases from 0.25 to 1, the maximum QoS is improved by approximately 6.3 Mb/s and 5.6 Mb/s in JOA and SOA, respectively.

Fig. 3.20 shows the performance of the maximum QoS for different algorithms. In the legend, 'HS' refers to the proposed handover scheme that is used in conjunction with load balancing algorithms while 'nonHS' refers to the direct handover strategy. It shows that the proposed handover scheme is able to enhance the user QoS. Specifically, the proposed handover algorithm achieves a data rate improvement of 2 Mb/s over the 'nonHS' scheme. Apart from JOA and SOA, two benchmark algorithms are considered for comparison, where the AP assignment and the resource allocation are undertaken separately. In the first benchmark algorithm, random AP allocation and the max-min fairness scheduler are used, termed as 'RMF'. In the second benchmark algorithm, random AP allocation and the proportional fairness scheduler are used, termed as 'RPF'. It is shown that the maximum QoS achieved by RMF and RPF are very close, and this maximum QoS in JOA and SOA are approximately 8 Mb/s and 3 Mb/s higher than that in RMF and RPF, respectively. Moreover, the performance of the system average data rate for these four algorithms is evaluated and given in Table. 3.5. It can be seen that the average data rate in SOA is slightly higher than that in RMF and RPF, and JOA outperforms the other three algorithms. For the the average data rate, JOA achieves an improvement of 50% compared to SOA.

A lower handover efficiency means that additional capacity would be sacrificed because of the increased handover overhead. Theoretically, it is possible that the handover time is longer than T_p and the handover efficiency is 0. In that case, users cannot select other APs because the handovers can not be finished during the current state. Thus, the achievable data rate during this state is zero if users try to switch APs.
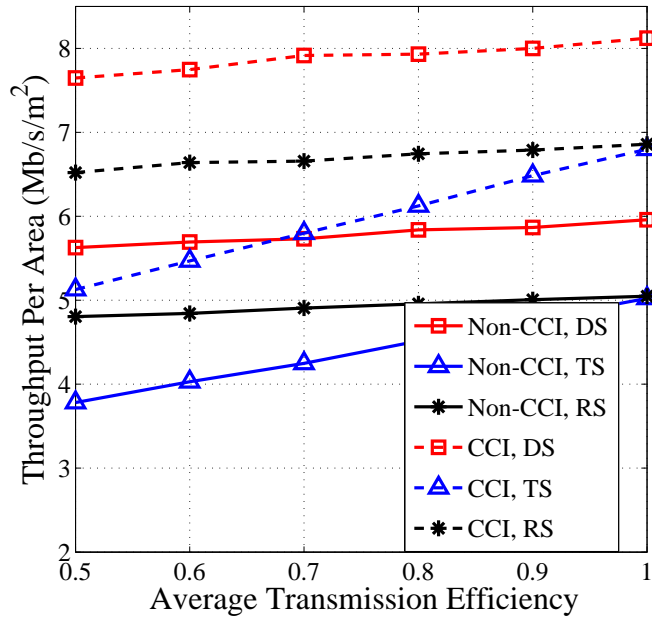
Figure 3.20: *The maximum QoS with the average handover efficiency for four different algorithms. ($\Phi = 0.1$)*

η	JOA (Mb/s)	SOA (Mb/s)	RMF (Mb/s)	RPF (Mb/s)
0.5	28.42	18.77	18.05	18.21
1	38.61	26.94	25.89	26.51

Table 3.5: *System average data rate ($\Phi = 0.1$)*

3.3.6 Discussion

In this section, a dynamic load balancing scheme for indoor LiFi and RF hybrid networks is proposed, and the handover overhead caused by user mobility is considered. Two load balancing algorithms, JOA and SOA, are proposed which jointly and separately optimise APA and RA, respectively. In order to achieve the maximum unified QoS, the optimum fairness coefficient and data rate threshold in both algorithms are obtained by using numerical simulations. Simulation results show that in a typical indoor scenario, the maximum QoS for more than 90% of the users in JOA is approximately 1.3 times higher than that in SOA. Also, the average data rate in JOA is 1.5 times higher than that in SOA. However, the computational complexity of JOA is significantly higher, and in some instances, it can be more then 1000 times greater than that of SOA. This means that SOA can offer a better performance/complexity trade-off than JOA for system load balancing.

3.4   Fuzzy Logic based dynamic LB Scheme

In Section 3.2 and Section 3.3, dynamic load balancing with handover for hybrid LiFi/RF networks is studied. As shown in the handover scheme proposed in Section 3.2.1, the APA and the RA can only consider the handover effect between the current state and the next state. However, fast user movement and the occasional strong blockage or angular misalignments of LiFi signals would prompt ping-pong handovers between LiFi and RF APs, and this effect was not taken into account in the earlier study. In this section, a novel dynamic handover scheme based on fuzzy logic (FL) is proposed [77]. The fuzzy logic method can combine a large number of input information (e.g. instantaneous and average CSI, user speed and required data rate of users) to determine a suitable load balancing solution with low-complexity, the aim of which is to improve the system throughput [78–80].

3.4.1   System setup

Referring to Section 2.1-2.2, an indoor hybrid LiFi/RF network is considered. It is assumed that there are N_l LiFi APs, and the entire scenario is covered by a single RF AP. The set of LiFi APs is denoted by $\mathcal{C}_{\mathcal{L}} = \{l| \ l \in [1, N_l], l \in \mathbb{N}\}$, and the RF AP set is denoted by $\mathcal{C}_{\mathcal{R}} = \{r\}$. The optical modulation bandwidth is reused in each LiFi attocell, and the optical CCI in the overlap area is treated as noise in this model. The hybrid network serves multiple users that are stationary or roaming in the indoor scenario. Note, these users could be internet-of-things (IoT) devices or mobile handsets. The set of users is denoted by $\mathcal{U}$. In each quasi-static state, every user has a random required data rate, denoted by λ_μ, which follows an independent identical Poisson distribution. The system CU determines the AP assignment and time resource allocation for each user, and it is connected to all of the APs through error free communication links. The sequence number of the states is denoted by a natural number n. When a user is allocated to different APs in two adjacent states, a handover is prompted, and the handover overhead is also considered in the performance analysis. The SINR (or SNR) for the LiFi and RF links is based on Eq. (3.55) and Eq. (3.56). Adaptive bit loading is used for both LiFi and RF systems, and the modulation and coding scheme is given in Table 2.1. The link data rate between user μ and LiFi AP α is denoted by $\dot{D}_{\mu,\alpha}$. The link data rate between user μ and the RF AP is denoted by $D_{\mu,r}$.

In the indoor scenario, it is possible that the LoS links of LiFi are blocked by surrounding

objects, people moving or angular misalignments of transmitter and receiver field of views (FoVs). These events are random and unpredictable. Here it is assumed that the blocking events follow the Bernoulli distribution, which indicates whether the LiFi reception is blocked or not [24]. Its probability mass function is expressed as:

$$I(k) = \begin{cases} 1-p, & k=1 \\ p, & k=0 \end{cases}, \tag{3.101}$$

where p denotes the LiFi LoS blocking probability. The LiFi link data rate with blocking considered is expressed as $D_{\mu,\alpha} = k\dot{D}_{\mu,\alpha}$, where k is a binary random variable according to (3.101).

In each state, the CU allocates the most suitable AP to each user. In order to reduce the complexity, the set of allocatable APs for users only contains the RF AP and the LiFi AP with the highest SINR, which can be expressed as $\mathcal{Y}_\mu = \{l_\mu, r\}$, where r is the RF AP; and $l_\mu = \arg\max_{\alpha \in \mathcal{C}_\mathcal{L}} \text{SINR}_{\mu,\alpha}$, where $\text{SINR}_{\mu,\alpha}$ is according to (3.55).

3.4.2 Dynamic Load Balancing Scheme with Fuzzy Logic

3.4.2.1 Dynamic handover scheme

In the dynamic hybrid LiFi/RF network, the CU determines the AP assignment and resource allocation for users periodically. When a user is assigned to different APs, a handover is prompted. In general, the handover overhead in an indoor scenario is in the order of milliseconds. The overhead time can be modelled as a Poisson random process, and the probability mass function (PMF) of the overhead is given in Eq. (3.3). In this study, it is assumed that all of the handovers follow an independent and identical Poisson distribution, and the Poisson parameter is denoted by ζ. Due to the overhead, users achieve zero data rates during the handover period. The number of states considered in the dynamic handover scheme is denoted by N_s.

In order to reduce the data rate loss during user movement, a load balancing scheme is designed and the following information is considered to be known at the CU in each state: i) the SINR between users and the APs belonging to $\mathcal{Y}_\mu$; ii) the average SINR achieved by l_μ during the last M states; iii) the speed of users; and iv) the required data rate. In each state, the CU determines the AP allocation and resource allocation based on the FL method, which will be given in this subsection.

3.4.2.2 FL based load balancing scheme

In this subsection, a FL based scheme for load balancing in each state is proposed. The FL method yields a truth value in a certain range instead of making a 'hard decision'. In general, there are four steps in a fuzzy logic system: fuzzification, rule evaluation, defuzzification and decision making [77, 78].

1) Fuzzification: This process is to convert the inputs of the FL system into crisp values with membership functions (MFs). In this study, the input contains four types of variables, namely, the instantaneous SINR of LiFi AP l_μ; the average SINR of LiFi AP l_μ during the last M states; the user speed; and the required data rate. It is assumed that each user uploads all of the input information to the CU in each state without delay. In this process, each type of input is represented by three grades: low, medium and high. For each grade, a value between 0 and 1 is returned to describe how much the input fits that grade. The triangular function is applied as the MF, which is described by:

$$f_{\text{TRI}}(x; a, b) = \begin{cases} 0, & x \le a \\ \frac{x-a}{b-a}, & a < x \le b \\ 1, & x > b \end{cases}, \tag{3.102}$$

and the fuzzified values for the three grades can be expressed as:

$$
\begin{aligned}
\text{Low:} \quad & 1 - f_{\text{TRI}}(x; c_1, c_2), \\
\text{Medium:} \quad & \begin{cases} f_{\text{TRI}}(x; c_1, c_2), & x \le c_2 \\ 1 - f_{\text{TRI}}(x; c_2, c_3), & x > c_2 \end{cases}, \\
\text{High:} \quad & f_{\text{TRI}}(x; c_2, c_3),
\end{aligned}
\tag{3.103}
$$

where x is the input; and $c_1 \le c_2 \le c_3$ are the breakpoints of the MF for each type of input. Fig. 3.21 shows an example of fuzzification for the input of the required data rate, where $c_1 = 1$, $c_2 = 5$, $c_3 = 9$ (Mb/s). As shown, given an input of 2.5 Mb/s, the fuzzified values of the three grades for the required data rate can be calculated, which are 0.625, 0.375 and 0, respectively. The other types of inputs are dealt with in the similar way, and the corresponding breakpoints can be determined based on the statistical information of the input data. In this step, each user obtains a fuzzy set that consists of 12 crisp values to describe all of the four types of inputs in the three grades.
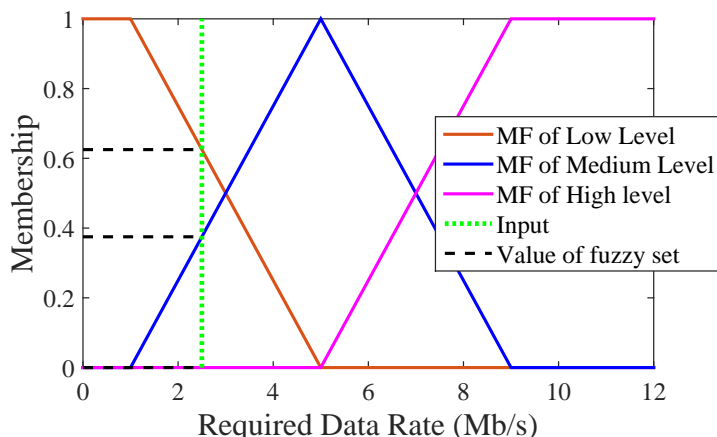
Figure 3.21: *Fuzzification*

Rule No.	Ins. SINR	Ave. SINR	Speed	Required Rate	AP Allocation
1	*not* Low	-	Low	-	LiFi
2	-	*not* Low	Low	-	LiFi
3	-	*not* Low	*not* High	Low	LiFi
4	-	-	High	-	RF
5	Low	-	*not* Low	*not* Low	RF
6	Low	Low	-	-	RF
7	*not* High	Low	Low	-	RF
8	-	Low	Medium	-	RF

Table 3.6: *Fuzzy Rules (Combining operation: multiplication)*

2) Rule Evaluation: In this procedure, the crisp values in the fuzzy set of inputs are combined based on the fuzzy rules to determine the 'score' of the outputs. The output of the AP allocation for each user has two possibilities: the best LiFi AP l_μ and the RF AP. The fuzzy rules are defined in Table 3.6. These rules are heuristic and self-explanatory. Essentially, they are intuitive guidelines on why a specific user is allocated to its best LiFi AP or the RF AP, denoted by 'LiFi' and 'RF' respectively in Table 3.6. For example, users with low instantaneous LiFi SINR but high average SINR can still be allocated to a LiFi AP because it is probably caused by transient LoS blockage of objects (rule 2 and 3); or allocating the RF AP to users with high speed is beneficial due to no handover prompted (rule 4); Users that move around the LiFi cell edge should be served by RF to avoid ping-pong effect (rule 6-8). The result of the rule evaluation step yields an output set for each user, which contains 8 crisp values for each user and represents how much this user should be allocated to the LiFi AP or the RF AP.
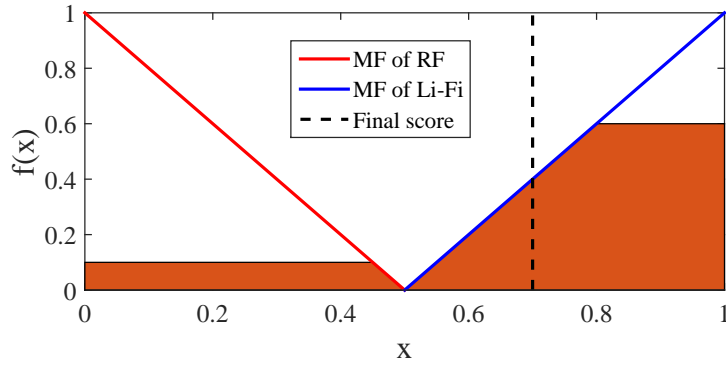
Figure 3.22: *Defuzzification*

3) Defuzzification: This process determines the final score of the AP allocation for each user. According to the rule evaluation step, the maximal score of output state 'LiFi' from rule 1 to rule 3, denoted by v_l, and the maximal score of output state 'RF' from rule 4 to rule 8, denoted by v_r, constitute a fuzzy set of output. Fig. 3.22 shows the defuzzification process of the proposed FL algorithm. Similar to fuzzification, a MF of each output state (LiFi or RF) is applied to describe the relationship between that state and the score. The shaded area shown in Fig. 3.22 represents the weight of each state in the fuzzy set. The centre of gravity of this fuzzy set is calculated for the final score [77], which is expressed as:

$$\omega_\mu = \frac{\int_0^1 f(x)x \, \mathrm{d}x}{\int_0^1 f(x) \, \mathrm{d}x},$$ (3.104)

where $f(x)$ is the upper edge of the shaded area based on the rule evaluation process, which is written as:

$$f(x) = \begin{cases} \min(f_{\mathrm{MR}}(x), v_r), \ 0 \le x \le 0.5 \\ \min(f_{\mathrm{ML}}(x), v_l), \ 0.5 < x \le 1 \end{cases},$$

(3.105)

where $f_{\mathrm{MR}}(x) = 1 - f_{\mathrm{TRI}}(x; 0, 0.5)$ is the MF of the output state RF; and $f_{\mathrm{ML}}(x) = f_{\mathrm{TRI}}(x; 0.5, 1)$ is the MF of output state LiFi. The final score ω_μ for user μ ranges from 0 and 1, and describes the preference for LiFi AP allocation. For example, the user with a score of 0.8 is more preferable to connect to their best LiFi APs than one with a score of 0.5.

4) Decision Making: In this step, the AP allocation is determined by the CU according to the final score of each user. The set of users for which the LiFi AP with the highest SINR is α

Algorithm 7 Decision-making Algorithm

1: Initialisation: $\omega_\mu, \mathcal{U}_\alpha, \bar{S}_L \to +\infty, \bar{S}_R = 0, \mathcal{C}_\alpha = \varnothing \ (\alpha \in \mathcal{C}_\mathcal{L})$, and $\mathcal{C}_r = \mathcal{U}$.

2: **while** $|\bar{S}_L - \bar{S}_R| \leq \varepsilon$ **do**

3:     **for all** each LiFi AP $\alpha \in \mathcal{C}_\mathcal{L}$ **do**

4:         **if** $\mathcal{U}_\alpha \neq \varnothing$ **then**

5:             $\dot{\mu} = \max_{\mu \in \mathcal{U}_\alpha} \omega_\mu$;

6:             $\mathcal{C}_\alpha \Leftarrow \dot{\mu}$;

7:             Remove $\dot{\mu}$ from $\mathcal{U}_\alpha$;

8:             Remove $\dot{\mu}$ from $\mathcal{C}_r$;

9:             Calculate the satisfaction for each assigned user based on (3.107);

10:         **end if**

11:     **end for**

12:     Calculate the satisfaction for users belonging to set $\mathcal{C}_r$.

13:     Calculate the average satisfaction $\bar{S}_L$ and $\bar{S}_R$.

14: **end while**

---

is denoted by $\mathcal{U}_\alpha$. The TDMA method is applied for resource allocation in each cell. The proportion of the time resource for user μ is expressed as:

$$k_{\mu,\alpha} = \frac{\lambda_\mu / D_{\mu,\alpha}}{\sum_{i \in \mathcal{C}_\alpha} \lambda_i / D_{i,\alpha}}, \tag{3.106}$$

where λ_μ is the required data rate of user μ; $D_{\mu,\alpha}$ is the link data rate between user μ and AP α; and $\mathcal{C}_\alpha$ is the set of users allocated to AP α. Accordingly, users served by the same AP can achieve equal satisfaction. The user satisfaction, denoted as the quality of service (QoS), can be expressed as:

$$S_{\mu,\alpha} = \max\{1, \frac{k_{\mu,\alpha} D_{\mu,\alpha}}{\lambda_\mu}\} = \max\{1, \frac{1}{\sum_{i \in \mathcal{C}_\alpha} \lambda_i / D_{i,\alpha}}\}. \tag{3.107}$$

Note that the average QoS achieved by LiFi APs and the RF AP are defined as $\bar{S}_L = \sum_{\alpha \in \mathcal{C}_\mathcal{L}} S_{\mu,\alpha}$ and $\bar{S}_R = \sum_{\alpha \in \mathcal{C}_\mathcal{R}} S_{\mu,\alpha}$. This process follows two principles: i) the users that belong to $\mathcal{U}_\alpha$ and that achieve high scores have priority to gain access to the LiFi AP α; and ii) the average satisfaction values achieved by LiFi and RF are equal. The decision-making algorithm is summarised in Algorithm 7.

Breakpoint	Ins. SINR [dB]	Ave. SINR [dB]	Speed [m/s]	Required Rate [Mb/s]
c_1	1	1	0.1	1
c_2	5	5	0.6	5.5
c_3	11	11	1.1	10

Table 3.7: *Breakpoints Setup for the FL-based LB scheme*

3.4.3 Simulation Results

3.4.3.1 Simulation setup

Referring to Fig. 3.23, a 18 m × 18 m indoor office with 36 LiFi APs and one RF AP is considered as the simulation scenario. The deployment of LiFi APs follows a square lattice topology which models a regular light placement commonly used in large offices and public places. The RF AP is deployed in the centre of the room. The movement of users follows the random way point model [71], with movement speed uniformly distributed between 0 and 1.2 m/s. The required data rate of users follows a Poisson distribution with parameter 5 Mb/s.

According to (3.101), users may be blocked in the indoor scenario, and the duration of blocking time follows a Poisson distribution with parameter 1000 ms [81]. The breakpoints c_1, c_2 and c_3 for each type of input of FL system is given in Table 3.7. The other simulation parameters are given in Table 3.8.
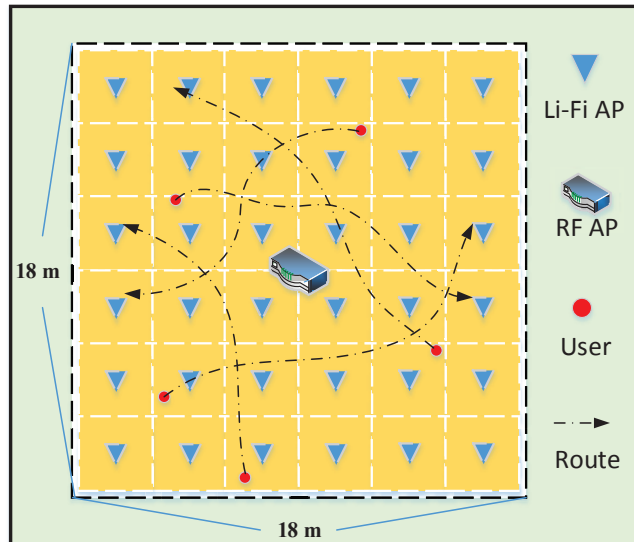
Figure 3.23: *Simulation Scenario of LiFi/RF Hybrid Network*

Name of Parameters	Value
Range of optical power of the LiFi APs, P_{opt}	20 W
LiFi baseband modulation bandwidth, B_{L}	20 MHz
The physical area of a PD, A_p	1 cm^2
Half-intensity radiation angle, $\theta_{1/2}$	60 deg.
Gain of optical filter, $T_s(\theta)$	1.0
Receiver FoV semi-angle, Θ_F	60 deg.
Refractive index, χ	1.5
Optical to electric conversion efficiency, γ	0.53 A/W
Transmitted power of the RF AP, P_{R}	20 dBm
RF modulation bandwidth, B_{R}	80 MHz
Noise power spectral density of LiFi, N_{L}	10^{-19} A^2/Hz
Variance of AWGN in RF systems, σ^2	-57 dBm
LiFi LoS blocking probability, p	0.1
Number of states for average LiFi link data rate, M	10
Duration of a state, T_p	100 ms
The number of states N_s	6000

Table 3.8: *Simulation parameters for the FL-based LB scheme*
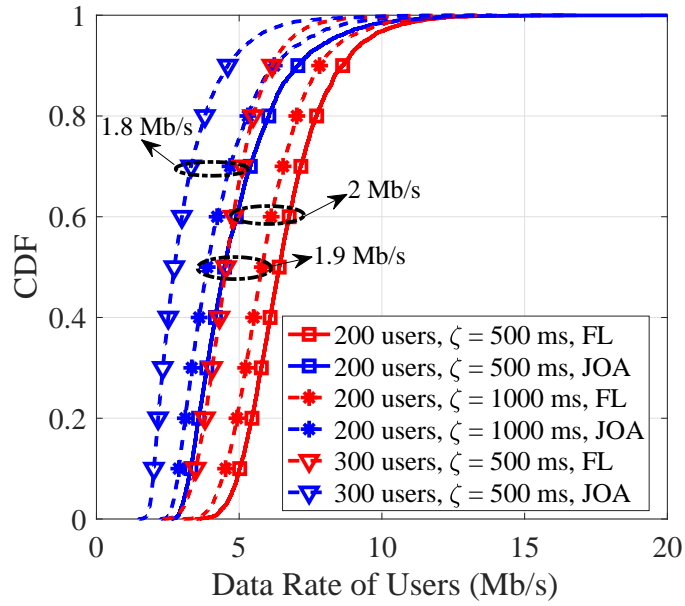
Figure 3.24: *CDF of user data rate (Proportional fairness scheduler is considered in JOA).*

3.4.3.2 Simulation Results

The cumulative distribution function (CDF) of the user data rate with the proposed dynamic handover scheme is evaluated and presented in Fig. 3.24. Also, a conventional algorithm is considered [34], to optimise the system throughput only based on the SINR of LiFi and RF links and the handover overhead in the current state. In this scheme, the RF AP would be assigned to users when they are at the LiFi cell edge or outside the LiFi coverage, and the LiFi APs serve users which are close to the cell centre. Thus, when users move through LiFi attocells continuously, a ping-pong pattern of handover occurs. In the legend of Fig. 3.24, the proposed scheme is denoted by 'FL'. Also, JOA with handover scheme which is presented in Section 3.2.1 is considered as benchmark algorithm in this simulation. As shown, the data rate performance of the proposed scheme is better than that with the conventional algorithm. In the case of 200 users and 500 ms average handover overhead, the gain of user data rate is approximately 2 Mb/s. This means that the proposed handover scheme achieves less data rate loss than the benchmark algorithm. The user data rates with both schemes decrease with an increase in the handover overhead. When the overhead is set to 1000 ms, the gain achieved by the proposed scheme slightly decreases to 1.9 Mb/s. Also, the number of users has an influence on the data rate performance. The difference between the two schemes is 1.8 Mb/s with 300
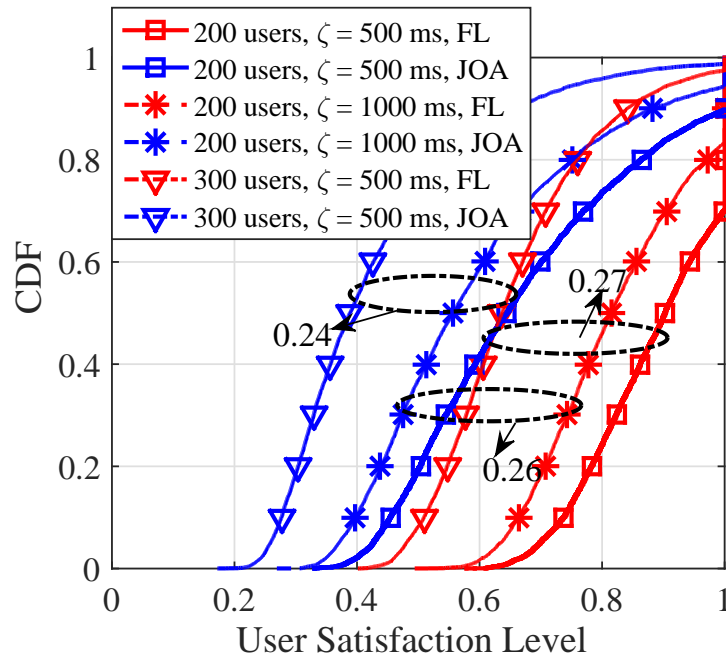
Figure 3.25: *CDF of user QoS (Proportional fairness scheduler is considered in JOA).*

users and 500 ms of average overhead. In the practical indoor scenarios, the proposed algorithm can improve the data rate performance by 40%, compared to the conventional load balancing algorithms.

In Fig. 3.25, the performance of the user QoS is presented, and the user QoS is calculated according to (3.107). As shown, the proposed scheme outperforms the benchmark algorithm, and the difference between the two algorithms is approximately 0.27 in the case of 200 users and $\zeta = 500$ ms. Specifically, Fig. 3.25 shows that 30% of users can achieve a full satisfaction level ($S_{\mu,\alpha} = 1$) using the FL method; this is only 10% of users when the conventional algorithm is used. Similarly, an increase in the number of users or in the handover overhead results in a decrease in user QoS.

3.4.4 Discussion

In this section, a LiFi/RF hybrid network in a practical indoor scenario is considered, and a FL based dynamic load balancing scheme is proposed to mitigate the handover effects. Information on user speed and time-average LiFi SINR is employed in the proposed algorithm so that users with fast movement or who experience transient shadowing effect can be allocated to more suitable APs than determined by the conventional algorithm, and also a ping-pong pattern of

handover is avoided. The simulation shows that the FL based dynamic load balancing scheme has less data rate loss than the conventional load balancing algorithms, and a 40% performance improvement is achieved in terms of both data rate and user QoS.

3.5 Summary

In this chapter, the dynamic load balancing for hybrid LiFi/RF networks with handover is investigated. Firstly, an optimisation-based LB scheme with proportional fairness is proposed, and the throughput performance of the hybrid LiFi/WiFi system is theoretically analysed. Also, the effects of the handover overhead on handover locations and user throughput are simulated and discussed. It has been shown that the WiFi and LiFi throughputs in the hybrid network are related despite the independent spectrum transmission. The LiFi throughput can be improved by increasing the WiFi throughput due to efficient load balancing. In Section 3.3, the dynamic load balancing with a variety of fairness schemes is studied, where two specific algorithms JOA and SOA that optimise the APA and the RA in each quasi-static state are proposed. Moreover, a unified data rate requirement of users is considered as a QoS metric and user outage probability is introduced. Simulation results show that SOA can offer a better performance/complexity trade-off than JOA for system load balancing. In Section 3.4, a fuzzy logic (FL) based dynamic LB scheme which jointly handles APA, RA and handover is proposed. Unlike the optimisation-based schemes, this FL scheme uses not only the CSI, but also the user speed and desired data rate to determine whether a handover needs to be prompted. Simulation shows that the proposed scheme outperforms the conventional LB algorithms, and the performance improvement is approximately 40% in terms of both data rate and user satisfaction level.

Chapter 4

Load Balancing with Shadowing Effects for HLRNs

4.1 Introduction

As shown in Chapter 1 and 2, the hybrid LiFi/RF network is able to mitigate the spatial fluctuation of data rate, offering a system throughput greater than that of stand alone LiFi or RF networks [34]. Most published research considers an ideal system model of hybrid networks, especially the LiFi channel model. In order to attain a more accurate evaluation of the system performance, three practical factors must be taken into account:

i). Blockage: In general, the signals of line of sight (LoS) paths contribute to most received signal power in a LiFi system [82]. In an indoor scenario, opaque objects such as people and furniture can block the LoS optical channel and this would significantly compromise the data rate performance. Therefore, the shadowing effect in a LiFi system needs to be considered.

ii). Receiving orientation angle (ROA): In most published research, the LiFi receiver is always assumed to be oriented perpendicularly upwards and for simplicity the incidence angle is set equal to the angle of irradiation. However, it has been shown in [43] that this incidence angle varies depending on the users' behaviour pattern and would significantly affect the receive SNR. Therefore a random ROA needs to be considered in the LiFi system model.

iii). User data rate requirement: Published research with respect to hybrid networks focuses on the improvement of system throughput and user fairness [23, 34, 83]. In general, each user has a required data rate in a short period to support certain wireless services such as browsing a web page, on-line video stream and voice over Internet protocol (VoIP). On the one hand, achieving a lower data rate than required would affect the quality of service (QoS) of users. On the other hand, a higher data rate than the requirement may lead to inefficient use of precious resources and possibly result in an overload of other cells. Therefore, user data rate requirements should be considered in the system load balancing (LB) for hybrid networks.

The system throughput and user satisfaction levels in hybrid LiFi/RF networks can be enhanced by using efficient LB techniques, which address two main issues: AP assignment (APA) and resource allocation (RA). In [23, 34], the APA and the RA are jointly optimised, and an iterative algorithm is given to find an optimal solution. In order to reduce the computational complexity, a LB scheme that separately optimises the APA and the RA is proposed in [18, 83], but the achievable data rates are significantly compromised. Therefore a novel LB scheme that can offer a proper performance/complexity trade-off is necessary. Moreover, when considering user data rate requirement, a piecewise function is normally needed to quantify the satisfaction of users because a data rate higher than the one required no longer increases the users' satisfaction level [84]. The conventional joint optimisation methods are NP-hard problems [23, 34]. Taking the user data rate requirement into account would further increase the complexity and result in a mathematically intractable problem. In this study, an evolutionary game theory (EGT) based LB scheme is proposed, where the problems of APA and RA are jointly handled. This algorithm accommodates the user data rate requirement for resource allocation and a novel RA scheme that makes full use of the communication resources is proposed. This EGT algorithm can greatly improve the system throughput while achieving low computational complexity.

4.1.1 Evolutionary game theory

In recent literature, game theory has been extensively applied to network selection and interference management problem in heterogeneous wireless networks [85–87]. The Nash equilibrium (NE) is the most commonly used solution to the non-cooperative game because it ensures that no player can improve its payoff without compromising another player. However, when there are multiple NEs in the game, a refined solution is required to ensure users' payoff reaches a stable status. Evolutionary equilibrium (EE), which is based on the EGT, can provide such a refined solution where a group of players will not change their chosen strategies over time [88, 89].

In the EGT model, each user selects a strategy by replication and adapts its selection for a better payoff (i.e. user satisfaction) until no user can increase their payoff by unilaterally changing strategy. An EGT based method is used in [85] to solve the problem of network selection in an environment where multiple networks are available. In [86], the EGT based subcarrier and power allocation for small-cell networks are proposed. In [87], the authors used a stochastic geometry-based approach to analyse the stability of equilibrium of the evolutionary game

in macro/micro heterogeneous wireless networks. In this study, an EGT based system load balancing scheme for an indoor LiFi/RF network is proposed with user data rate requirement taken into account. Different from conventional EGT based approaches, the proposed algorithm jointly deals with the APA and the RA rather than only focuses on the network selection. Specifically, the max-min fairness and the proportional fairness schedulers are used in the RA. Also, an enhanced proportional fairness scheduler is proposed to improve the efficiency of resource utilisation.

4.1.2 Main contributions

- An EGT based load balancing scheme is proposed for hybrid LiFi/RF networks where the following practical issues are considered: i). channel blockages; ii). LiFi ROA; iii). user data rate requirement. The proposed algorithm jointly handles the APA and the RA, and the optimality of this algorithm is analysed in this study.

- When considering user data rate requirement, conventional fairness schedulers such as max-min fairness and proportional fairness may lead to inefficient use of communication resources. In the proposed EGT based algorithm, an enhanced proportional fairness scheduler for resource allocation is proposed to avoid inefficient use of transmission resources. The performance of user satisfaction for both conventional and proposed fairness schedulers is evaluated by computer simulations.

- The effects of blockages and the ROA, which are the channel characteristics of LiFi, are analysed in this study. To the best of the authors' knowledge, it is the first time an investigation on how these two issues affect the system load balancing in hybrid LiFi/RF networks has been conducted.

The rest of this chapter is organised as follows. The practical hybrid LiFi/RF network model is introduced in Section 4.2. The EGT based load balancing scheme is given in Section 4.3. The performance evaluation is presented in Section 4.4 and a summary is drawn in Section 4.5.

4.2 System Model

In this study, an indoor scenario covered by a hybrid LiFi/RF network is considered, where N_l LiFi APs and N_r RF APs are deployed. The system model of hybrid LiFi and RF networks

can be seen in Section 2.1-2.2. In the LiFi system, the photon detector (PD) at each LiFi receiver may have horizontal and vertical tilts, as shown in Fig. 2.2. The direction vector of the PD in Cartesian coordinates is given in Eq. (2.5), and the angle of incidence to the PDs is shown in Eq. (2.7). Due to the field of view (FoV) of the LED and PDs, each LiFi AP covers a confined cell, termed as an optical attocell. Since an attocell can significantly reduce the spread of signals outside a given zone determined by the light cone, LiFi APs are able to reuse the same bandwidth in a radical manner. Optical inter-cell interference (ICI) is treated as an additive noise [90]. In this study, a square lattice topology is used for the deployment of LiFi APs so as to model a regular lighting placement used in large offices and public places. Direct current biased orthogonal frequency division multiplexing (DCO-OFDM) is applied for LiFi transmission. In addition, a RF system working at 2.4 GHz covers the whole indoor scenario. When more than one RF AP is considered, the RF ICI is not negligible. It is assumed that the RF APs use different channels, and the spectrum used by each RF AP is non-overlapping.

Assume that the channel state information (CSI) in both LiFi and RF systems changes slowly and is constant in a short period of T_p, which contains numbers of transmission time intervals (TTIs). During a period of T_p, the load distribution is considered to be fixed in the hybrid network. In this study, user movement is not taken into account, and the EGT based dynamic load balancing scheme with handover will be subject to future research.

Time division multiple access (TDMA) is used at each LiFi and RF cell to serve multiple users [34]. The portion of the time resource allocated to user μ in a signal frame is denoted by $k_{\mu,\alpha}$, where α is the index of the serving AP and $k_{\mu,\alpha} \in [0,1]$. The data rate requirement of each user during time T_p is denoted by λ_μ. The number of users is denoted by N_μ; the set of LiFi APs is denoted by $\mathcal{C}_{\mathcal{L}} = \{l|\ l \in [1, N_l], l \in \mathbb{N}\}$; the set of RF APs is denoted by $\mathcal{C}_{\mathcal{R}} = \{r|\ r \in [1, N_r], r \in \mathbb{N}\}$; and the total number of the APs is denoted as $N_{\text{ap}} = N_l + N_r$.

In this chapter, the blockage caused by opaque objects in LiFi attocells is considered. According to [91], an object which generates a shadow in an indoor scenario is approximately modelled by a cylinder, 1.2 m (height) and 0.8 m (diameter). The shape of the shadow caused by this cylinder is assumed to be a rectangle. As shown in Fig. 4.1, the length of the rectangle is defined as the distance between the cylinder bottom and the shadow of the cylinder top, and the width of the rectangle is the diameter of the cylinder. It is assumed that the PDs in the shadows cannot receive any LoS optical signal from the blocked LiFi APs.
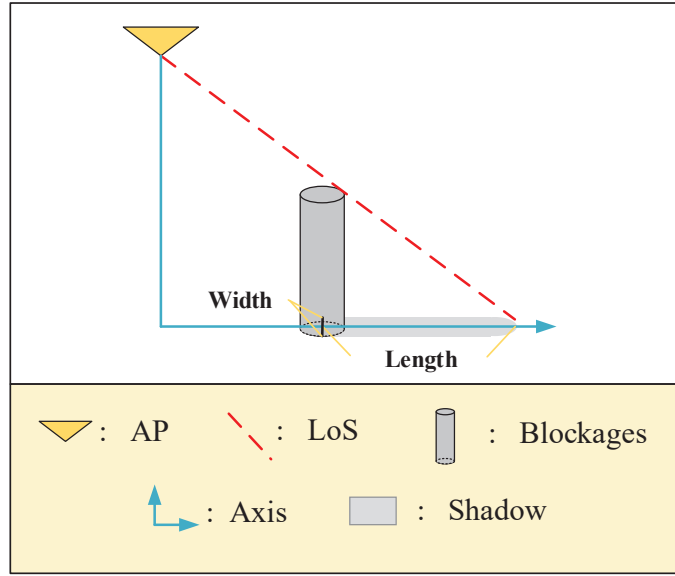
Figure 4.1: *Illustration of the blockages for LiFi links*

The LiFi channel impulse response in the frequency domain can be modelled as [53]:

$$
H_{\mu,\alpha}(f) = \begin{cases} (\eta_{\text{LoS}} + H_{\text{me}}(f))H_{\text{fe}}(f), & \text{LoS not blocked} \\ H_{\text{me}}(f)H_{\text{fe}}(f), & \text{LoS blocked} \end{cases}, \tag{4.1}
$$

where η_{LoS} is the path loss of a LoS channel, given in Eq. (2.3); $H_{\text{me}}(f)$ is the channel gain caused by the multi-path propagation and the diffuse effect, given in Eq. (2.8); and $H_{\text{fe}}(f)$ is the front-end device frequency response, given in Eq. (2.9), which are presented in Section 2.3.

The signal-to-interference-plus-noise ratio (SINR) for user μ connected to AP α in a LiFi link is given in Eq. (3.55). In addition, the RF channel model has been shown in Section 2.4. Since there is no ICI in the RF system, the SINR is equivalent to SNR on each sub-carrier, which is shown in Eq. (3.56).

The OFDM technology is used in both LiFi and RF systems, and the number of OFDM sub-carriers is denoted by K_m. Due to the channel fading in the frequency domain, adaptive M-QAM modulation is used on different OFDM sub-carriers [53]. In this study, the spectrum efficiency achieved on each subcarrier depends on the achievable SINR (or SNR), which can be obtained from the modulation and coding scheme (MCS) given in Table 2.1 [77]. Since the baseband bandwidth in the LiFi system is B_{L}, the OFDM bandwidth would be $2B_{\text{L}}$, and the

LiFi link data rate between user μ and AP α can be written as [13]:

$$Z_{\mu,\alpha} = \frac{2B_{\mathrm{L}}}{K_m} \sum_{i=1}^{\frac{K_m}{2}-1} q_{\mathrm{L}}(i),$$ (4.2)

where $q_{\mathrm{L}}(i)$ is the spectrum efficiency on sub-carrier i in the LiFi system, according to Eq. (3.55). The link communication data rate of RF can be written as:

$$\Upsilon_{\mu,\alpha} = \frac{B_{\mathrm{R}}}{K_m} \sum_{j=0}^{K_m-1} q_{\mathrm{R}}(j),$$ (4.3)

where $q_{\mathrm{R}}(j)$ is the spectrum efficiency on sub-carrier j in the RF system, according to Eq. (3.56).

In order to reduce the complexity of AP selection, the receivers only select from the candidate APs with the highest link data rate performance in the stand-alone LiFi or RF system. Without loss of generality, it is assumed that the link data rates between user μ and the APs follows:

$$\begin{cases} Z_{\mu,l_1} \geq \ldots Z_{\mu,l_i} \geq Z_{\mu,l_{i+1}} \ldots \geq Z_{\mu,l_{N_l}}, & l_i \in \mathcal{C_L} \\ \Upsilon_{\mu,r_1} \geq \ldots \Upsilon_{\mu,r_j} \geq \Upsilon_{\mu,r_{j+1}} \ldots \geq \Upsilon_{\mu,r_{N_r}}, & r_j \in \mathcal{C_R} \end{cases}.$$

The AP resource of user μ can be defined as:

$$\mathcal{S}_\mu = \{l_1, r_1\}.$$ (4.4)

For simplicity, the link data rate between user μ and its candidate AP $\alpha \in \mathcal{S}_\mu$ is denoted by $\gamma_{\mu,\alpha}$, which can be expressed as:

$$\gamma_{\mu,\alpha} = \begin{cases} Z_{\mu,\alpha}, & \alpha \in \mathcal{C_L} \cap \mathcal{S}_\mu \\ \Upsilon_{\mu,\alpha}, & \alpha \in \mathcal{C_R} \cap \mathcal{S}_\mu \end{cases}.$$

4.3   Load Balancing Game

In this section, a new load balancing scheme is proposed, where the APA and the RA are formulated as an evolutionary game. Also, the replicator dynamic is used to model the strategy adaptation process for network load balancing [87]. The evolutionary equilibrium is considered to be the solution of the formulated load balancing game, and the stability and optimality of this

algorithm are analysed.

4.3.1 Game setup

The load balancing game can be formulated as follows:

1. Players Set ($\mathcal{U}$): The users in the hybrid network are the players in the game, and the number of players is denoted by $N_\mu = |\mathcal{U}|$.

2. Strategy Set ($\mathcal{S}_\mu$): The strategy set for each player is in accordance with Eq. (4.4). Each player can select one AP from $\mathcal{S}_\mu$.

3. Population: In the proposed game, each player should be allocated to an AP. The set of players connected to AP α ($\alpha \in \mathcal{C}_\mathcal{L} \cup \mathcal{C}_\mathcal{R}$) is denoted by $\mathcal{U}_\alpha$, where the number of players in this set is denoted by $N_\alpha = |\mathcal{U}_\alpha|$.

4. Payoff Function: The payoff of a player quantifies the satisfaction level of that player's action of AP selection, and this is considered as the user QoS. In general, player μ would be satisfied when its data rate is higher than the requirement λ_μ. Otherwise, the satisfaction level would decrease along with the data rate. Intuitively, the payoff function of user μ that is allocated to AP α can be written as:

$$\pi_{\mu,\alpha} = \min\left\{ k_{\mu,\alpha} \frac{\gamma_{\mu,\alpha}}{\lambda_\mu}, \ 1 \right\}, \tag{4.5}$$

where $k_{\mu,\alpha}$ is the time resource portion provided by host AP α; and $\gamma_{\mu,\alpha}$ is the link data rate between player μ and AP α.

4.3.2 Resource allocation

Since TDMA is used in this study, the time slot resource would be allocated to users in each cell by serving APs. Here the portion of time slot resource allocated by AP α for user μ is denoted by $k_{\mu,\alpha}$. In this study, the β-proportional fairness function shown in Eq. (2.16) is used, which is repeated here:

$$\psi_\beta(x) = \begin{cases} \ln(x), & \beta = 1 \\ \dfrac{x^{1-\beta}}{1-\beta}, & \beta \geq 0, \ \beta \neq 1 \end{cases}, \tag{4.6}$$

where x is the user satisfaction level, defined as the user QoS; and β is the fairness coefficient. Particularly, when $\beta = 0$, a linear utility function is obtained, which achieves a maximal system throughput. In this case, each AP only serves the user with the best channel state information (CSI) whereas the other users have zero data rates. This scheduler finally leads to an ineffective network load balancing. Thus, the situation of $\beta = 0$ is not under consideration.

In the cell covered by AP α, the resource allocation problem with the β-proportional fairness function can be formulated as:

$$\max_{k_{\mu,\alpha}} \sum_{\mu \in \mathcal{U}_\alpha} \psi_\beta \left(k_{\mu,\alpha} \frac{\gamma_{\mu,\alpha}}{\lambda_\mu} \right) \tag{4.7}$$

$$\text{s.t.} \quad \sum_{\mu \in \mathcal{U}_\alpha} k_{\mu,\alpha} \leq 1; \tag{4.8}$$

where $\mathcal{U}_\alpha$ is the set of players allocated to AP α. The Lagrangian multiplier method is used to solve this problem. The Lagrangian function is given by:

$$F(k_{\mu,\alpha}, \omega) = \sum_{\mu \in \mathcal{U}_\alpha} \psi_\beta \left(k_{\mu,\alpha} \frac{\gamma_{\mu,\alpha}}{\lambda_\mu} \right) + \omega \left(1 - \sum_{\mu \in \mathcal{U}_\alpha} k_{\mu,\alpha} \right), \tag{4.9}$$

where ω is the Lagrangian multiplier for the constraint in Eq. (4.8). The optimal $k_{\mu,\alpha}$ can be obtained by making the gradient of the Lagrangian function in Eq. (4.9) equal to 0, which is written as:

$$\frac{\partial F(k_{\mu,\alpha}, \omega)}{\partial k_{\mu,\alpha}} = \frac{\partial \psi_\beta(k_{\mu,\alpha}\gamma_{\mu,\alpha}/\lambda_\mu)}{\partial k_{\mu,\alpha}} - \omega = 0, \tag{4.10}$$

where according to Eq. (4.6),

$$\frac{\partial \psi_\beta(k_{\mu,\alpha}\gamma_{\mu,\alpha}/\lambda_\mu)}{\partial k_{\mu,\alpha}} = \frac{\gamma_{\mu,\alpha}}{\lambda_\mu} \left(k_{\mu,\alpha} \frac{\gamma_{\mu,\alpha}}{\lambda_\mu} \right)^{-\beta}, (\beta > 0). \tag{4.11}$$

It can be derived from Eq. (4.10) and Eq. (4.11) that:

$$k_{\mu,\alpha} = \left(\frac{\gamma_{\mu,\alpha}}{\lambda_\mu} \right)^{\frac{1}{\beta} - 1} \omega^{-\frac{1}{\beta}}. \tag{4.12}$$

According to Eq. (4.12) and Eq. (4.8), it can be further calculated that:

$$\omega^{\frac{1}{\beta}} = \sum_{\mu \in \mathcal{U}_\alpha} \left(\frac{\gamma_{\mu,\alpha}}{\lambda_\mu} \right)^{\frac{1}{\beta} - 1}. \tag{4.13}$$

Combining Eq. (4.12) and Eq. (4.13), the optimum $k_{\mu,\alpha}$ can be expressed as:

$$k_{\mu,\alpha} = \frac{(\gamma_{\mu,\alpha}/\lambda_\mu)^{\frac{1}{\beta}-1}}{\sum_{i\in\mathcal{U}_\alpha}(\gamma_{i,\alpha}/\lambda_i)^{\frac{1}{\beta}-1}} \qquad (\beta > 0). \tag{4.14}$$

In this study, three fairness schedulers are considered, which are max-min fairness (MF), proportional fairness (PF) and enhanced proportional fairness (EPF).

i). *MF*: The MF is achieved with $\beta \to +\infty$ [74], and the optimal portion of allocated time resource can be expressed as:

$$k_{\mu,\alpha}^{(\mathrm{MF})} = \lim_{\beta\to+\infty} \frac{(\gamma_{\mu,\alpha}/\lambda_\mu)^{\frac{1}{\beta}-1}}{\sum_{i\in\mathcal{U}_\alpha}(\gamma_{i,\alpha}/\lambda_i)^{\frac{1}{\beta}-1}} = \frac{(\gamma_{\mu,\alpha}/\lambda_\mu)^{-1}}{\sum_{i\in\mathcal{U}_\alpha}(\gamma_{i,\alpha}/\lambda_i)^{-1}}. \tag{4.15}$$

Combining Eq. (4.5) and Eq. (4.15), the user payoff with MF scheduler can be written as:

$$\pi_{\mu,\alpha}^{(\mathrm{MF})} = \min\left\{\frac{1}{\sum_{i\in\mathcal{U}_\alpha}\lambda_i/\gamma_{i,\alpha}}, \ 1\right\}, \tag{4.16}$$

where the operation $\min\{e_1, e_2\}$ represents the minimum between e_1 and e_2. It can be seen that all players served by AP α achieve equal payoffs.

ii). *PF*: The PF scheduler is realised by $\beta = 1$ [74]. According to Eq. (4.15), the optimal RA portion can be written as follows:

$$k_{\mu,\alpha}^{(\mathrm{PF})} = \left.\frac{(\gamma_{\mu,\alpha}/\lambda_\mu)^{\frac{1}{\beta}-1}}{\sum_{i\in\mathcal{U}_\alpha}(\gamma_{i,\alpha}/\lambda_i)^{\frac{1}{\beta}-1}}\right|_{\beta=1} = \frac{1}{N_\alpha}, \tag{4.17}$$

where N_α is the number of users in $\mathcal{U}_\alpha$. The user payoff of proportional scheduler is therefore expressed as:

$$\pi_{\mu,\alpha}^{(\mathrm{PF})} = \min\left\{\frac{\gamma_{\mu,\alpha}}{\lambda_\mu N_\alpha}, \ 1\right\}. \tag{4.18}$$

In the PF scheduler, receivers in each cell share the same portion of time slot resource. Nevertheless, an inefficient use of resources may occur when users require low data rates. This issue will be handled by the EPF scheduler.

iii). *EPF*: Unlike the PF scheduler, the EPF scheduler can avoid inefficient use of resources by allocating the redundant time slot resources of over-achieving users to those who achieve low user satisfaction. Specifically, the RA is initially undertaken through the PF scheduler, as shown

---

Algorithm 8 : Enhanced proportional fairness scheduler in each cell.

1: Initialisation: The set of users served by AP α is denoted by $\mathcal{U}_{\text{RA}} = \mathcal{U}_\alpha$; total time resource $K_r = 1$; and the set of users over-achieving is denoted by $\mathcal{U}_{\text{Waste}} \neq \varnothing$.

2: **while** $\mathcal{U}_{\text{RA}} \neq \varnothing$ and $\mathcal{U}_{\text{Waste}} \neq \varnothing$ **do**

3:    Allocate time resource to users in $\mathcal{U}_{\text{RA}}$ using proportional fairness scheduler:

$$k_{\mu,\alpha}^{(\text{EPF})} = \frac{K_r}{N_{\text{RA}}}, \tag{4.20}$$

   where N_{RA} is the number of users in $\mathcal{U}_{\text{RA}}$.

4:    Update $\mathcal{U}_{\text{Waste}}$: $\mathcal{U}_{\text{Waste}} = \{\mu | \ k_{\mu,\alpha}^{(\text{EPF})} \gamma_{\mu,\alpha}/\lambda_\mu > 1, \mu \in \mathcal{U}_{\text{RA}}\}$. The resource portion allocated to users in $\mathcal{U}_{\text{Waste}}$ is changed to $k_{\mu,\alpha}^{(\text{EPF})} = \lambda_\mu/\gamma_{\mu,\alpha}$.

5:    Update $\mathcal{U}_{\text{RA}}$: $\mathcal{U}_{\text{RA}} = \mathcal{U}_{\text{RA}} - \mathcal{U}_{\text{Waste}}$.

6:    Update total time resource:

$$K_r = K_r - \sum_{\mu \in \mathcal{U}_{\text{Waste}}} \frac{\lambda_\mu}{\gamma_{\mu,\alpha}}. \tag{4.21}$$

7:    **if** $\mathcal{U}_{\text{RA}} = \varnothing$ **then**

8:       The resource that have not been used can be allocated to all users with proportional fairness:

$$k_{\mu,\alpha}^{(\text{EPF})} = k_{\mu,\alpha}^{(\text{EPF})} + K_r/N_\alpha. \tag{4.22}$$

9:    **end if**

10: **end while**

---

in Eq. (4.17). After that, the redundant time slot resources of users achieving data rates higher than the requirements will be re-allocated to the other users via the PF scheduler to improve their user QoS performance. This re-allocation process is iteratively conducted until no user receives redundant resources. The EPF scheduler achieves a high level of resource utilisation as well as a near-proportional fairness. The RA process using the EPF scheduler is summarised in Algorithm 8. The payoff of each user achieved by the EPF scheduler can be expressed as:

$$\pi_{\mu,\alpha}^{(\text{EPF})} = \frac{k_{\mu,\alpha}^{(\text{EPF})} \gamma_{\mu,\alpha}}{\lambda_\mu}, \tag{4.19}$$

where $k_{\mu,\alpha}^{(\text{EPF})}$ is the resource portion for user μ which can be obtained from Algorithm 8.

4.3.3   AP assignment

In the context of the evolutionary game for load balancing, the players iteratively adapt their strategies of AP selection to enhance the payoffs. The duration of each iteration is considered

as a TTI. The strategy adaptation process of AP selection and the corresponding population evolution can be modelled as follows. In the t-th iteration, the average payoff of players served by AP α is expressed as:

$$\bar{\pi}_\alpha^{(t,j)} = \frac{1}{N_\alpha} \sum_{\mu \in \mathcal{U}_\alpha} \pi_{\mu,\alpha}^{(t,j)}, \ j \in \{\text{MF}, \text{PF}, \text{EPF}\}, \tag{4.23}$$

where $\pi_{\mu,\alpha}^{(t,j)}$ is the payoff for user μ. The global average payoff of all players in this hybrid network can therefore be obtained:

$$\bar{\pi}^{(t,j)} = \frac{1}{N_\mu} \sum_{\alpha \in \mathcal{C}_\mathcal{L} \cup \mathcal{C}_\mathcal{R}} N_\alpha \bar{\pi}_\alpha^{(t,j)}, \ j \in \{\text{MF}, \text{PF}, \text{EPF}\}. \tag{4.24}$$

The AP selection strategy of each player is based on its previous payoff, the average payoff of each cell and the global average payoff in the last iteration, denoted by $\pi_{\mu,\alpha}^{(t-1,j)}$, $\bar{\pi}_\alpha^{(t-1,j)}$ and $\bar{\pi}^{(t-1,j)}$, respectively. The strategy shift for any player occurs randomly and follows the rule that the player with a lower value of payoff would be more likely to change its strategy. This is termed as the 'mutation and selection mechanism' in EGT [87]. Based on this principle, the mutation probability for a strategy shift in the t-th iteration is designed as:

$$p_\mu^{(t,j)} = \begin{cases} 1 - \dfrac{\pi_{\mu,\alpha}^{(t-1,j)}}{\bar{\pi}^{(t-1,j)}}, & \pi_{\mu,\alpha}^{(t-1,j)} < \bar{\pi}^{(t-1,j)} \\ 0, & \pi_{\mu,\alpha}^{(t-1,j)} \geq \bar{\pi}^{(t-1,j)} \end{cases}. \tag{4.25}$$

When a player is 'mutated', an AP selection for this player is required. The new AP is determined by maximising the estimated payoff in the current iteration, which can be expressed as:

$$\alpha^{(t,j)} = \arg\max_{i \in \mathcal{S}_\mu} \hat{\pi}_{\mu,\alpha}^{(t,j)} \tag{4.26}$$

$$\text{s.t.} \quad \hat{\pi}_{\mu,\alpha}^{(t,j)} = \begin{cases} \pi_{\mu,i}^{(t-1,j)}, & i = \alpha^{(t-1,j)} \\ \dot{\pi}_{\mu,i}^{(t,j)}, & i \neq \alpha^{(t-1,j)} \end{cases};$$

$$j \in \{\text{MF}, \text{PF}, \text{EPF}\}, \tag{4.27}$$

where $\alpha^{(t,j)}$ is the AP selected by player μ at the t-th iteration; $\dot{\pi}_{\mu,i}^{(t,j)}$ is the estimated payoff if the player is served by a different AP from $\alpha^{(t-1,j)}$ which here is denoted as υ for simplicity. The estimated payoff $\dot{\pi}_{\mu,\upsilon}^{(t,j)}$ is greatly related to the fairness achieving schedulers considered in

this work as follows:

i). *MF*: According to Eq. (4.16), the payoff of users served by the same AP is equal to their average payoff. When player μ is served by AP υ, the total time resource for other players allocated to this AP would decrease to $1 - k_{\mu,\upsilon}$. Since each player served by υ ultimately achieves an equal payoff after player μ joins in. The estimated payoff of player μ can be written as:

$$\dot{\pi}_{\mu,\upsilon}^{(t,\mathrm{MF})} = (1 - k_{\mu,\upsilon})\bar{\pi}_{\upsilon}^{(t-1,\mathrm{MF})}. \tag{4.28}$$

Also, the payoff of user μ can be expressed as:

$$\dot{\pi}_{\mu,\upsilon}^{(t,\mathrm{MF})} = k_{\mu,\upsilon}\frac{\gamma_{\mu,\upsilon}}{\lambda_{\mu}}. \tag{4.29}$$

Combining Eq. (4.28) and Eq. (4.29), it can be derived that:

$$\dot{\pi}_{\mu,\upsilon}^{(t,\mathrm{MF})} = \frac{\gamma_{\mu,\upsilon}\bar{\pi}_{\upsilon}^{(t-1,\mathrm{MF})}}{\lambda_{\mu}\bar{\pi}_{\upsilon}^{(t-1,\mathrm{MF})} + \gamma_{\mu,\upsilon}}. \tag{4.30}$$

ii). *PF*: In the PF scheduler, users in a specific cell achieve an equal time resource portion. When a new user joins the cell served by AP υ in the current iteration, the allocated portion of resources for each user becomes:

$$k_{\mu,\upsilon}^{(t-1,\mathrm{PF})} = \frac{1}{N_{\upsilon}^{(t-1,\mathrm{PF})} + 1} = \frac{k_{\upsilon}^{(t-1,\mathrm{PF})}}{1 + k_{\upsilon}^{(t-1,\mathrm{PF})}}, \tag{4.31}$$

where $N_{\upsilon}^{(t-1,\mathrm{PF})}$ is the total number of users served by AP υ in the last iteration; and $k_{\upsilon}^{(t-1,\mathrm{PF})} = 1/N_{\upsilon}^{(t-1,\mathrm{PF})}$ is the corresponding resource portion of users according to Eq. (4.17). Therefore, the estimated payoff of player μ in the t-th iteration can be written as:

$$\dot{\pi}_{\mu,\upsilon}^{(t,\mathrm{PF})} = \min\left\{\frac{\gamma_{i,\upsilon}}{\lambda_i(N_{\upsilon}^{(t-1,\mathrm{PF})} + 1)}, 1\right\}. \tag{4.32}$$

iii). *EPF*: It has been shown that the EPF scheduler is able to enhance the average user payoff performance by minimising the excess of time slot resources while achieving a proportional fairness. The EPF scheduler results in varying RA per user depending on their requirements of time resources. When a player is 'mutated', a simple method to estimate user payoff is to use the expression in Eq. (4.32) with $k_{\upsilon}^{(t-1,\mathrm{EPF})} = 1/N_{\upsilon}^{(t-1,\mathrm{EPF})}$, which is applied in this study. The

---

Algorithm 9 : EGT based centralised load balancing algorithm using MF, PF and EPF schedulers.

1: Initialisation: A random AP from $\mathcal{S}_\mu$ is assigned to player μ; each AP allocates the time resource to the connected players using one of the three fairness schemes; the CU calculates the average payoff of each player $\pi_{\mu,\alpha}^{(0,j)} = \bar{\pi}_\alpha^{(0,j)}$, the global average payoff $\bar{\pi}^{(0,j)}$ with $j \in \{\text{MF}, \text{PF}, \text{EPF}\}$, k_υ and $k_\upsilon^{\max}$; and $t \leftarrow 1$. This algorithm is executed by the CU.

2: **for all** each player $\mu \in \mathcal{U}$ **do**

3:     The CU calculates the mutation probability $p_{\mu 1}^{(t,j)}$ according to Eq. (4.25);

4:     The CU generates a random number with uniform distribution between 0 and 1, denoted as δ.

5:     **if** $\delta < p_\mu^{(t,j)}$ **then**

6:         The mutation occurs and player μ is assigned to an AP based on Eq. (4.26).

7:     **else**

8:         Player μ is still assigned to the original AP.

9:     **end if**

10: **end for**

11: **for all** each AP $\alpha \in \mathcal{C}_\mathcal{L} \cup \mathcal{C}_\mathcal{R}$ **do**

12:     The CU calculates the time resource portion for players in each cell, according to Eq. (4.15), (4.17) and Algorithm. 8.

13: **end for**

14: The CU stores the parameters $\bar{\pi}_\upsilon^{(t,\text{MF})}$ and $N_\upsilon^{(t,\text{PF})}$ and $N_\upsilon^{(t,\text{EPF})}$ ($\upsilon \in \mathcal{C}_\mathcal{L} \cup \mathcal{C}_\mathcal{R}$) for payoff estimation.

15: $t \leftarrow t + 1$ and repeat from Step 2 until no AP switch occurs.

---

estimated payoff of player μ with EPF taken into account can be expressed as follows:

$$\dot{\pi}_{\mu,\upsilon}^{(t,\text{EPF})} = \min \left\{ \frac{\gamma_{i,\upsilon}}{\lambda_i(N_\upsilon^{(t-1,\text{EPF})} + 1)}, 1 \right\}. \tag{4.33}$$

4.3.4   Load balancing algorithm

In the evolutionary game, players are randomly mutated with a probability according to Eq. (4.25). If a mutation occurs, the player selects an AP based on Eq. (4.26). On the one hand a player can possibly stay with the original AP when it experiences a mutation. On the other hand a new AP could be selected by players in each iteration. The parameters that are needed to estimate the payoff for the three schedulers (MF, PF and EPF) are $\bar{\pi}_\upsilon^{(t-1,\text{MF})}$ (MF) and N_υ (PF and EPF), respectively. If no strategy shift occurs for any player, the load balancing algorithm converges.

Lemma 4. *In the proposed game, the load balancing algorithm always converges.*

Proof. Without loss of generality, the average payoff of users served by each AP in the t-th iteration can be expressed as:

$$\bar{\pi}_{n_1}^{(t,j)} \leq ...\bar{\pi}_{n_i}^{(t,j)} \leq \bar{\pi}_{n_{i+1}}^{(t,j)}... \leq \bar{\pi}_{n_{N_{\text{ap}}}}^{(t,j)},$$

$$n_i \in \mathcal{C}_{\mathcal{L}} \cup \mathcal{C}_{\mathcal{R}}, \ \ j \in \{\text{MF}, \text{PF}, \text{EPF}\}. \tag{4.34}$$

The maximal difference between two average payoffs is denoted as $w^{(t,j)} = \bar{\pi}_{n_{N_{\text{ap}}}}^{(t,j)} - \bar{\pi}_{n_1}^{(t,j)}$. In the next iteration, the players served by AP $n_{N_{\text{ap}}}$ would not change the AP because their mutation probability is zero according to Eq. (4.25), and no player would join the AP n_1 due to the low estimated payoff based on Eq. (4.26). Thus, it can be seen that $\bar{\pi}_{n_{N_{\text{ap}}}}^{(t+1,j)} \leq \bar{\pi}_{n_{N_{\text{ap}}}}^{(t,j)}$ and $\bar{\pi}_{n_1}^{(t+1,j)} \geq \bar{\pi}_{n_1}^{(t,j)}$ would be satisfied, resulting in $w^{(t,j)} \geq w^{(t+1,j)}$. Also, based on Eq. (4.34), it can be seen that $w^{(t,j)} \geq 0$ is achieved. According to the monotonically bounded theorem, there is:

$$\lim_{t \to +\infty} w^{(t,j)} = w, \ \ w \geq 0, \tag{4.35}$$

where w is a constant. After $w^{(t,j)}$ converges, the difference between $\bar{\pi}_{n_{N_{\text{ap}}}-1}^{(t,j)}$ and $\bar{\pi}_2^{(t,j)}$ also follows the monotonically bounded theorem and will converge. By such analogy, the average payoffs for all APs tend to be constant. Thus the network load balancing can achieve convergence. $\qquad\square$

The proposed EGT load balancing algorithm contains the following steps: i) users change their strategies unilaterally to find better serving APs in the AP assignment step; 2) the users served by the same AP are allocated the time slot resource according to the RA schemes, i.e. MF, PF and EPF; 3) repeat step i) and ii) until no user can change the strategy unilaterally to improve their payoff. The EGT technique is often implemented in a distributed fashion to achieve low computational complexity. However, a distributed EGT algorithm requires coordination of all users. In particular, each user needs to keep sending their strategy selections back to the APs until the algorithm converges, and this process consumes communication resources. However, the EGT algorithm can also be realised in a centralised manner, where the central unit (CU) undertakes the AP selection for users virtually following the EGT algorithm. After the CU works out the final AP selection results, users will be assigned to their serving APs for data transmission. An advantage is that the EGT algorithm for system load balancing can be carried out rapidly by consuming few communication resources in a centralised network. In this study, an indoor hybrid LiFi/RF network is considered. An EGT based centralised load balancing
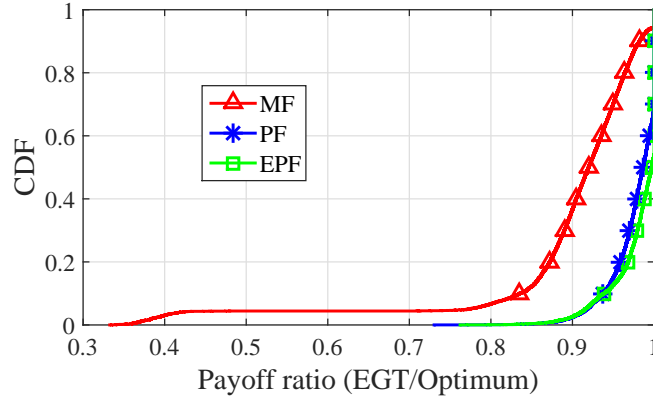
Figure 4.2: *Ratios of EGT payoffs to the global optima (1000 independent and identical simulations are considered.)*

algorithm is proposed, where the CU selects the AP for each user in each iteration based on the users' CSI. This approach supports typical software defined networking (SDN) architectures [92–94]. The EGT-based centralised load balancing algorithm is summarised in Algorithm 9.

4.3.5 Evolutionary Equilibrium and Optimality Analysis

Definition 1. *A strategy profile $\mathcal{A}_\mu = \{\alpha_\mu | \mu \in \mathcal{U}\}$ is an Evolutionary Equilibrium (EE) (referred to as the Nash Equilibrium in the evolutionary game [95]) of the proposed load balancing game if at the equilibrium $\mathcal{A}_\mu$, no player can further increase their payoff by unilaterally changing its strategy, i.e.:*

$$\pi_{\mu,\alpha_\mu} \geq \pi_{\mu,\beta_\mu}, \ \ \alpha_\mu \neq \beta_\mu, \ \alpha_\mu, \beta_\mu \in \mathcal{S}_\mu \tag{4.36}$$

where $\pi_{\mu,x}$ represents the payoff function for user μ allocated to AP x, according to Eq. (4.5).

It can be seen that when network load balancing converges, an EE is achieved. According to Lemma 4, the EE has the perfect self-stability property, and thus the players at the EE can achieve a mutually satisfactory solution. As a consequence, the EE can be regarded as the solution of the proposed evolutionary game. However, this does not mean that the optimal solution of maximising the average payoff of users has been achieved. Since a closed-form optimal solution of system load balancing is mathematically intractable, an exhaustive search is used to find this global optimum.

When considering N_μ users and N_{ap} APs in the hybrid LiFi/RF network, there are $N_{\mathrm{ap}}^{N_\mu}$ pos-

107

Name of Parameters	Value
Height of the room, h_w	2 m
The range of optical transmit power in the LiFi system, P_{opt}	20 W
Modulation bandwidth for LED lamp, B_L	100 MHz
Noise power spectral density of LiFi, N_L	10^{-19} A^2/Hz
The physical area of a PD, A_p	1 cm^2
Half-intensity radiation angle, $\theta_{1/2}$	60 deg.
Gain of optical filter, $T_s(\theta)$	1.0
Refractive index, χ	1.5
Cut-off frequency of diffuse optical channel, f_c	30 MHz
Cut-off frequency of front-end filtering effect, f_0	30 MHz
Optical to electric conversion efficiency, κ	0.53 A/W
Transmit power for each RF AP, P_R	20 dBm
Total transmitted bandwidth in RF system, B_R	80 MHz
Noise power of RF, σ^2	-57 dBm

Table 4.1: *Simulation parameters for the evaluation of the EGT-based LB scheme*

sibilities of AP assignments, which are denoted by $\mathbf{g}^{(i)}$, $i = 1, 2...N_{ap}^{N_\mu}$. Given a certain $\mathbf{g}^{(i)}$, the time resource portions using MF, PF and EPF schedulers can be computed based on Eq. (4.15), (4.17) and Algorithm 8, respectively. Subsequently, the global optimum of the system load balancing problem can be determined using an exhaustive search. The ratios of the payoffs achieved by the EGT algorithm to the global optima are shown in Fig. 4.2. It can be seen that the EGT algorithm with three fairness achieving schedulers has a performance close to the optimum. Specifically, 70% of players using the MF scheduler can achieve a payoff over 90% of the global optimum. The PF and EPF schedulers have better performance than MF, where the payoff achieved by 80% of players is greater than 95% of the optimum. Therefore, it can be concluded that the EGT technique achieves near-optimal performance.

Particular, the number of users evaluated in the optimality analysis is 10 and a larger amount of users are not considered because of the high complexity to find the optimum. Therefore, the simulation result shown in this section can only justify the optimality performance in the case of small amount of users. In future work, the optimality analysis for large number of users will be studied, where distributed parallel computing may be used to reduce the computing time.
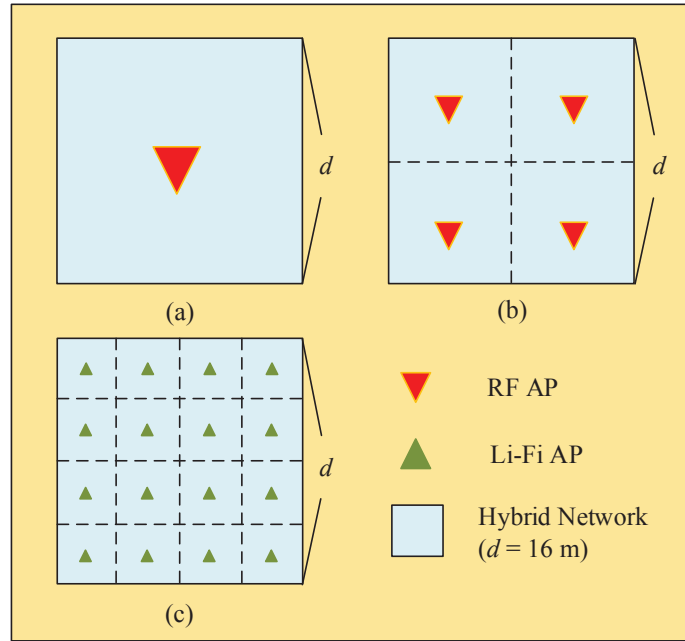
Figure 4.3: *Square topology for LiFi and RF network: (a). 1 RF AP; (b). 4 RF APs; (c). 16 LiFi APs.*

4.4 Performance Evaluation

4.4.1 System setup

In this study, a 16 m $\times$ 16 m indoor office space is considered. Two RF AP deployment scenarios are used as shown in Fig. 4.3 (a-b), and the LiFi AP deployment is shown in Fig. 4.3 (c). The users and the blocking objects are uniformly distributed, and the number of objects is denoted by N_B. The required data rate of each user follows a Poisson distribution with the parameter λ. The vertical ROA of each PD follows a uniform distribution ranging between 0 and θ_{PD}. In this study, the period of interest T is set to be 500 ms [96], and the channels and the data rate requirements of users are assumed to be fixed in this duration. According to [97], the TTI is set to be 2 ms. As a consequence, the maximum iteration number of the proposed algorithm is 250. Other parameters related to the simulation are given in Table 4.1. The payoff in the proposed algorithm is considered as the user QoS, which is between 0 and 1. When payoff is 0, users achieve zero data rates. When payoff is 1, users achieve data rates higher than or equal to the requirements.

In order to evaluate the performance of the proposed EGT based LB scheme, three benchmark

Algorithm	Addition	Multiplication	Exponentiation
EGT(MF,PF&EPF)	$O(N_\mu N_{ap} I_E)$	$O(N_\mu N_{ap} I_E)$	0
JOA	$O(N_\mu N_{ap} I_J)$	$O(N_\mu N_{ap} I_J)$	$O(N_\mu N_{ap} I_J)$
TAA	$O(N_\mu N_{ap})$	$O(N_\mu)$	0
RAA	$O(N_\mu)$	$O(N_\mu)$	0

Table 4.2: *Computation complexity comparison between the EGT based scheme and benchmarks*
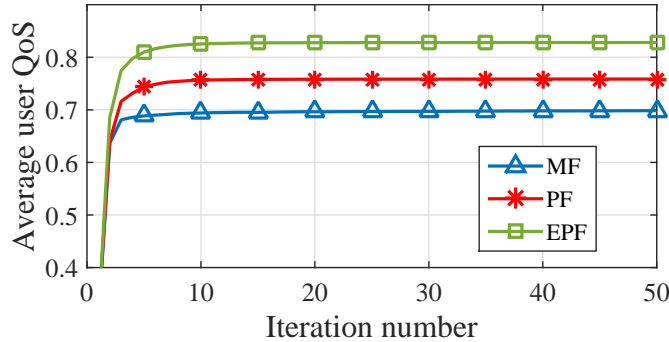
Figure 4.4: *The average user QoS corresponding to the iteration number (1 RF AP, $\lambda = 25$ Mb/s, $N_B = 10$, $\theta_{PD} = 0$, $N_\mu = 200$ and FoV = 90°).*

algorithms are implemented for comparison:

i). Joint optimisation algorithm (JOA): In the JOA benchmark, APA and RA are jointly optimised with proportional fairness considered [23, 34, 74, 77], which has been shown in Section 3.3.2.

ii). Threshold-based access algorithm (TAA): In the TAA benchmark, the APA and the RA are separately optimised. Specifically, the APA is determined by using an optimal data rate threshold and the RA is performed using the proportional fairness scheduler [83].

iii). Random access algorithm (RAA): In the RAA benchmark, APA and RA are also undertaken separately. Different from the TAA, each user randomly chooses the AP from $\mathcal{S}_\mu$ in the APA step. In the RA step, the RAA is conducted in the same way as the TAA.

4.4.2 Complexity analysis

As shown in Fig. 4.4, the proposed EGT algorithm reaches a steady state after several iterations. Specifically, the number of iterations for convergence is denoted by I_E, and I_E is around 10 for all of the curves shown in Fig. 4.4. During the interval T, there are 250 TTIs, and only 10 TTIs

are taken for convergence. Therefore 96% of the TTI can be used for signal transmission.

Figure 4.5: *Evaluation of user QoS with different RF setups. ($N_B = 10$, $\theta_{PD} = 0$, $N_\mu = 200$ and FoV = $90°$)*
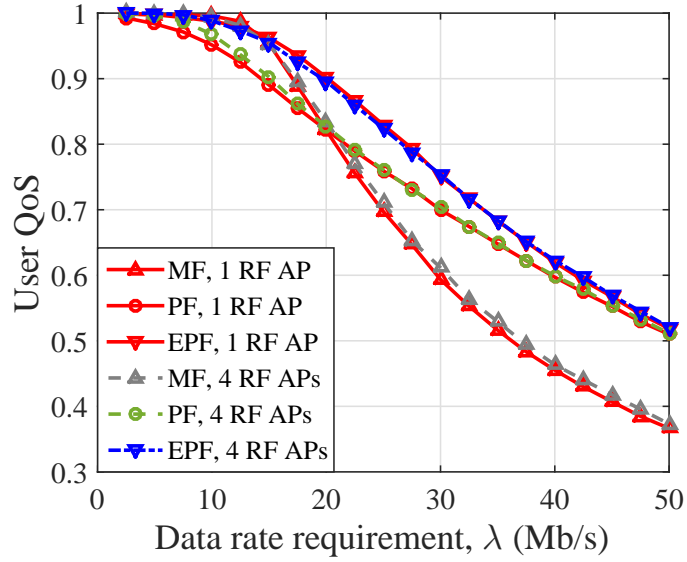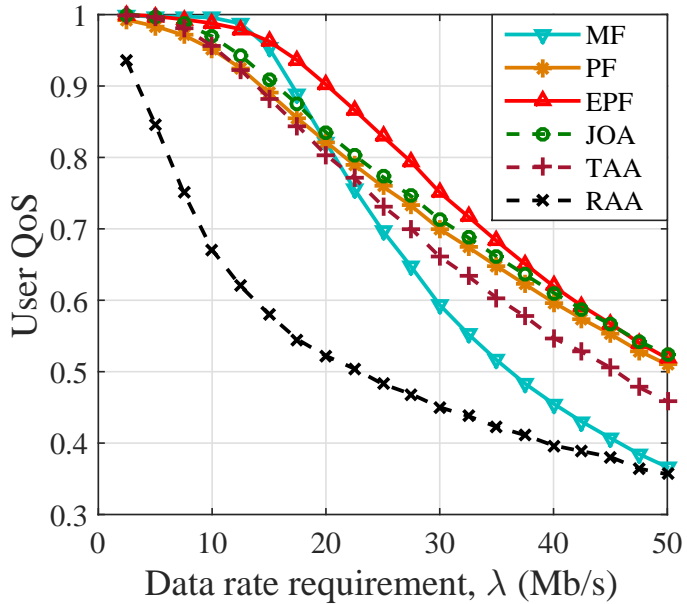

Figure 4.6: *Evaluation of user QoS achieved by different load balancing algorithms. (1 RF AP, $N_B = 10$, $\theta_{PD} = 0$, $N_\mu = 200$ and FoV = $90°$)*

In this study, JOA, TAA and RAA are simulated as the benchmarks for performance evaluation. The computational complexity of these algorithms is summarised in Table 4.2, where I_J is the iteration number in JOA [24]. The EGT algorithm with three RA schedulers achieves a lower complexity than JOA because the EGT algorithm includes no exponential operation but JOA does. However, the complexity of the EGT algorithm is higher than TAA and RAA due to the iterative computation.

4.4.3   Evaluation of user QoS

The user QoS performance with different RF AP deployments is shown in Fig. 4.5. It can be found that the user QoS with 1 RF AP exhibits similar performance to the case with 4 RF APs. On the one hand, 4 RF APs can reduce the path loss between users and APs, resulting in a higher receive SINR than in the case of 1 RF AP. On the other hand, according to Eq. (4.4), each user only uses the best LiFi and RF AP as the candidates for AP assignment, and the best LiFi attocell is generally covered by the best RF AP. In the network with 1 RF AP, when a LiFi attocell is overloaded, users in this attocell will be transferred to the RF cell so that the system load can be well balanced. However, in the network with 4 RF APs, since each user can only be served by either the best RF AP or the best LiFi AP, the hybrid network would be naturally divided into four independent regions. The users in one region cannot be served by the APs in other regions. Therefore, it is difficult to achieve efficient load balancing over the entire network, resulting in a decrease in the user QoS to the scenario with 1 RF AP. Accordingly, even though the scenario with 4 RF APs provides users with a low path loss and a high level of SINR, the user QoS cannot be significantly enhanced over the scenario with 1 RF AP.

The average QoS as a function of required user data rate is shown in Fig. 4.6. It can be seen that the EGT algorithm with EPF outperforms the other schemes. In addition, the MF algorithm results in a steeper slope of user QoS than the PF algorithm, which attains a better user QoS with $\lambda \leq 25$ Mb/s. Compared with the three benchmark systems where the proportional fairness is taken into account, the proposed EGT algorithm with PF performs between JOA and TAA/RAA. However, when the EPF scheme is used in the EGT based algorithm, the user QoS is much higher than achieved by all benchmark techniques. This is because the EPF scheme can minimises the inefficient use of transmission resources. The performance of JOA with EPF scheme is not presented due to high computational complexity. Compared with JOA, a benefit of the proposed EGT scheme is that some complicated RA scheme such as EPF can be

considered as the AP assignment and RF are separated undertaken.
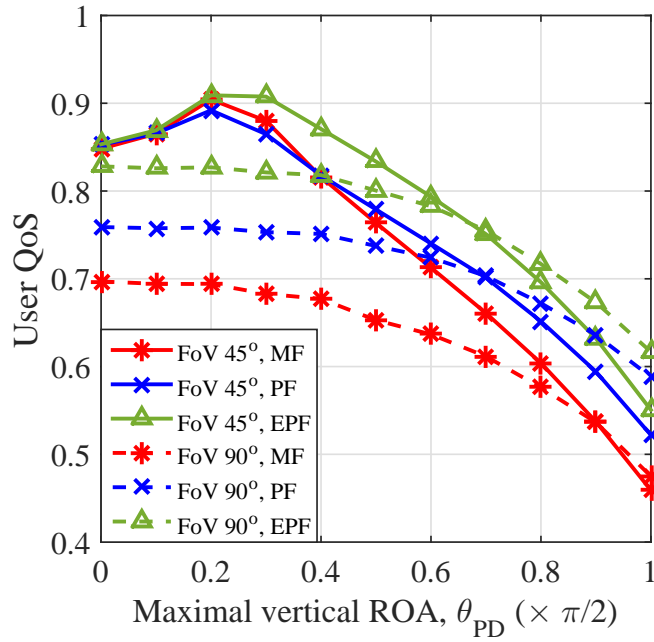
Figure 4.7: *The user QoS with maximal vertical ROA θ_{PD} (1 RF AP, $N_B = 10$, $N_\mu = 200$, $\lambda = 25$ Mb/s); users are fixed and have a random ROA in each simulation.*

Figure 4.8: *The average data rate with different blockage densities. (1 RF AP, $N_\mu = 200$, FoV $= 90°$, $\theta_{PD} = 0$ and $\lambda = 25$ Mb/s)*

Figure 4.9: *The CDF of user QoS achieved by EGT algorithms. (1 RF AP, $N_B = 10$, $N_\mu = 200$, FoV $= 45°$ and $\lambda = 25$ Mb/s)*

Figure 4.10: *CDF of user data rate with different blockage densities. (1 RF AP, $N_\mu = 200$, FoV $= 90°$, $\theta_{PD} = 0$ and $\lambda = 25$ Mb/s)*

In this study, it is assumed that the user QoS should be at least greater than 0.9 in order to guarantee the basic requirement of wireless services. It can be seen that in the hybrid LiFi/RF network with 200 users, an average user data rate of 20 Mb/s can be achieved by the EGT based algorithm.

4.4.4 Effect of vertical ROA

The receive SINR of LiFi is affected by the vertical ROA, φ_2. As shown in Section 2.3.1, φ_2 follows a uniform distribution ranging between 0 and θ_{PD}, where θ_{PD} is the maximal vertical ROA (MVR). In the LiFi system, the vertical ROA is able to affect the angle of incidence of LiFi signals. When the angle of incidence is less than the FoV, LiFi signals can be received by users. Otherwise, users can only be served by the RF APs. The effect of the MVR, θ_{PD}, on the performance of user payoff (or user QoS) is shown in Fig. 4.7. When the FoV is 45°, the QoS firstly increases than decreases with an increase in θ_{PD}. The optimum is attained approximately at $\theta_{\mathrm{PD}} = 25°$. On the one hand, when the vertical ROA tends to be zero, users at the edge of LiFi attocells may achieve a larger angle of incidence than FoV so that they can only be served by the RF AP, resulting in inefficient load balancing. On the other hand, a large θ_{PD} will lead to a severe path loss of LiFi signals, which decreases the LiFi data rates. With FoV = 90°, the angle of incidence of users at any location can basically be less than the FoV. Therefore, the user QoS decreases with an increase in θ_{PD} due to the path loss effects in the LiFi system.

Here a comparison of user QoS between $\theta_{\mathrm{PD}} = 0$ and 30° is made and demonstrated in Fig. 4.9, where the FoV is 45°. In the case of $\theta_{\mathrm{PD}} = 0$, LiFi receivers are perpendicular to the ground, and the angle of irradiance is equal to the angle of incidence in the LoS optical channel. Since users have a FoV of 45°, they can only receive LoS LiFi signals in a confined area, where the angle of irradiance of signals from LiFi APs should be less than 45°. This confined area is defined as the serving area. It can be seen that with $\theta_{\mathrm{PD}} = 0$, the user QoS mainly falls into two different ranges that are $0.1 \leq \mathrm{QoS} \leq 0.6$ and $\mathrm{QoS} = 1$, corresponding to the two situations that are users in the serving area and users outside the area. However, when users have a vertical ROA ranging from 0 to 30° ($\theta_{\mathrm{PD}} = 30°$), each LiFi AP is capable of serving users with a maximal angle of irradiance as large as 75°, leading to an enhancement of system load balancing. Therefore, it can be concluded that a proper vertical ROA in conjunction with a small FoV can improve the user QoS.
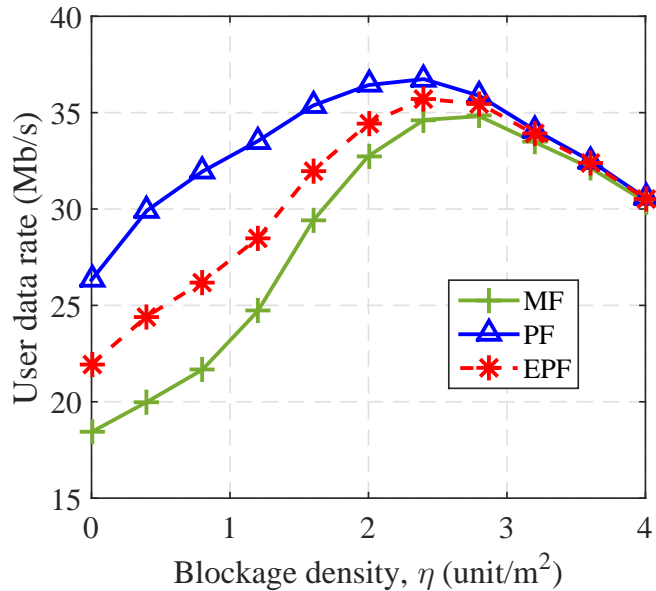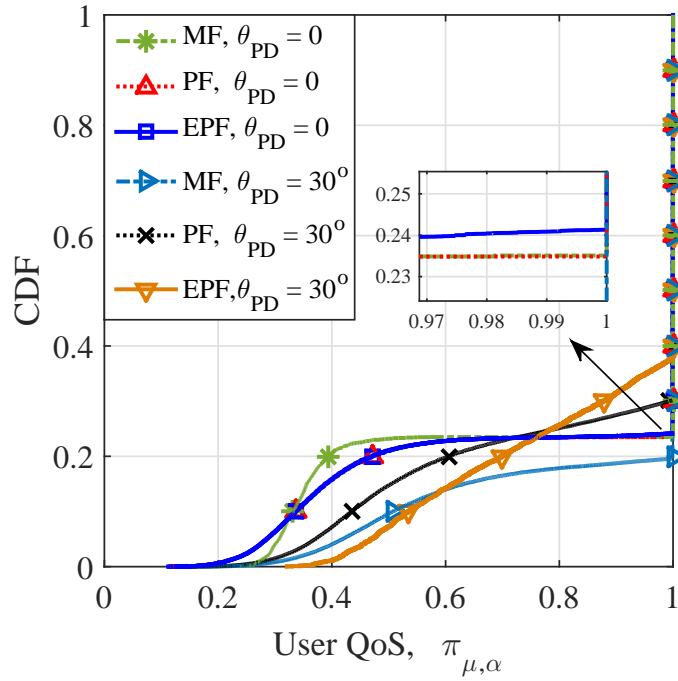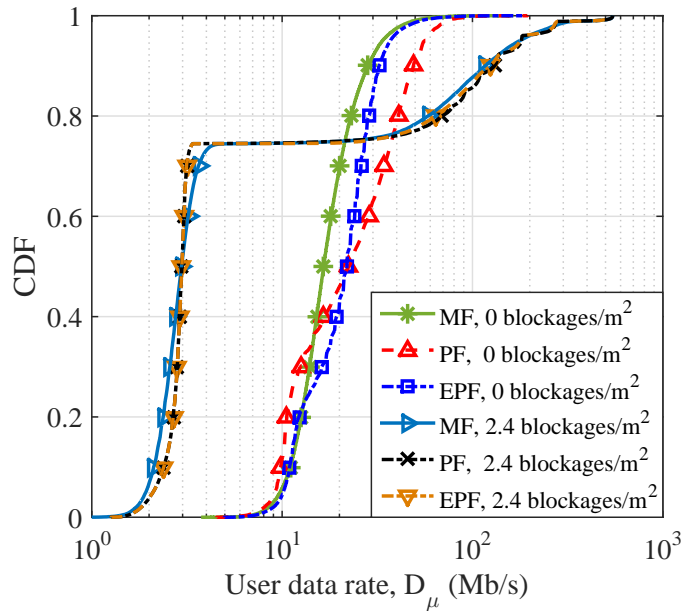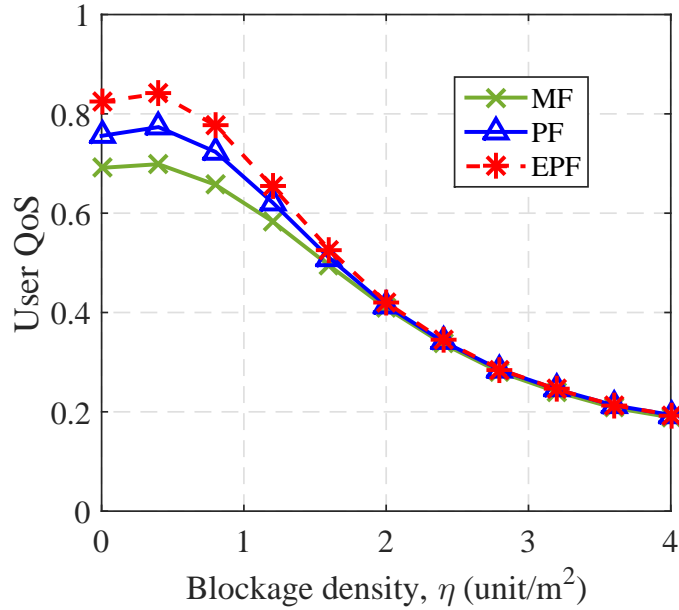
Figure 4.11: *Average user QoS with different blockage densities. (1 RF AP, $N_\mu = 200$, FoV = 90°, $\theta_{PD} = 0$ and $\lambda = 25$ Mb/s)*

4.4.5   Effect of blockage and shadow

In this subsection, the shadowing effect resulting from blockages in the LiFi system is studied. The number of blockages are denoted by N_B, and the blockage density is defined as $\eta_b = N_B/S$, where S is the area of the simulation scenario. The average user data rate corresponding to the blockage density is shown in Fig. 4.8. The data rate of user μ is denoted by $D_\mu = k_{\mu,\alpha}\gamma_{\mu,\alpha}$, where α is the serving AP of user μ. It can be seen that the average user data rate is a concave function with respect to the blockage density, η_b. With a small value of η_b, users served by LiFi may experience interference from neighbouring LiFi APs. When η_b increases, the interference signals are more likely to be blocked and the achievable SINR in LiFi channels is therefore improved. If the expected LiFi signals are blocked, the RF APs will be automatically allocated to those users by the CU. As shown in Fig. 4.8, the optimal data rate appears at $\eta_b = 2.4$. However, a further increase of η_b results in a decrease in the average data rate. This is because most of the users have to be allocated to the RF APs due to the blockage of LiFi LoS channels, which leads to a reduction of network throughput.

For different blockage situations, the CDF of the user data rate is shown in Fig. 4.10. It can be seen that the achievable data rates with blockages have a much larger range than those without blockages. When η_b is set to be 2.4 unit/m² (the optimal η_b in Fig. 4.8), the user data rates

would basically be classified into two groups: [0, 4] Mb/s and [30, 600] Mb/s. Compared with the non-blockage case, 72% of the users in the blockage scenario experience a data rate degradation, while the remaining users achieve a significant data rate improvement. This means that although a blockage density of 2.4 unit/m^2 results in the largest average user data rate, more than half of the users in this case have to be served by RF APs and achieve a low data rate. Moreover, 28% of the users can obtain plenty of LiFi communication resources but their achievable data rates are much higher than required. Fig. 4.11 shows that when considering the required data rate of users, the QoS increases at the low blockage densities but decreases with a further increase in η_b. This indicates that an increase in blockage density cannot provide a better user experience despite achieving an improvement of the sum data rate.

4.5   Summary

In this chapter, in order to model a practical hybrid LiFi/RF network scenario, three factors are taken into account: blockages, LiFi ROA and user data rate requirement. An EGT based load balancing algorithm is proposed to improve the user QoS. Also, an enhanced proportional fairness scheduler is proposed to maximise the usage of communication resources in the RA step. The effects of the maximal vertical ROA and blockages on the hybrid network are evaluated and discussed. Three conclusions are drawn based on the simulation results: (i) The proposed EGT load balancing algorithm achieves a better performance/complexity trade-off than the conventional algorithms. In addition, when the EPF scheme is used, a high level of user QoS can be attained due to a more efficient exploitation of transmission resources; (ii) When the FoV of LiFi receivers is 90°, the average user QoS decreases with an increase in the maximal vertical ROA θ_{PD}. However, when considering a small FoV, there is an optimum of the maximal vertical ROA that can optimise the QoS performance, leading to improved system load balancing ; (iii) Given the simulation scenario, an optimal blockage density of $\eta_b = 2.4$ unit/m^2 can maximise the system sum data rate. However, when considering user data rate requirement, the user QoS decreases with an increase in η_b as the blockages cause an inefficient allocation of communication resources.

Chapter 5
Optimisation of Packet Flow Assignment for HLRNs

5.1 Introduction

In hybrid LiFi and RF networks (HLRNs), an efficient AP assignment can significantly affect the overall quality of service (QoS). Many current research efforts have been paid towards improving the performance of hybrid networks. In [23, 24], a centralised load balancing (LB) scheme is proposed, aiming to maximise the system sum data rate with certain fairness schedulers. In [81, 98, 99], dynamic load balancing is studied, where handovers between different APs are considered. In [99], a fuzzy logic based scheme is proposed, which readily integrates static load balancing with direct handover schemes. In [81], a Markov decision process (MDP) based vertical handover scheme was proposed for hybrid networks consisting of one LiFi AP and one RF AP. This work aims to find a trade-off solution to reduce the handover cost without significantly sacrificing the system throughput. The aforementioned works primarily focus on the improvement of data rate performance. In Chapter 3 and 4, the optimisation-based LB schemes and the evolutionary game theory based LB scheme for HLRNs are proposed, which also concentrate on load balancing in the physical layer. However, the system delay, which is essential to the user's QoS, also needs to be studied for hybrid networks. In [21], the delay modelling of hybrid visible light communication (VLC) and wireless fidelity (WiFi) networks has been investigated. In this work, the M/D/1 queuing model is considered and the capacities with respect to the asymmetric VLC/WiFi and hybrid VLC/WiFi networks are compared. In [1], the analysis of system delay in hybrid LiFi/RF networks is undertaken, where M/M/1 model is applied. However, all of these works assume that the LiFi users achieve an equal data rate. In practice, the LiFi data rate significantly depends on the distance between the LiFi APs and the users [17]. Therefore, the distribution of user data rates must be taken into account when the system delay is evaluated.

In this chapter, a two-tier buffer framework for hybrid LiFi/RF networks is considered. Specifically, the arrival packets will be initially queued in the buffer of a central unit (CU). The CU

coordinates all of the APs and carries out AP assignment for packet flow. According to the AP assignment results, the packets in the CU buffer will be delivered to the buffers of serving APs, and then transmitted to the target users via wireless channels. In this study, the notion of a 'LiFi service ratio' is introduced, which signifies the proportion of users that are served by LiFi APs. With the practical distribution of LiFi data rates considered, an analytical solution to the optimum LiFi service ratio is derived. Based on this optimum LiFi service ratio, a novel AP assignment scheme is proposed which is able to minimise the overall system delay. The main contributions of this paper are summarised below:

- An analytical solution to the optimum LiFi service ratio for hybrid LiFi/RF networks is provided. A comparison between the analytical results and simulation results is conducted.

- Based on the analytical optimum LiFi service ratio, a low-complexity cross-layer load balancing scheme for hybrid LiFi/RF network is proposed to minimise the average packet delay.

- For various AP assignment schemes, the effects of different network setups on the packet delay are numerically studied.

The rest of the chapter is organised as follows. The system model of the hybrid LiFi/RF network is introduced in Section 5.2. The system delay is analysed and an AP assignment scheme to minimise packet delay is proposed in Section 5.3. The performance evaluation is given in Section 5.4 and the summary is presented in Section 5.5.

5.2 System Model

Referring to Fig. 5.1, a downlink hybrid LiFi/RF network for an indoor environment is considered. This hybrid network is covered by several LiFi attocells and a RF cell. The system model of hybrid LiFi and RF networks refers to Section 2.1-2.2. The deployment of LiFi APs follows a square lattice topology which models a regular light placement commonly used in large offices and public places. The set of LiFi APs is denoted by $\mathcal{C}_{\mathcal{L}} = \{l|l \in [1, N_l], l \in \mathbb{N}\}$, where N_l is the number of LiFi APs. It is assumed that the photo diode (PD) at each user is oriented perpendicularly to the ceiling. This means that the angle of irradiance is equal to the angle of incidence in the LoS optical channel. The RF AP is considered to offer a ubiquitous coverage
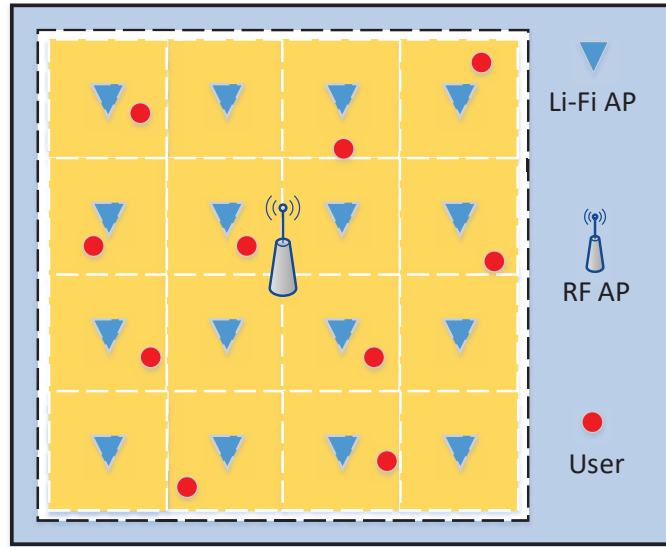
Figure 5.1: *Square topology for hybrid LiFi and RF networks*

over the indoor scenario. Users are uniformly distributed in this network. Each user can receive signals through either LiFi or RF links. The set of users is denoted by $\mathcal{U}$ with $|\mathcal{U}| = N$.

5.2.1 Hierarchical Buffer Framework

In this study, a two-tier buffer framework for hybrid LiFi/RF networks is considered, which consists of a CU buffer and $N_l + 1$ AP buffers. The sizes of these two kinds of APs are assumed to be infinite. Due to the varying channel state information (CSI) of mobile users, the network load balancing should be undertaken in regular intervals, denoted by T_p. It is assumed that the CSI in both LiFi and RF systems remains constant for a short period which is defined as a quasi-static state, and changes at the beginning of the next state. The arrival packets initially queue up at the CU buffer, and then are delivered to the buffers of target APs, according to the AP assignment result carried out by the CU at the beginning of each quasi-static state. The packets arriving at each AP buffer will line up and be processed when it comes to the head of the queue. The arrival process of packets follows a Poisson distribution, and λ (packets/s) denotes the average arrival rate of the packets. The packet size follows an exponential distribution, where the average packet size is denoted by L_{ave}. The required user data rate can be expressed as: $\lambda_0 = \lambda L_{\text{ave}}/N$.

5.2.1.1 Delay in the CU Buffer

The data packets from remote content providers initially queue at the CU buffer. Following the first-in-first-out rule, each packet is delivered to the target AP via Ethernet cables with a data rate of R_b. Let $t_{a,cu}^{<m>}$ denote the arrival time of the m-th packet at the CU buffer. The queuing time of this packet in the CU buffer can be expressed as:

$$\tau_{q,cu}^{<m>} = [\tau_{q,cu}^{<m-1>} + \tau_{p,cu}^{<m-1>} - (t_{a,cu}^{<m>} - t_{a,cu}^{<m-1>})]^+, \qquad (5.1)$$

where $\tau_{p,cu}^{<m-1>}$ is the packet transmission time from the CU buffer to the host AP; and $[.]^+$ is the maximum operator, $\max(\,.\,, 0)$. For the first packet, the queuing time is zero, i.e. $\tau_{q,cu}^{<1>} = 0$. According to Eq. (5.1), the arrival time of the m-th packet at the buffer of serving AP can be expressed as:

$$t_{a,ap}^{<m>} = t_{a,cu}^{<m>} + \tau_{q,cu}^{<m>} + \tau_{p,cu}^{<m>}. \qquad (5.2)$$

Therefore, the delay of the m-th packet in the CU buffer can be expressed as:

$$\Delta T_{\text{CU}}^{<m>} = \tau_{q,cu}^{<m>} + \tau_{p,cu}^{<m>}. \qquad (5.3)$$

5.2.1.2 Delay in AP Buffers

Based on the AP assignment determined by the CU, all of the packets will be allocated to the target APs. The arrival packets queue in line in each AP buffer and would be processed by the corresponding APs independently, following the first-in-first-out rule. Similar to Eq. (5.1), the arrival time of the q-th packet at the target user can be expressed as:

$$t_{a,user}^{<q>} = t_{a,ap}^{<q>} + \tau_{q,ap}^{<q>} + \tau_{p,ap}^{<q>}, \qquad (5.4)$$

where $\tau_{p,ap}^{<q>}$ is the packet transmission time from the AP to the user; and $\tau_{q,ap}^{<q>}$ is the queuing time at the AP buffer. The delay for the q-th packet in the AP buffer can be expressed as:

$$\Delta T_{\text{AP}}^{<q>} = \tau_{q,ap}^{<q>} + \tau_{p,ap}^{<q>}. \qquad (5.5)$$

Therefore, the total delay for the p-th packet in the hybrid LiFi/RF network is written as:

$$\Delta T^{<p>} = \Delta T_{\text{CU}}^{<p>} + \Delta T_{\text{AP}}^{<p>}. \qquad (5.6)$$

5.2.2 Downlink capacity achieved by LiFi and RF APs

In this study, the LiFi channel model shown in Section 2.3.1 is considered, where field-of-view (FoV) path loss, front-end filtering effect and multi-path effect are taken into account. The link data rate between user μ and LiFi AP α is denoted as $R_{\mu,\alpha}$. The RF channel model is given in Section 2.4.1, and the link data rate between user μ and the RF AP is denoted by $R_{\mu,\text{RF}}$. In order to reduce the complexity of AP assignment, the receivers are only served by the LiFi AP with the highest link data rate performance or the RF AP. It is assumed that α_μ denotes the LiFi AP which offers highest link data rate to user μ.

In hybrid LiFi/RF networks, LiFi AP offers very high spatial spectral efficiency. Thus, users achieving a high quality of optical channels will be assigned to a LiFi AP, and those with a low quality of optical channels are assigned to the RF AP. Without loss of generality, the achievable LiFi data rates of each user follows:

$$R_{\mu_1,\alpha_{\mu_1}} \geq ...R_{\mu_2,\alpha_{\mu_2}} \geq R_{\mu_{N-1},\alpha_{\mu_{N-1}}} ... \geq R_{\mu_N,\alpha_{\mu_N}};$$
$$\mu_i \in \mathcal{U}, i = 1, 2, ...N.$$

It is assumed that the first n users with the highest LiFi data rate are assigned to LiFi APs and users from μ_{n+1} to μ_N are served by the RF AP. The parameter $\gamma = n/N$ is defined as the "LiFi service ratio". The average data rate achieved by LiFi can be written as a function with respect to γ, expressed as:

$$C_L(\gamma) = \frac{1}{\lfloor \gamma N \rfloor} \sum_{i=1}^{\lfloor \gamma N \rfloor} R_{\mu_i,\alpha_{\mu_i}}, \tag{5.7}$$

where $\lfloor . \rfloor$ is the floor operator. In addition, the average data rate achieved by RF corresponding to γ can be written as:

$$C_R(\gamma) = \frac{1}{N - \lfloor \gamma N \rfloor} \sum_{i=\lfloor \gamma N \rfloor + 1}^{N} R_{\mu_i,\text{RF}}. \tag{5.8}$$

In this study, the polynomial fitting method is applied to find the closed-form solutions to $C_L(\gamma)$ and $C_R(\gamma)$ [17]. As shown in Fig. 5.1, a square topology of LiFi APs is considered and the RF AP is settled in the centre of the network. It is assumed that users are uniformly distributed in this hybrid LiFi/RF network, and Monte Carlo simulations are undertaken to estimate $C_L(\gamma)$ and $C_R(\gamma)$. Fig. 5.2 shows that $C_L(\gamma)$ is a monotonic function of γ, and this function can be fitted by a first-order polynomial very well. Therefore, a first-order polynomial is used to
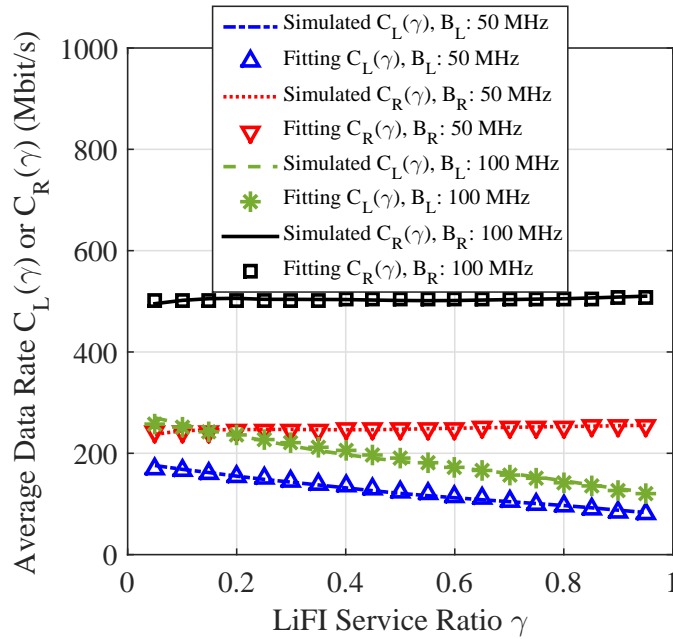
Figure 5.2: *Fitting of average LiFi and RF data rates in each cell (Simulation parameters are given in Table .4.1)*

express $C_L(\gamma)$:

$$C_L(\gamma) = X_L\gamma + Y_L, \tag{5.9}$$

where $X_L < 0$ is the first-order coefficient; $Y_L > 0$ is the zero-order coefficient. In addition, it is shown that $C_R(\gamma)$ remains stable regardless of the variance of γ, which can be approximated as a constant, denoted by:

$$C_R(\gamma) = Y_R, \tag{5.10}$$

where $Y_R > 0$ is a constant.

5.3 Optimisation of Packet Flow Assignment

5.3.1 Problem Formulation

In order to minimise the average packet delay in the hybrid LiFi/RF system, the optimisation of packet flow assignment is analysed. It is assumed that the arrival packets to each AP follow a Poisson process. The service time achieved by each server (the CU and each LiFi and RF AP) can be approximated to follow an exponential distribution. The proof is given as follows:

The service time of each server is defined as the ratio of packet size and achievable data rate. It

is assumed that the packet size has an exponential distribution with parameter $\hat{\lambda} = 1/L_{\text{ave}}$. The processing data rate of the CU buffer is constant, denoted by R_b. Thus, the service time at the CU buffer follows an exponential distribution, with the parameter of R_b/L_{ave}.

With regard to the LiFi AP buffer, the cumulative distribution function (CDF) of the processing data rate of users is shown in Fig. 5.3. It can be seen that the achievable data rate varies from zero to a maximum value, denoted as R_{max}, which is close to a uniform distribution. In this study, the processing data rate at the LiFi AP buffer is approximated to follow a uniform distribution, ranging from R_{min} to R_{max}. The probability distribution function (PDF) of the LiFi user data rate can be expressed as:

$$f_x(x) = \frac{1}{R_{\text{max}} - R_{\text{min}}}.\tag{5.11}$$

The PDF of packet size following exponential distribution with parameter $\hat{\lambda}$ can be expressed as:

$$f_y(y) = \hat{\lambda} e^{-\hat{\lambda} y}.\tag{5.12}$$

The PDF of the service time at each LiFi AP buffer is expressed as:

$$\begin{aligned}
f(z) &= \int_{-\infty}^{+\infty} |x|\, f_y(zx)\, f_x(x)\ \mathrm{d}x \\
&= \frac{1}{z(R_{\text{max}} - R_{\text{min}})} \left(R_{\text{min}} e^{-z\hat{\lambda} R_{\text{min}}} - R_{\text{max}} e^{-z\hat{\lambda} R_{\text{max}}} + \frac{e^{-z\hat{\lambda} R_{\text{min}}} - e^{-z\hat{\lambda} R_{\text{max}}}}{\hat{\lambda} z} \right)
\end{aligned}\tag{5.13}$$

By applying the Taylor series expansion, the PDF of the service time can be re-written as:

$$\begin{aligned}
f(z) = \\
\sum_{n=0}^{n=+\infty} \frac{\hat{\lambda}}{n+2} \frac{R_{\text{min}}^{n+1} + R_{\text{min}}^n R_{\text{max}} + R_{\text{min}}^{n-1} R_{\text{max}}^2 + ... + R_{\text{min}} R_{\text{max}}^n + R_{\text{max}}^{n+1}}{n!} (-\hat{\lambda} z)^n
\end{aligned}\tag{5.14}$$

Note that $R_0 = (R_{\text{min}} + R_{\text{max}})/2$ is defined as the mean of R_{min} and R_{max}. Particularly, with $R_{\text{min}} = R_{\text{max}} = R_0$, the PDF of the service time can be simplified to:

$$f_0(z) = \lim_{R_{\text{min}}=R_{\text{max}}=R_0} f(z) = \hat{\lambda} R_0 e^{-\hat{\lambda} R_0 y}.\tag{5.15}$$

In this case, the service time strictly follows an exponential distribution. In Fig. 5.4, the PDF of

Empirical CDF
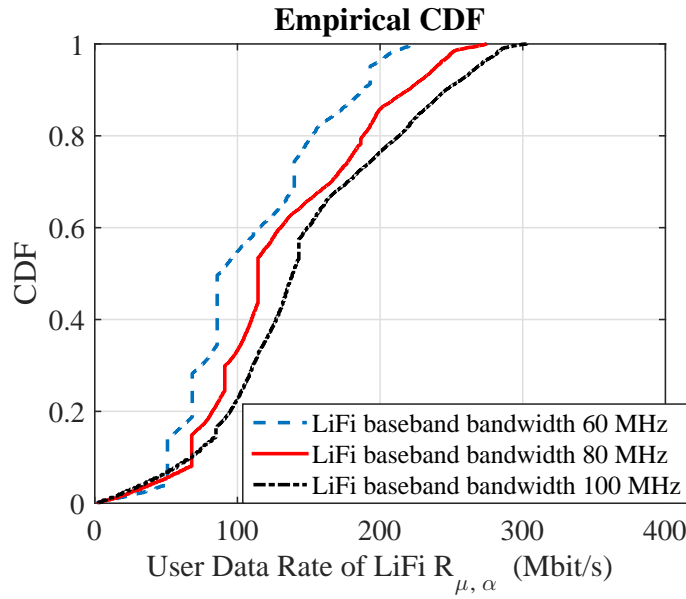
Figure 5.3: *CDF of user data rate served by LiFi APs*

$f_0(z)$ and $f(z)$ are compared, according to the hybrid network setup. It can be seen that $f(z)$ is very close to $f_0(z)$. Therefore, service time at the LiFi AP buffer can be approximated to follow an exponential distribution with the parameter of R_0/L_{ave}. The approximation of service time at the RF buffer is similar to the LiFi service time. In sum, the service time of CU and each AP can be considered to have an exponential distribution.

As is shown, the packet queues in the CU buffer and in each AP buffer can be characterised by the M/M/1 queueing model [100]. The average delay of packets in the hybrid network is expressed as:

$$D_{\text{total}} = D_{\text{CU}} + D_{\text{AP}}, \tag{5.16}$$

where $D_{\text{CU}} = 1/(R_{\text{b}}/L_{\text{ave}} - \lambda)$, is the average queueing time and processing time of packets in the CU buffer; and the average queueing and processing time of packets in the AP buffer is written as:

$$D_{\text{AP}} = \frac{\gamma}{C_L(\gamma)/L_{\text{ave}} - \gamma\lambda/N_l} + \frac{1-\gamma}{C_R(\gamma)/L_{\text{ave}} - (1-\gamma)\lambda}. \tag{5.17}$$

The optimisation problem to minimise the average packet delay in the hybrid LiFi/RF network
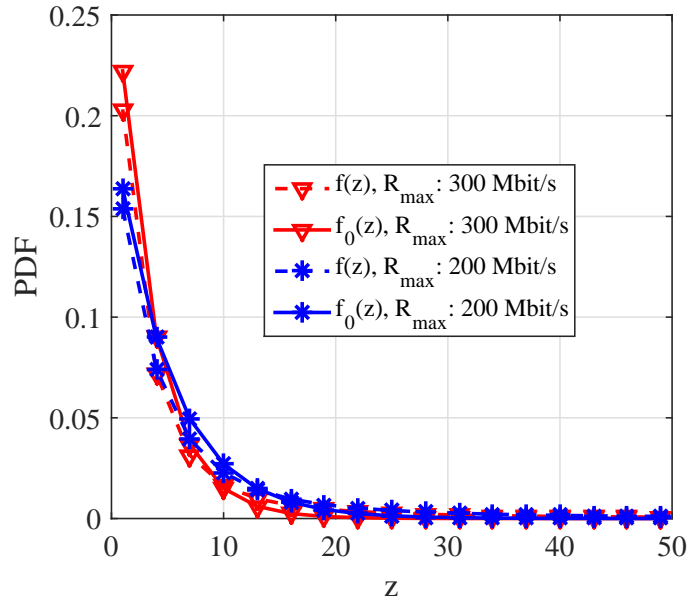
Figure 5.4: *Comparison between PDF $f(z)$ and $f_0(z)$. ($R_{min} = 0$, and the other parameters are shown in Table. 4.1)*

can be formulated as:

$$\min_{\gamma} \quad D_{\text{CU}} + D_{\text{AP}} \tag{5.18}$$

$$\text{s.t.} \quad 0 \leq \gamma \leq 1; \tag{5.19}$$

$$C_L(\gamma)/L_{\text{ave}} - \gamma\lambda/N_l > 0; \tag{5.20}$$

$$C_R(\gamma)/L_{\text{ave}} - (1 - \gamma)\lambda > 0; \tag{5.21}$$

5.3.2 Analysis of feasible region

In order to avoid traffic blockages in the AP buffers, the variable γ should meet the constraints in Eq. (5.20) and (5.21). According to the constraint in Eq. (5.20), it can be obtained that:

$$\gamma < \frac{Y_L N_l}{L_{\text{ave}}(\lambda - X_L N_l)}, \tag{5.22}$$

where $\frac{Y_L N_l}{L_{\text{ave}}(\lambda - X_L N_l)} > 0$ is always satisfied due to $X_L < 0$ and $Y_L, N_l, L_{\text{ave}}, \lambda > 0$. Also, according to the constraint in Eq. (5.21), it can be obtained that:

$$\gamma > 1 - \frac{Y_R}{\lambda L_{\text{ave}}}, \tag{5.23}$$

127

where $1 - Y_R/\lambda L_{\text{ave}} < 1$ is always satisfied.

Based on Eq. (5.22) and Eq. (5.23), it can be derived that

$$1 - \frac{Y_R}{\lambda L_{\text{ave}}} < \gamma < \frac{Y_L N_l}{L_{\text{ave}}(\lambda - X_L N_l)}. \tag{5.24}$$

Combining the condition in Eq.(5.19), the feasible region can be expressed as

$$\gamma_{\min} \leq \gamma \leq \gamma_{\max} \tag{5.25}$$

where $\gamma_{\min} = \max\{1 - \frac{Y_R}{\lambda L_{\text{ave}}}, 0\}$ is the lower bound of the feasible region and $\gamma_{\max} = \min\{\frac{Y_L N_l}{L_{\text{ave}}(\lambda - X_L N_l)}, 1\}$ is the upper bound of the feasible region. The condition that $\gamma_{\min}$ is included in the feasible region is $1 - \frac{Y_R}{\lambda L_{\text{ave}}} < 0$ and the condition that $\gamma_{\max}$ is included is $\frac{Y_L N_l}{L_{\text{ave}}(\lambda - X_L N_l)} > 1$.

In order to guarantee that the feasible region is effective, the condition below should be satisfied:

$$1 - \frac{Y_R}{\lambda L_{\text{ave}}} < \frac{Y_L N_l}{L_{\text{ave}}(\lambda - X_L N_l)}. \tag{5.26}$$

Otherwise, the feasible region will be a null set.

5.3.3 Solution to the optimisation problem

In this section, the solution to the optimisation problem in Eq. (5.18) is provided. The objective function of this optimisation problem is expressed as:

$$G(\gamma) = \frac{1}{R_b/L_{\text{ave}} - \lambda} + \frac{\gamma L_{\text{ave}}}{(X_L - \lambda L_{\text{ave}}/N_l)\gamma + Y_L} + \frac{(1 - \gamma)L_{\text{ave}}}{\lambda L_{\text{ave}}\gamma + Y_R - \lambda L_{\text{ave}}} \tag{5.27}$$

Its first order derivative corresponding to γ can be expressed as:

$$\frac{\mathrm{d}G(\gamma)}{\mathrm{d}\gamma} = \frac{\frac{\mathrm{d}g_0(\gamma)}{\mathrm{d}\gamma}g_1(\gamma) - \frac{\mathrm{d}g_1(\gamma)}{\mathrm{d}\gamma}g_0(\gamma)}{g_1^2(\gamma)}, \quad (g_1(\gamma) > 0) \tag{5.28}$$

where we have

$$\begin{cases} g_0(\gamma) = x_0\gamma^2 + y_0\gamma + z_0 \\ g_1(\gamma) = x_1\gamma^2 + y_1\gamma + z_1 \end{cases}; \tag{5.29}$$

128

and the coefficients in Eq. (5.29) are listed as follows:

$$x_0 = \lambda L_{\text{ave}}^2(1 + 1/N_l) - L_{\text{ave}}X_L,$$

$$x_1 = \lambda L_{\text{ave}}(X_L - \lambda L_{\text{ave}}/N_l),$$

$$y_0 = Y_R L_{\text{ave}} + X_L L_{\text{ave}} - Y_L - \lambda L_{\text{ave}}^2(1 + 1/N_l),$$

$$y_1 = \lambda L_{\text{ave}}Y_L + (Y_R - \lambda L_{\text{ave}})(X_L - \lambda L_{\text{ave}}/N_l),$$

$$z_0 = Y_L L_{\text{ave}}, \quad z_1 = Y_L(Y_R - \lambda L_{\text{ave}}). \tag{5.30}$$

The optimum γ can be obtained by making the gradient of the objective function in Eq. (5.28) equal to 0, which can be written as:

$$\frac{\mathrm{d}g_0(\gamma)}{\mathrm{d}\gamma}g_1(\gamma) - \frac{\mathrm{d}g_1(\gamma)}{\mathrm{d}\gamma}g_0(\gamma) = 0. \tag{5.31}$$

By using the coefficients in Eq. (5.30), the function in Eq. (5.31) can be transferred to:

$$(x_0y_1 - x_1y_0)\gamma^2 + 2(x_0z_1 - x_1z_0)\gamma + y_0z_1 - y_1z_0 = 0. \tag{5.32}$$

It can be seen from Eq. (5.32) that there are at most two extreme points for the objective function. The discriminant of the function in Eq. (5.32) is denoted by:

$$\Delta = 4(x_0z_1 - x_1z_0)^2 - 4(x_0y_1 - x_1y_0)(y_0z_1 - y_1z_0). \tag{5.33}$$

When $\Delta > 0$ is satisfied, the set of extreme points for the objective function can be expressed as:

$$\mathcal{R} = \{\frac{2(x_1z_0 - x_0z_1) + \sqrt{\Delta}}{2(x_0y_1 - x_1y_0)}, \frac{2(x_1z_0 - x_0z_1) - \sqrt{\Delta}}{2(x_0y_1 - x_1y_0)}\}. \tag{5.34}$$

When $\Delta = 0$ is achieved, the set of extreme points can be written as:

$$\mathcal{R} = \{\frac{x_1z_0 - x_0z_1}{x_0y_1 - x_1y_0}\}. \tag{5.35}$$

When $\Delta < 0$ is satisfied, the set of extreme points is $\mathcal{R} = \varnothing$.

According to the feasible region of the optimisation problem shown in Eq. (5.25), the optimum γ can be obtained by finding the minimum $G(\gamma)$ among $\gamma \in \bar{\mathcal{R}}$, where there is $\bar{\mathcal{R}} =$

$\{\gamma_{\min}, \gamma_{\max}\} \cup \mathcal{R}$. The cardinality of $\bar{\mathcal{R}}$ varies from 2 to 4, depending on the discriminant in Eq. (5.33). Therefore, it can be seen that finding the optimum γ^* requires very low computational complexity. The optimum γ^* can be expressed as:

$$\gamma^* = \arg \min_{\gamma \in \mathcal{R}} G(\gamma) \tag{5.36}$$

$$\text{s.t.} \quad \gamma_{\min} \leq \gamma \leq \gamma_{\max}. \tag{5.37}$$

Particularly, if $\gamma_{\min}$ and $\gamma_{\max}$ are not included in the feasible region, it can be attained from Eq. (5.18) that $G(\gamma_{\min}) = G(\gamma_{\max}) = +\infty$. Since $G(\gamma)$ is a continuous function in the feasible region, an optimum γ^* must exist in this case which can minimise $G(\gamma)$, and this optimum γ^* should belong to $\mathcal{R}$.

5.3.4 Flow assignment scheme

In this subsection, the packet flow scheme based on the optimum LiFi service ratio is proposed, which is summarised in Algorithm. 10. Initially, the users achieving zero LiFi data rate due to severe ICI are assigned to the RF AP. The set of users that can be served by either a LiFi AP or the RF AP is denoted by $\mathcal{U}_b$. The set of users who can receive the highest LiFi data rate from the LiFi AP α is denoted by $\mathcal{U}_\alpha$. If $|\mathcal{U}_b|/|\mathcal{U}| \leq \gamma^*$ is satisfied, the RF cell is overloaded. In this case, each user belonging to $\mathcal{U}_b$ should be assigned to the LiFi AP which can offer them the highest link data rate. Otherwise, the users in set $\mathcal{U}_b$ which have poor-quality of LiFi channel in set $\mathcal{U}_b$ need to assigned to the RF AP.

In the M/M/1 model based packet delay analysis, the numbers of users served by all LiFi APs are assumed to be equal. In the practical scenario, users are generally uniformly distributed in the network, and Step. 1 in the proposed scheme is able to guarantee that the number of users served by each LiFi AP tend to be the same. In addition, it can be seen that in this proposed flow assignment scheme, the optimum LiFi service ratio γ^* is essential. However, the optimum γ^* derived from the M/M/1 model may have a bias to the practical optimum γ^*. This is because four approximations are used in the M/M/1 model based analysis: i). the distribution of the average data rate achieved by APs expressed in Eq. (5.9) and (5.10); (ii) the distribution of the user data rate in each cell, shown in Appendix. A; (iii). the distribution of service time of each AP, shown in Appendix. A; and (iv). the same number of users served by each LiFi AP. In Section IV, the accuracy of the analytical optimum γ^* will be evaluated via simulations.

Algorithm 10 Packet flow assignment scheme for hybrid LiFi/RF networks.

1: Initialisation: the set of users that can achieve LiFi data rate greater than zero is denoted by $\mathcal{U}_b$; and the set of users who can receive the highest LiFi data rate from the LiFi AP α is denoted by $\mathcal{U}_\alpha$.

2: **if** $|\mathcal{U}_b|/|\mathcal{U}| \leq \gamma^*$ **then**

3:      Users belonging to $\mathcal{U}_b$ are assigned to the LiFi APs which can offer users the highest LiFi data rates.

4: **else**

5:      **while** $|\mathcal{U}_b|/|\mathcal{U}| > \gamma^*$ **do**

6:          Find the LiFi AP with maximal number of users in set $\mathcal{U}_\alpha$, denoted by:

$$\alpha^* = \arg \max_{\alpha \in \mathcal{C}_\mathcal{L}} |\mathcal{U}_\alpha|. \tag{5.38}$$

7:          The LiFi AP α^* will drop the user that belongs to $\mathcal{U}_{\alpha^*}$ and achieves lowest link data rate, which can be expressed as:

$$\mu^* = \arg \min_{\mu \in \mathcal{U}_{\alpha^*}} R_{\mu,\alpha^*}. \tag{5.39}$$

8:          The user μ^* will be assigned to the RF AP. Update the set $\mathcal{U}_b$ and $\mathcal{U}_{\alpha^*}$ using the following expressions:

$$\mathcal{U}_b = \mathcal{U}_b - \mu^*; \tag{5.40}$$

$$\mathcal{U}_{\alpha^*} = \mathcal{U}_{\alpha^*} - \mu^*; \tag{5.41}$$

9:      **end while**

10: **end if**

5.4 Performance Evaluation

5.4.1 Simulation Setups

As shown in Fig. 5.1, a 16 m $\times$ 16 m indoor office simulation scenario is considered, where 16 LiFi APs are deployed following a square topology. A RF AP is located at the centre offering ubiquitous wireless coverage. All of the users are uniformly distributed in the simulation scenario. Three benchmark AP assignment schemes, max-fairness, max-sum-rate and threshold-based, are used for comparison. In the 'max-fairness' scheme, the overall user fairness in the hybrid network is maximised [61, 74]. The 'max-sum-rate' scheme enables the system to achieve a maximal sum data rate with proportional fairness considered [24, 98]. In the 'threshold-based' scheme, a threshold of the LiFi link data rate is used for AP assignment.

Name of Parameters	Value
Height of the room, w	2.5 m
The range of optical transmit power in LiFi system, P_{opt}	20 W
Noise power spectral density of LiFi, N_L	$10^{-19}\ A^2$/Hz
The physical area of a PD, A_p	1 cm^2
Cut-off frequency of LiFi front-end filtering effect, f_0	60 MHz
Cut-off frequency of diffuse optical channel, f_c	60 MHz
Half-intensity radiation angle, $\theta_{1/2}$	60 deg.
Gain of optical filter, $T_s(\theta)$	1.0
Refractive index, χ	1.5
Optical to electric conversion efficiency, κ	0.53 A/W
Transmit power for each RF AP, P_R	20 dBm
Noise power of RF, σ^2	-57 dBm
Average packet size, $L_{\text{p,ave}}$	500 Bytes
Number of users, N	80

Table 5.1: *Simulation parameters for evaluation of packet flow assignment schemes*
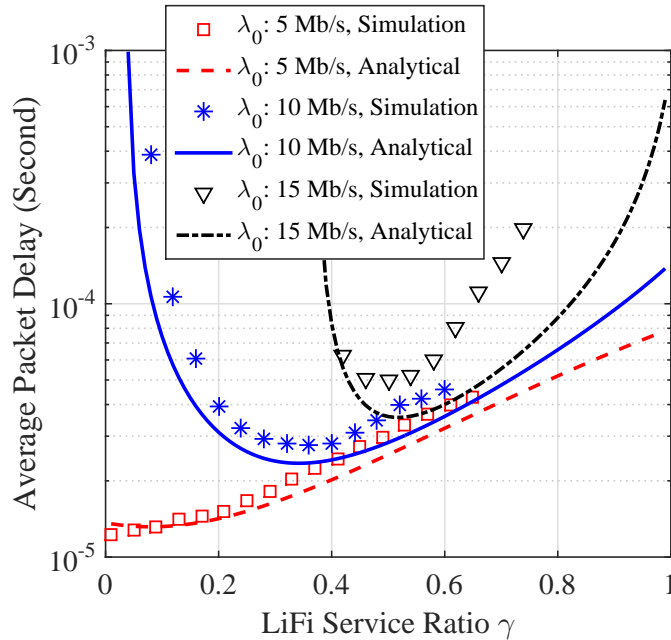
Figure 5.5: *Analytical and simulation results of average packet delay corresponding to LiFi service ratio γ. ($B_L = 50$ MHz and $B_R = 150$ MHz)*

Figure 5.6: *Comparison of optimal LiFi service ratio between simulation results and analytical results, corresponding to LiFi bandwidth B_L. (The 3 dB bandwidth of LiFi channels is 60 MHz.)*

Figure 5.7: *Comparison of optimal LiFi service ratio between simulation results and analytical results, corresponding to RF bandwidth B_R.*

Users that achieve a higher LiFi link data rate than the threshold are allocated to the LiFi APs, and the others with a lower LiFi SINR are served by the RF AP [18]. The parameters in the simulation are summarised in Table 5.1.

5.4.2 Performance Analysis

In this section, the performance of the average packet delay in hybrid LiFi/RF networks is evaluated. In Fig. 5.5, the average packet delay is depicted as a function of the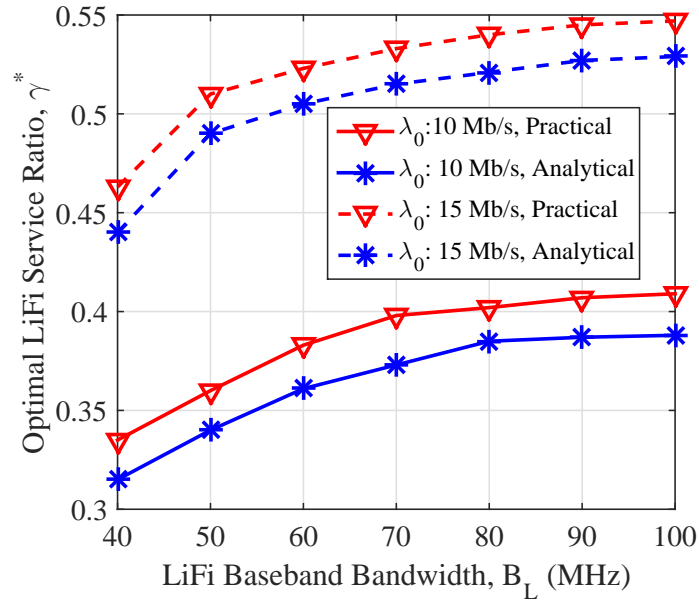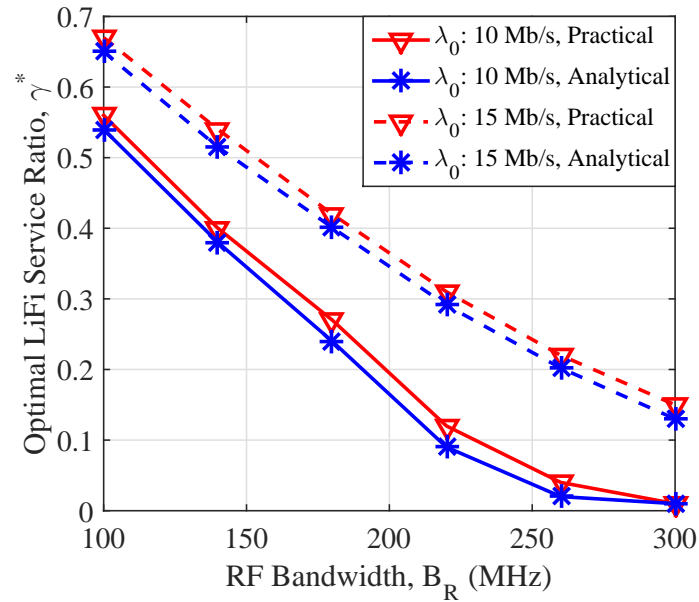 LiFi service ratio γ, for both the analytical results and the simulation results. The curve of the theoretical packet delay comes from the M/M/1 model based analysis, shown in Eq. (5.18). The simulation results are achieved by the proposed packet flow assignment scheme with different values of γ. It can be seen that the analytical results are slightly lower than the simulation results with different values of required user data rate λ_0 due to the four approximations used in the M/M/1 model based analysis, which has been discussed in Section III.E. This can be equivalent to a longer average service time for the simulation results. Particularly, the gap between these two curves tends to be small at the optimum. Also, it can be seen from Eq. (5.3.1) that the gap will increase with the arriving packet rate. In addition, when having $\lambda_0 = 5$ Mbit/s , the average packet delay increases along with the LiFi service ratio γ. This means that the RF AP is able to serve most of the users due to the low data rate requirement. When λ_0 increases to 10 Mbit/s and 15 Mbit/s, the average packet delay becomes a convex function with respect to γ. This is because a small γ can lead to the congestion in the RF AP buffer while a large γ will make the LiFi attocells overloaded.

In Fig. 5.6 and Fig. 5.7, the analytical optimum γ^* and practical optimum γ^* obtained by the simulations are shown. It can be seen that the analytical γ^* is close to the practical γ^*. Fig. 5.6 also shows that both the analytical γ^* and the practical γ^* increase towards a saturation point with the LiFi baseband bandwidth B_L. This is because the front-end effects of LEDs in the LiFi APs function as a low pass filter. The channel gains of the high frequency subcarrier in LiFi systems is lower than that of low frequency subcarriers. In Fig. 5.7, the optimum γ^* is presented as a function of the RF bandwidth B_R. Similarly, the curves of analytical γ^* are very close to those of practical γ^* for different values of B_R. When B_R increases, both analytical and practical γ^* decrease and tend to zero. This is because according to the M/M/1 queueing theory, the average packet delay is inversely proportional to the difference between the processing packet rate and the arrival packet rate. When the capacity of the RF AP is large
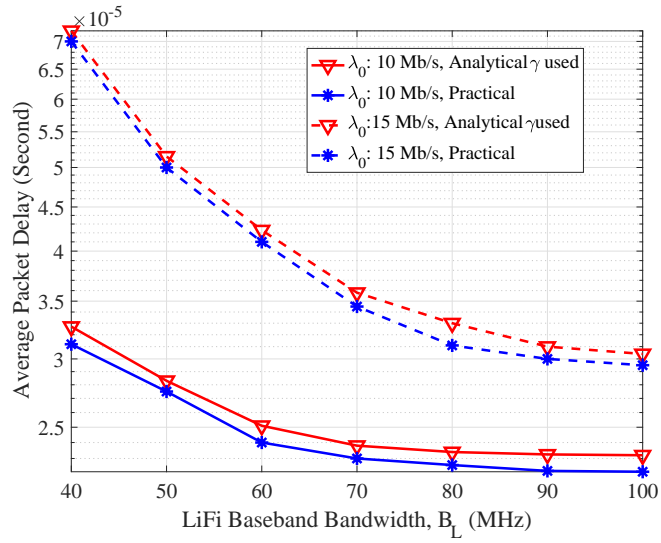
Figure 5.8: *Comparison of average packet delay between optimal simulation results and analytical optimal ratio based results, corresponding to LiFi bandwidth B_L.*

enough, the RF AP can achieve a larger packet rate difference than the LiFi AP. Therefore, in this case, most of the users will be assigned to the RF AP.

In Fig. 5.8 and Fig. 5.9, the minimal average packet delay achieved by using the proposed packet flow scheme is shown. The analytical γ^* and the practical γ^* are used in the proposed scheme, respectively. It can be seen that the minimal average packet delay achieved by the analytical γ^* based scheme is very close to that by using practical γ^*. Moreover, the analytical γ^* are calculated according to Eq. (5.36), requiring very low computational complexity. However, there is no closed-form solution to the practical γ^*, which has to be obtained via thousands of simulations. This signifies that in the proposed packet flow scheme, the practical γ^* can be replaced by the analytical γ^* so as to reduce the computational complexity.

The performance of the average packet delay by using different packet flow schemes is evaluated and presented in Fig. 5.10. In the legend, 'Optimum' and 'Proposed' represent the flow assignment scheme using the analytical γ^* and the practical γ^*, respectively. It can be seen that the average packet delay achieved by the analytical γ^* based flow assignment scheme is very close to the practical γ^* based scheme. In addition, compared with the three benchmarks schemes, the proposed scheme can reduce up to 90% of the packet delay while offering the same user packet rates. In Fig. 5.11, the system throughput performance by using different flow assignment scheme is presented. It appears that the system throughput by proposed scheme decreases with an increase in λ_0. Specifically, with $\lambda_0 \leq 19$ Mb/s, the proposed scheme is able to
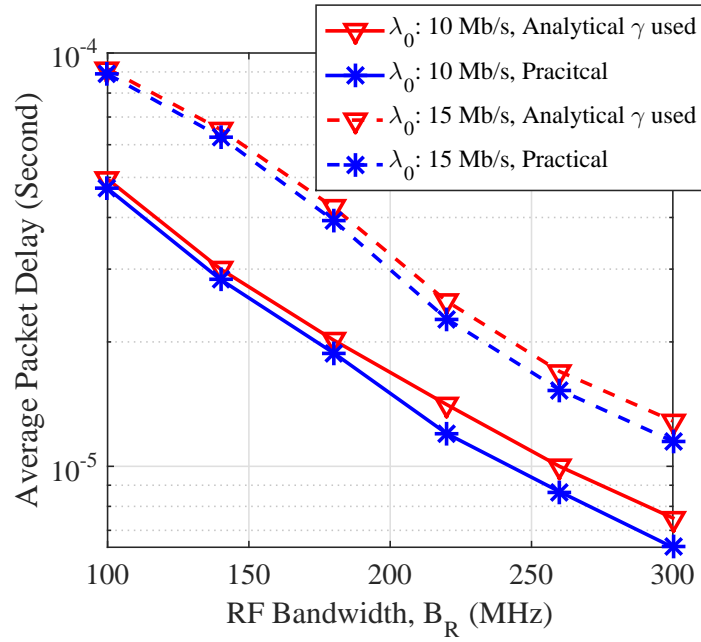
Figure 5.9: *Comparison of average packet delay between optimal simulation results and analytical optimal ratio based results, corresponding to RF bandwidth B_R.*

Algorithm	Addition	Multiplication	Exponentiation
Proposed scheme	$O(NN_{ap})$	$O(N)$	0
max-fairness scheme	$O(NN_{ap}I_F)$	$O(NN_{ap}I_F)$	0
max-sum-rate scheme	$O(NN_{ap}I_S)$	$O(NN_{ap}I_S)$	$O(NN_{ap}I_S)$
threshold-based scheme	$O(NN_{ap})$	$O(N)$	0

Table 5.2: *Computation complexity comparison between the proposed scheme and benchmarks*

achieve a higher throughput than max-sum-rate scheme where proportional fairness scheduler is considered. In addition, the proposed scheme outperforms the other two benchmark algorithm in terms of system throughput. Particularly, the throughput performance shown in Fig. 5.11 is the maximal data rate without any delay constraint. If the packet delay in Fig. 5.10 is realised, the maximal data rate of each user will just be the required data rate λ_0.

According to [61, 98], the computational complexity of the proposed scheme as well as the three benchmark schemes is summarised in Table. 5.2, where N is the number of users; $N_{ap} = N_l+1$ is the number of the APs; and I_F and I_S are the iteration numbers required in the 'max-fairness' scheme and the 'max-sum-rate' scheme, respectively. It is shown that the proposed scheme is able to achieve the lowest computation complexity among all schemes. Therefore, it can be concluded that comparing with the state-of-the-art load balancing schemes for hybrid LiFi/RF
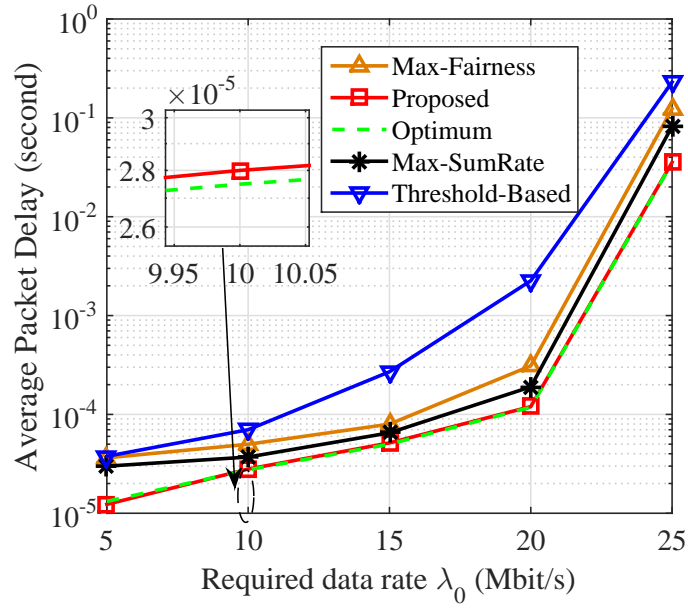
Figure 5.10: *Comparison of packet delay by using different flow assignment schemes. ($B_L = 50$ MHz, $B_R = 150$ MHz)*
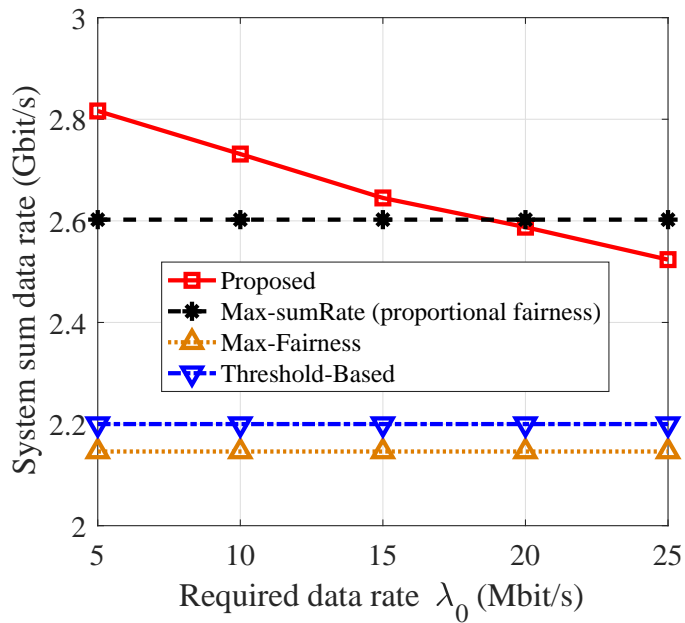
Figure 5.11: *Comparison of system sum data rate by using different flow assignment schemes. ($B_L = 50$ MHz, $B_R = 150$ MHz)*

networks, the proposed flow assignment scheme can achieve a minimum average packet delay with reduced computational complexity.

5.5 Summary

In this chapter, the optimum LiFi service ratio is derived in order to minimise system delay for hybrid LiFi/RF networks. A low-complexity AP assignment scheme based on the analytical optimal LiFi service ratio is proposed. Three conclusions can be drawn from the results: (i) the analytical optimum of the LiFi service ratio is close to the practical results; (ii) the optimal LiFi service ratio increases with the LiFi bandwidth, but tends to be saturated because of the low-pass filtering effect of LiFi front-end devices; (iii) the proposed flow assignment scheme by using the analytical optimum of LiFi service ratio outperforms the conventional load balancing schemes in term of average packet delay at reduced computational complexity.

Chapter 6
Conclusions, Limitations and Future Research

6.1   Summary and Conclusions

In this thesis, hybrid LiFi and RF networks (HLRN) with mobile users are considered and downlink network load balancing for HLRN is investigated. In the indoor scenario, the channel state information (CSI) for LiFi and RF link varies slowly. Therefore, in each short period, the CSI can be considered to be fixed for HLRN, and such a short period is referred to as a quasi-static state. Downlink load balancing consists of static load balancing in each state and handover. Specifically, static load balancing contains access point assignment (APA) and resource allocation (RA). In this thesis, several novel load balancing schemes have been developed to optimise the overall throughput and to improve users' quality of service (QoS), including users' satisfaction level and packet delay. In addition, the effects of handover, blockages in LiFi links, random orientation of photo diodes on the system data rate performance have been evaluated.

In Chapter 2, the relevant background of LiFi technology and hybrid LiFi and RF networks has been presented. Initially, the brief history of optical wireless communications is introduced and the overall communication architecture of HLRN is provided. After that, the LiFi channel model including field-of-view (FoV) path loss, front-end low pass filtering effects and multipath effect caused by reflections. Then, the optical orthogonal frequency division multiplexing (O-OFDM) transmission is depicted. Specifically, we focus on the direct current (DC) optical OFDM (DCO-OFDM) technology because of its high spectral efficiency. In DCO-OFDM, a DC bias added to the modulated signal ensures that the output signals are positive. Also, at least half of the OFDM sub-carriers are used to realise the Hermitian conjugate of the complex-valued symbols so that the strict positive and real number constraint is satisfied after the Fourier transform. Moreover, the multiple access technology in LiFi systems is investigated. It has been found that the orthogonal frequency division multiple access (OFDMA) outperforms the time division multiple access (TDMA) technique in terms of both data rate and user fairness due to the efficient use of high frequency subcarriers. In addition, a novel low complexity

OFDMA based resource allocation scheme is proposed. This RA scheme exploits the unique characteristics of LiFi channels functioning as a low pass filter to reduce the computational complexity. Simulations show that the OFDMA outperforms the time division multiple access (TDMA) technique in terms of both data rate and user fairness due to the efficient use of high frequency subcarriers. Finally, the system model for RF networks is introduced. The 2.4 GHz spectrum band is considered for RF transmission and OFDM-TDMA is considered for multiple access in order to reduce the complexity.

In Chapter 3, the dynamic load balancing with handover considered for HLRN is studied. First, the handover scheme between two neighbouring quasi-static states is proposed. Then, the optimisation of static load balancing is investigated. The AP assignment and the RA are formulated as an optimisation problem which is used to maximise the system sum data rate under certain user fairness conditions. In Section 3.2, an optimisation-based load balancing scheme with proportional fairness is proposed, and the throughput performance of the hybrid LiFi/WiFi network is theoretically analysed. It has been shown that the WiFi (or RF) and LiFi throughputs in the hybrid network are related despite the independent spectrum transmission. The LiFi throughput can be enhanced by increasing the WiFi throughput due to efficient load balancing. Following that, a comprehensive study of dynamic load balancing with a variety of fairness schemes is provided. Two specific load balancing algorithms, joint optimisation algorithm (JOA) and separate optimisation algorithm (SOA) are proposed. A unified data rate requirement of users is considered as a QoS metric and user outage probability is introduced. Simulation results show that JOA can achieve an optimal performance of system throughput while requiring high computational complexity. SOA achieves a lower data rate than JOA at a reduced complexity. Finally, a fuzzy logic (FL) based dynamic load balancing scheme that jointly handles AP assignment, RA and handover is proposed. This FL based scheme uses CSI, user speed and users' data rate requirement to determine whether a handover is prompted. It is shown that compared with conventional load balancing scheme, the FL based scheme improve 40% in terms of both data rate and user satisfaction level due to the reduction of handover frequency.

In Chapter 4, an evolutionary game theory (EGT) based load balancing scheme is proposed in order to reduce the computational complexity of conventional load balancing approaches. In the EGT based load balancing scheme, APA and RA are handled separately, resulting in a low complexity. In addition, the EGT based scheme optimises APA and RA iteratively by using the relation between them so that a near optimal performance of system throughput can

be achieved. In this chapter, three factors are taken into account in order to model a practical HLRN: blockages in LiFi channels, random orientation angle and user data rate requirement. Also, in the RA step in the EGT scheme, an enhanced proportional fairness (EPF) scheduler is proposed to maximise the usage of communication resources. Three conclusions are drawn based on the simulation results: i). The EGT load balancing scheme can achieve a better trade-off between data rate performance and computational complexity; ii). The proposed EPF scheduler can achieve a higher user QoS than conventional schedulers in the RA step due to a more efficient exploitation of transmission resources; iii). When the FoV of LiFi receivers is 90°, the average user QoS decreases with an increase in the maximum vertical ROA θ_{PD}. However, when considering a small FoV, there is an optimum of the maximal vertical ROA that can optimise the QoS performance, leading to improved system load balancing; However, when considering user data rate requirement, the user QoS decreases with an increase in the blockage density as blockages cause an inefficient allocation of communication resources.

In Chapter 5, the optimisation of packet flow assignment for HLRN is investigated. Unlike the load balancing on the physical layer, we focus on the performance improvement on packet delay instead of system sum data rate. Initially, a two-layer buffer framework including central unit (CU) buffer and AP buffers for HLRN is introduced. The arrival packets will be firstly queued in the CU buffer. According to the AP assignment results, the packets in the CU buffer will be delivered to the AP buffers. In this chapter, a notion of 'LiFi service ratio' is introduced, which signifies the proportion of users that are served by LiFi APs. Moreover, an optimisation analysis of LiFi service ratio for HLRN is provided. Based on the analytical optimal LiFi service ratio, a low-complexity flow assignment scheme is proposed in order to minimise the packet delay. Three conclusions can be drawn from the results: (i) the analytical optimum of the LiFi service ratio is close to the practical results; (ii) the optimal LiFi service ratio increases with the LiFi bandwidth, but tends to be saturated because of the low-pass filtering effect of LiFi front-end devices; (iii) the proposed flow assignment scheme by using the analytical optimum of LiFi service ratio outperforms the conventional load balancing schemes in term of average packet delay at reduced computational complexity.

6.2 Limitations and Future Research

In the analysis presented in this thesis, a multitude of factors related to load balancing for HLRN have been considered. However, in order to reduce the analytical complexity, some assumptions

are introduced to simplify the system models. In Chapter 2, the spatial multiplexing in both LiFi and RF systems is not taken into account [101]. Multiple light emitting diodes (LEDs) are essentially used to lighten an indoor environment. Therefore, multiple input and multiple output (MIMO) system can be naturally employed in an indoor VLC scheme [102]. There is an amount of research on the VLC MIMO technique. A MIMO approach to model an indoor VLC system has been introduced in [103] and the capacity of an optical MIMO system is studied in [104], with a low-speed optical system demonstrated. In [105], research on space-time coding for diffuse optical communications is investigated. In [106], several preliminary experiments with a simple MIMO interconnect are reported. Also, multiple LEDs can be used for space division multiple access (SDMA) systems. It has been shown in [107] that an angle diversity LiFi transmitter that consists of several LED lamps and generates multiple narrow beams in different directions simultaneously can realise SDMA. This can significantly improve the system throughput by increasing bandwidth reuse. In addition, multiple antennas in the RF system have not been considered. By using MIMO techniques, the uplink and downlink system throughput can be improved [108], because the techniques such as space time block coding and beamforming employed in the MIMO system helps in achieving extension of cell coverage and interference cancellation. Moreover, the data rate increase in both LiFi and RF stand-alone networks can affect the system load balancing and handover strategies in HLRNs. This topic that load balancing with advanced antennas technology in HLRNs will be studied in our future research.

In the LiFi channel model, the non-line-of-sight (NLoS) transmission is modelled by considering the effects of internal room surfaces only. In order to simulate a more precise reflective channel, random objects such as human bodies and furniture need to be taken into account. Though a number of related research has investigated several different communication environments, the generic characteristics of the effects of objects on NLoS LiFi channels still remain unknown [109]. This is because there are too many uncertain factors about the random objects such as the type and the surface reflectivity. Also, the geometry of the random objects are not as simple as a flat plane. Therefore, it is more difficult to characterise the effects of random objects on NLoS channel than merely considering indoor surfaces. In order to evaluate the data rate performance in HLRNs more accurately, more research on modelling LiFi NLoS channel should be undertaken.

The OFDMA-based RA scheme for LiFi systems has been investigated in Section 2.3.3, and a

novel low-complexity OFDMA scheme has been proposed. Despite the inconspicuous multi-user diversity, the OFDMA RA scheme outperforms the TDMA in LiFi systems due to an efficient use of high-frequency resources. However, TDMA instead of OFDMA is employed when studying load balancing in this thesis. This is because TDMA has a much simpler solution for RA than OFDMA, and using OFDMA may lead to an intractable problem for load balancing optimisation. In our future work, the OFDMA-based load balancing algorithms for HLRNs will be studied. Particularly, by using the low-complexity OFDMA-based RA scheme and well-designed AP allocation schemes, the computational complexity of LB in OFDMA-based HLRNs could be reduced.

In Chapter 3, the handover scheme in HLRNs is studied. However, the difference between the horizontal handover and the vertical handover is not considered. In fact, vertical handovers are implemented across heterogeneous cells of access systems, which differ in several aspects such as bandwidth, data rate, frequency of operation, etc. The different characteristics of the networks involved make the implementation of vertical handovers more challenging as compared to horizontal handovers. In future work, some experimental analysis of horizontal and vertical handovers in HLRNs is expected, and more efficient handover schemes will be developed.

When studying dynamic hybrid LiFi/RF networks, user movement should be considered and modelled properly. Specifically, user movement contains moving routes/speed and random orientations of LiFi receivers. For user moving routes/speed, the random way point model is usually applied in the published research. However, this model is far from being implemented in practical situations. Users in the shopping mall definitely have different moving performance from those in the office scenarios. In addition, the random orientations of LiFi receivers will affect the user data rate, which should be carefully modelled. It has been shown in [110, 111] that physical and geometrical parameters have a significant effect on VLC communications and must be considered in VLC channel models. In Chapter 4, a uniform distribution of vertical orientations of LiFi receivers is assumed. This may not be accurate in practical scenarios according to users' behaviour. Therefore, in order to make a more effective performance evaluation of dynamic LB schemes, an accurate user movement model should be applied. A LB scheme which relies on an accurate movement model may significantly improve the user data rate and mitigate the influence caused by handover overhead. The modelling of user movement in LiFi networks will be investigated in our future work.

In Chapter 5, the media access control (MAC) layer load balancing in HLRNs is investigated.

Similar to conventional RF channels, an efficient and fair MAC protocol is required where nodes can contend for the channel and eventually transmit without collisions. There are several achievements through the research of VLC-based channel access mechanism for indoor communication [112–114]. In [115], authors test the VLC transceiver prototype design using a modified version of the 802.11 MAC protocol. The results show that performance of the protocol is in the acceptable range of 80-90% for only simple simulation scenarios. A significant difference between LiFi and conventional RF such as LTE, WiFi is that each LiFi AP covers a much smaller area than RF, leading to more frequent handover. Therefore, more research should be undertaken on LiFi MAC layer in order to develop an efficient LiFi MAC protocol. This will be included in our future work.

Finally, bi-directional load balancing is also planned for our future work. Besides dynamic LB for downlink network, coupling the LiFi and RF links for the uplink network allows it to offer high degrees of freedom and may require sophisticated network resource optimisation [116–118]. This work is very important because mobile units are becoming more and more powerful in terms of computing power and storage and the uplink may experience heavy traffic caused by mobile multimedia transmissions [119]. Properly distributing heavy traffic in both the uplink and downlink requires efficient traffic reshaping, which is an unknown problem in existing mobile networks.

Appendix A
List of Publications

This Chapter contains a list of published papers.

A.1 Journal Papers and Main Contributions

Y. Wang, X. Wu and H. Haas, "Load Balancing Game With Shadowing Effect for Indoor Hybrid LiFi/RF Networks," in *IEEE Transactions on Wireless Communications*, vol. 16, no. 4, pp. 2366-2378, April 2017.

Main contributions: In this paper, an evolutionary game theory (EGT) based load balancing scheme is proposed for hybrid LiFi/RF networks (HLRNs) where three practical issues are considered: i). LiFi channel blockages; ii). random orientation angle (ROA) of LiFi receivers; iii) user data rate requirement. The proposed algorithm jointly handles the access point (AP) assignment and resource allocation (RA). The optimality of the proposed algorithm is analysed. Moreover, when considering user data rate requirement, conventional fairness schedulers such as max-min fairness and proportional fairness may lead to inefficient use of communication resources. In the proposed EGT based algorithm, an enhanced proportional fairness scheduler for resource allocation is proposed to avoid inefficient use of transmission resources. The performance of user satisfaction for both conventional and proposed fairness schedulers is evaluated by computer simulations.

Y. Wang, D. A. Basnayaka, X. Wu and H. Haas, "Optimization of Load Balancing in Hybrid LiFi/RF Networks," in *IEEE Transactions on Communications*, vol. 65, no. 4, pp. 1708-1720, April 2017.

Main contributions: A novel dynamic load balancing scheme is proposed and the β-proportional fairness function is applied, where β is the fairness coefficient. The effect of β on user data rate performance in the hybrid network is evaluated. Two specific algorithms that optimise the AP assignment and the RA in each quasi-static state are proposed, termed as joint optimisation

algorithm (JOA) and separate optimisation algorithm (SOA) respectively. In this work, the optimality of JOA and the optimal threshold in SOA are analysed. A comparison of data rate performance and computational complexity between these two algorithms is made.

Y. Wang and H. Haas, "Dynamic Load Balancing With Handover in Hybrid LiFi and WiFi Networks," in *Journal of Lightwave Technology*, vol. 33, no. 22, pp. 4671-4682, Nov.15, 15 2015.

Main contributions: In this paper, a dynamic load balancing scheme with handover for hybrid LiFi and WiFi networks is proposed, where proportional fairness is taken into consideration. In this work, the service area is defined as the region within which users will be allocated to LiFi APs. By analysing the service areas of the LiFi APs, the throughput performance of the hybrid system is theoretically studied. Also, the relation between LiFi throughput and WiFi throughput is investigated. Moreover, the effects of the handover overhead on handover locations and user throughput are simulated and discussed.

Y. Wang, X. Wu and H. Haas, "Cross-layer Load Balancing Design for Hybrid LiFi/RF Networks," submitted to *Journal of Lightwave Technology*.

Main contributions: A two-tier buffer framework for HLRNs is proposed, which contains a central unit (CU) buffer and one buffer for each AP. Two multiple access technologies, carrier sense multiple access (CSMA) and time division multiple access (TDMA), are used in this hierarchical buffer model, and the quality of service (QoS) performance of these two techniques, including packet loss rate and packet latency is investigated and compared. Also, a dynamic load balancing scheme that handles the AP assignment, resource allocation and handover for hybrid networks is proposed. In order to decrease the packet delay, a packet dropping mechanism (PDM) that deletes the expired packets is included in the proposed load balancing scheme. In addition, an optimisation-based LB scheme is introduced as a benchmark and a comparison of QoS performance and computational complexity is carried out between the proposed scheme and the benchmark.

Y. Wang, X. Wu and H. Haas, "Optimisation of Flow Assignment for Hybrid LiFi/RF Networks," submitted to *IEEE Transactions on Wireless Communications*.

Main contributions: In this study, a downlink HLRN is considered and the notion of a LiFi service ratio is introduced, which signifies the proportion of users that are served by LiFi APs.

146

An analytical solution to the optimum LiFi service ratio for HLRNs is provided. A comparison between the analytical results and simulation results is conducted. Based on the analytical optimum LiFi service ratio, a low-complexity AP assignment scheme for hybrid LiFi/RF network is proposed to minimise the average packet delay. For various AP assignment schemes, the effects of different network setups on the packet delay are numerically studied.

A.2   Conference papers

Y. Wang, X. Wu and H. Haas, "OFDMA-Based Resource allocation in LiFi Networks," accepted by *2017 IEEE Global Communications Conference (GLOBECOM)*, *Singapore*.

Y. Wang, and H. Haas, "A Comparison of Load Balancing Techniques for Hybrid LiFi/RF Networks" accepted by *4th ACM Workshop on Visible Light Communication Systems (VLCS 2017)*, *Snowbird*.

Y. Wang, X. Wu and H. Haas, "Fuzzy logic based dynamic handover scheme for indoor Li-Fi and RF hybrid network," *2016 IEEE International Conference on Communications (ICC)*, *Kuala Lumpur*, 2016, pp. 1-6.

Y. Wang, X. Wu and H. Haas, "Analysis of area data rate with shadowing effects in Li-Fi and RF hybrid network," *2016 IEEE International Conference on Communications (ICC)*, *Kuala Lumpur*, 2016, pp. 1-5.

Y. Wang, X. Wu and H. Haas, "Distributed load balancing for Internet of Things by using Li-Fi and RF hybrid network," *2015 IEEE 26th Annual International Symposium on Personal, Indoor, and Mobile Radio Communications (PIMRC)*, *Hong Kong*, 2015, pp. 1289-1294.

Y. Wang, D. A. Basnayaka and H. Haas, "Dynamic load balancing for hybrid Li-Fi and RF indoor networks," *2015 IEEE International Conference on Communication Workshop (ICCW)*, *London*, 2015, pp. 1422-1427.

Y. Wang, S. Videv and H. Haas, "Dynamic load balancing with handover in hybrid Li-Fi and Wi-Fi networks," *2014 IEEE 25th Annual International Symposium on Personal, Indoor, and Mobile Radio Communication (PIMRC)*, *Washington DC*, 2014, pp. 575-579.

References

[1] S. Shao and A. Khreishah, "Delay Analysis of Unsaturated Heterogeneous Omnidirectional-Directional Small Cell Wireless Networks: The Case of RF-VLC Co-existence," *IEEE Transactions on Wireless Communications*, vol. PP, no. 99, pp. 1–1, 2016.

[2] Cisco, "Cisco Visual Networking Index: Forecast and Methodology, 2014-2019," 2015.

[3] Ericsson, "Mobility Report on the Pulse of the Networked Society," 2015.

[4] H. Haas, "LiFi: Conceptions, Misconceptions and Opportunities," in *IEEE Photonics Conference (IPC)*, pp. 680–681, 2016.

[5] H. Zhang, S. Chen, X. Li, H. Ji, and X. Du, "Interference Management for Heterogeneous Networks with Spectral Efficiency Improvement," *IEEE Wireless Communications*, vol. 22, pp. 101–107, April 2015.

[6] D. Lopez-Perez, I. Guvenc, G. de la Roche, M. Kountouris, T. Q. S. Quek, and J. Zhang, "Enhanced Intercell Interference Coordination Challenges in Heterogeneous Networks," *IEEE Wireless Communications*, vol. 18, pp. 22–30, June 2011.

[7] A. Tzanakaki, M. Anastasopoulos, I. Berberana, D. Syrivelis, P. Flegkas, T. Korakis, D. C. Mur, I. Demirkol, J. Gutierrez, E. Grass, Q. Wei, E. Pateromichelakis, N. Vucic, A. Fehske, M. Grieger, M. Eiselt, J. Bartelt, G. Fettweis, G. Lyberopoulos, E. Theodoropoulou, and D. Simeonidou, "Wireless-Optical Network Convergence: Enabling the 5G Architecture to Support Operational and End-User Services," *IEEE Communications Magazine*, vol. 55, pp. 184–192, October 2017.

[8] W. Abdallah and N. Boudriga, "Enabling 5G Wireless Access Using LiFi Technology: An OFDM Based Approach," in *18th International Conference on Transparent Optical Networks (ICTON)*, pp. 1–6, July 2016.

[9] T. Maksymyuk, M. Brych, Y. Klymash, M. Kyryk, and M. Klymash, "Game Theoretical Framework for Multi-Operator Spectrum Sharing in 5G Heterogeneous Networks," in *4th International Scientific-Practical Conference Problems of Infocommunications, Science and Technology (PIC S T)*, pp. 515–518, Oct 2017.

[10] B. Soleyman, A. Zaman, S. H. Rastegar, and V. Shah-Mansour, "RAT Selection Based on Association Probability in 5G Heterogeneous Networks," in *IEEE Symposium on Communications and Vehicular Technology (SCVT)*, pp. 1–6, Nov 2017.

[11] H. Haas, L. Yin, Y. Wang, and C. Chen, "What is LiFi," *Journal of Lightwave Technology*, vol. 34, pp. 1533–1544, March 2016.

[12] N. V. R. Kumar, A. Srikanth, A. Singha, and B. B. Sam, "Comparison of LIFI and WIFI and Study of Smart Meter-survey," in *2017 International Conference on Information Communication and Embedded Systems (ICICES)*, pp. 1–8, Feb 2017.

[13] D. Tsonev, H. Chun, S. Rajbhandari, J. McKendry, S. Videv, E. Gu, M. Haji, S. Watson, A. Kelly, G. Faulkner, M. Dawson, H. Haas, and D. O'Brien, "A 3-Gb/s Single-LED OFDM-Based Wireless VLC Link Using a Gallium Nitride uLED ," *IEEE Photonics Technology Letters*, vol. 26, pp. 637–640, Apr. 2014.

[14] M. Islim, R. X. Ferreira, X. He, E. Xie, S. Videv, S. Viola, S. Watson, N. Bamiedakis, R. V. Penty, I. H. White, A. E. Kelly, E. Gu, H. Haas, and M. D. Dawson, "Towards 10 Gb/s Orthogonal Frequency Division Multiplexing-based Visible Light Communication Using a GaN Violet Micro-LED," *Photon. Res.*, pp. A35–A43, 2017.

[15] D. Tsonev, S. Videv, and H. Haas, "Towards a 100 Gb/s Visible Light Wireless Access Network," *Optics Express*, vol. 23, pp. 1627–1637, 2015.

[16] E. Perahia and R. Stacey, "Next Generation Wireless LAN: 802.11n and 802.11ac ," *Cambridge University Press*, 2013.

[17] C. Chen, D. Basnayaka, and H. Haas, "Downlink Performance of Optical Attocell Networks," *Journal of Lightwave Technology*, vol. 34, pp. 137–156, Apr. 2016.

[18] D. A. Basnayaka and H. Haas, "Hybrid RF and VLC Systems: Improving User Data Rate Performance of VLC System," in *IEEE Vehicular Technology Conference (VTC Spring)*, May 2015.

[19] Y. Wang, X. Wu, and H. Haas, "Analysis of Area Data Rate with Shadowing Effects in LiFi and RF Hybrid Network," in *2016 IEEE International Conference on Communications (ICC)*, pp. 1–5, May 2016.

[20] X. Wu and H. Haas, "Access Point Assignment in Hybrid LiFi and WiFi Networks in Consideration of LiFi Channel Blockage," in *IEEE 18th International Workshop on Signal Processing Advances in Wireless Communications (SPAWC)*, pp. 1–5, July 2017.

[21] M. B. Rahaim, A. M. Vegni, and T. D. C. Little, "A Hybrid Radio Frequency and Broadcast Visible Light Communication System," in *IEEE Global Communications Conference Workshop (GLOBECOMW)*, pp. 792–796, Dec. 2011.

[22] S. Shao, A. Khreishah, M. B. Rahaim, H. Elgala, M. Ayyash, T. D. C. Little, and J. Wu, "An Indoor Hybrid WiFi-VLC Internet Access System," in *IEEE International Conference on Mobile Ad Hoc and Sensor Systems (MASS)*, pp. 569–574, Oct. 2014.

[23] X. Li, R. Zhang, and L. Hanzo, "Cooperative Load Balancing in Hybrid Visible Light Communications and WiFi," *IEEE Transactions on Communications*, vol. 63, pp. 1319–1329, Apr. 2015.

[24] F. Jin, R. Zhang, and L. Hanzo, "Resource Allocation Under Delay-Guarantee Constraints for Heterogeneous Visible-Light and RF Femtocell," *IEEE Transactions on Wireless Communications*, vol. 14, pp. 1020–1034, Feb. 2015.

[25] M. Kassar, B. Kervella, and G. Pujolle, "An Overview of Vertical Handover Decision Strategies in Heterogeneous Wireless Networks," *Computer Communications*, vol. 31, pp. 2607–2620, Jun. 2008.

[26] M. Kassab, J. Bonnin, and A. Belghith, "Fast and Secure Handover in WLANs: An Evaluation of the Signaling Overhead," in *IEEE Consumer Communications and Networking Conference (CCNC)*, pp. 770–775, Jan. 2008.

[27] A. Xhafa and O. Tonguz, "Reducing Handover Time in Heterogeneous Wireless Networks," in *IEEE Vehicular Technology Conference (VTC Fall)*, vol. 4, pp. 2222–2226 Vol.4, Oct. 2003.

[28] H.-H. Choi, "An Optimal Handover Decision for Throughput Enhancement," *IEEE Communications Letters*, vol. 14, pp. 851–853, Sep. 2010.

[29] R. Zhang, J. Wang, Z. Wang, Z. Xu, C. Zhao, and L. Hanzo, "Visible Light Communications in Heterogeneous Networks: Paving the Way for User Centric Design," *IEEE Wireless Communications*, vol. 22, pp. 8–16, April 2015.

[30] T. Komine and M. Nakagawa, "Fundamental Analysis for Visible Light Communication System Using LED Lights," *IEEE Transactions on Consumer Electronics*, vol. 50, pp. 100–107, Feb 2004.

[31] J. Grubor, S. Randel, K. D. Langer, and J. W. Walewski, "Broadband Information Broadcasting Using LED-Based Interior Lighting," *Journal of Lightwave Technology*, vol. 26, pp. 3883–3892, Dec 2008.

[32] X. Wu, M. Safari, and H. Haas, "Joint Optimisation of Load Balancing and Handover for Hybrid LiFi and WiFi Networks," in *2017 IEEE Wireless Communications and Networking Conference (WCNC)*, pp. 1–5, March 2017.

[33] D. J. T. Heatley, D. R. Wisely, I. Neild, and P. Cochrane, "Optical Wireless The Story So Far," *IEEE Communications Magazine*, vol. 36, pp. 72–82, Dec 1998.

[34] Y. Wang and H. Haas, "Dynamic Load Balancing with Handover in Hybrid LiFi and WiFi Networks," *Journal of Lightwave Technology*, vol. 33, pp. 4671–4682, Nov. 2015.

[35] A. H. and K. James, "A Novel Protocol Design in Hybrid Networks of Visible Light Communication and OFDMA System," in *2015 IEEE International Conference on Electrical, Computer and Communication Technologies (ICECCT)*, pp. 1–5, March 2015.

[36] M. S. Saud and M. Katz, "Implementation of a Hybrid Optical RF Wireless Network with Fast Network Handover," in *European Wireless 2017; 23th European Wireless Conference*, pp. 1–6, May 2017.

[37] M. Kashef, M. Abdallah, N. Al-Dhahir, and K. Qaraqe, "On the Impact of PLC Backhauling in Multi-User Hybrid VLC and RF Communication Systems," in *2016 IEEE Global Communications Conference (GLOBECOM)*, pp. 1–6, Dec 2016.

[38] Z. Ghassemlooy, W. Popoola, and S. Rajbhandari, "Optical Wireless Communications: System and Channel Modelling with MATLAB," in *Taylor & Francis*, 2012.

[39] P. Jayasinghe, A. Tlli, J. Kaleva, and M. Latva-Aho, "Direct Beamformer Estimation for Dynamic TDD Networks with Forward-Backward Training," in *IEEE 18th International Workshop on Signal Processing Advances in Wireless Communications (SPAWC)*, pp. 1–6, July 2017.

[40] Y. Sun, S. Lv, S. Liu, and Y. Zhang, "Density Based User Grouping for Massive MIMO Downlink in FDD System," in *IEEE 9th International Conference on Communication Software and Networks (ICCSN)*, pp. 448–453, May 2017.

[41] Z. Dong, T. Shang, Y. Gao, and Q. Li, "Study on VLC Channel Modeling Under Random Shadowing," *IEEE Photonics Journal*, vol. 9, pp. 1–16, Dec 2017.

[42] J. J. D. McKendry, D. Massoubre, S. Zhang, B. R. Rae, R. P. Green, E. Gu, R. K. Henderson, A. E. Kelly, and M. D. Dawson, "Visible Light Communications Using a CMOS-Controlled Micro-Light-Emitting-Diode Array," *Journal of Lightwave Technology*, vol. 30, pp. 61–67, Jan 2012.

[43] J. Kahn and J. Barry, "Wireless Infrared Communications," *Proceedings of the IEEE*, vol. 85, pp. 265–298, Feb. 1997.

[44] V. Jungnickel, V. Pohl, S. Nonnig, and C. von Helmolt, "A Physical Model of the Wireless Infrared Communication Channel," *IEEE Journal on Selected Areas in Communications*, vol. 20, pp. 631–640, Apr. 2002.

[45] J. R. Barry, J. M. Kahn, W. J. Krause, E. A. Lee, and D. G. Messerschmitt, "Simulation of Multipath Impulse Response for Indoor Wireless Optical Channels," *IEEE Journal on Selected Areas in Communications*, vol. 11, pp. 367–379, Apr 1993.

[46] F. Miramirkhani and M. Uysal, "Channel Modeling and Characterization for Visible Light Communications," *IEEE Photonics Journal*, vol. 7, pp. 1–16, Dec 2015.

[47] F. J. Lopez-Hermandez and M. J. Betancor, "DUSTIN: Algorithm for Calculation of Impulse Response on IR Wireless Indoor Channels," *Electronics Letters*, vol. 33, pp. 1804–1806, Oct 1997.

[48] E. F. Schubert, "Light-Emitting Diodes," *Cambridge University Press*, Sept. 2012.

[49] T. Komine, S. Haruyama, and M. Nakagawa, "Performance Evaluation of Narrowband OFDM on Integrated System of Power Line Communication and Visible Light Wireless Communication," in *2006 1st International Symposium on Wireless Pervasive Computing*, Jan 2006.

[50] S. Dimitrov and H. Haas, "Optimum Signal Shaping in OFDM-Based Optical Wireless Communication Systems," in *IEEE Vehicular Technology Conference (VTC Fall)*, pp. 1–5, Sep. 2012.

[51] W. Chu, J. Dang, Z. Zhang, and L. Wu, "Effect of Clipping on the Achievable Rate of Non-orthogonal Multiple Access with DCO-OFDM," in *9th International Conference on Wireless Communications and Signal Processing (WCSP)*, pp. 1–6, Oct 2017.

[52] Q. Wang, B. Song, D. Boland, B. Corcoran, and A. Lowery, "Efficient IFFT Implementation in an ACO-OFDM Transmitter," in *Opto-Electronics and Communications Conference (OECC) and Photonics Global Conference (PGC)*, pp. 1–3, July 2017.

[53] L. Wu, Z. Zhang, J. Dang, and H. Liu, "Adaptive Modulation Schemes for Visible Light Communications," *Journal of Lightwave Technology*, vol. 33, pp. 117–125, Jan. 2015.

[54] S. D. Dissanayake, K. Panta, and J. Armstrong, "A Novel Technique to Simultaneously Transmit ACO-OFDM and DCO-OFDM in IM/DD Systems," in *2011 IEEE GLOBE-COM Workshops (GC Wkshps)*, pp. 782–786, Dec 2011.

[55] H. Jang, S. Y. Yun, J. Shin, and Y. Yi, "Game Theoretic Perspective of Optimal CSMA," *IEEE Transactions on Wireless Communications*, vol. 17, pp. 194–209, Jan 2018.

[56] L. Zhang and Y. Sun, "The Optimal Assignment of Orthogonal Polyphase Sequences in CDMA Systems," *IEEE Communications Letters*, vol. 22, pp. 109–112, Jan 2018.

[57] M. Baghani, A. Mohammadi, and M. Majidi, "Downlink Resource Allocation in OFDMA Wireless Networks Under Power Amplifier Non-linearity," *IET Communications*, vol. 11, no. 18, pp. 2751–2757, 2017.

[58] S. Sesia, I. Toufik, and M. Baker, "LTE-The UMTS Long Term Evolution: From Theory to Practice," *A John Wiley and Sons, Ltd, Publication*, 2009.

[59] F. Seguel, I. Soto, D. Iturralde, P. Adasme, and B. Nuez, "Enhancement of the QoS in an OFDMA VLC System," in *International Symposium on Communication Systems, Networks and Digital Signal Processing (CSNDSP)*, pp. 1–5, July 2016.

[60] J. Fakidis, D. Tsonev, and H. Haas, "A Comparison between DCO-OFDMA and Synchronous One Dimensional OCDMA for Optical Wireless Communications," in *IEEE International Symposium on Personal, Indoor, and Mobile Radio Communications (PIMRC)*, pp. 3605–3609, Sept 2013.

[61] Y. Wang, X. Wu, and H. Haas, "Load Balancing Game with Shadowing Effect for Indoor Hybrid LiFi/RF Networks," *IEEE Transactions on Wireless Communications*, vol. 16, pp. 2366–2378, April 2017.

[62] R. Ibrahim, D. Voyer, M. E. Zoghbi, J. Huillery, A. Brard, C. Vollaire, B. Allard, and Y. Zaatar, "Novel Design for a Rectenna to Collect Pulse Waves at 2.4 GHz," *IEEE Transactions on Microwave Theory and Techniques*, vol. 66, pp. 357–365, Jan 2018.

[63] C. Hansen, "WiGig: Multi-gigabit wireless communications in the 60 ghz band," *Wireless Communications, IEEE*, vol. 18, pp. 6–7, December 2011.

[64] I. Stefan, H. Burchardt, and H. Haas, "Area Spectral Efficiency Performance Comparison between VLC and RF Femtocell Networks," in *Communications (ICC), 2013 IEEE International Conference on*, pp. 3825–3829, June 2013.

[65] Y. Zhou, A. Pahwa, and S.-S. Yang, "Modeling Weather-Related Failures of Overhead Distribution Lines," *Power Systems, IEEE Transactions on*, vol. 21, pp. 1683–1690, Nov 2006.

[66] S. Boyd and L. Vandenberghe, "Convex Optimization," *Cambridge University Press*, 2004.

[67] D. Bertsekas and J. Tsitsiklis, "Parallel and Distributed Computation:Numerical Methods," *Prentice-Hall, Inc,*, 1989.

[68] C. CHEN, S. Videv, D. Tsonev, and H. Haas, "Fractional Frequency Reuse in DCO-OFDM-based Optical Attocell Networks," *Lightwave Technology, Journal of*, vol. 33, pp. 3986–4000, Oct 2015.

[69] Z. Rong and S. Gray, "Beamforming Loss due to Tracking Error in Downlink SDMA," in *IEEE International Conference on Universal Personal Communications,*, vol. 1, pp. 441–444, Oct 1998.

[70] M. Chen, C. Ijaz, D. Tsonev, and H. Haas, "Analysis of Downlink Transmission in DCO-OFDM-Based Optical Attocell Networks," in *IEEE Global Communications Conference Exhibition and Industry Forum*, Dec. 2014.

[71] C. Tsao, Y.-T. Wu, W. Liao, and J.-C. Kuo, "Link Duration of the Random Way Point Model in Mobile Ad Hoc Networks," in *IEEE WCNC*, vol. 1, pp. 367–371, April 2006.

[72] D. A. Basnayaka and H. Haas, "Hybrid RF and VLC systems: Improving user data rate performance of VLC system," *IEEE Vehicular Technology Conference (VTC Spring)*, May 2014.

[73] A. Kamal and V. Mathai, "A Novel Cell Selection Method for LTE HetNet," in *International Conference on Communications and Signal Processing (ICCSP)*, pp. 738–742, April 2014.

[74] Q. Ye, B. Rong, Y. Chen, M. Al-Shalash, C. Caramanis, and J. Andrews, "User Association for Load Balancing in Heterogeneous Cellular Networks," *IEEE Transactions on Wireless Communications*, vol. 12, pp. 2706–2716, Jun. 2013.

[75] S. Low and D. Lapsley, "Optimization Flow Control. I. Basic Algorithm and Convergence," *IEEE/ACM Transactions on Networking*, vol. 7, pp. 861–874, Dec. 1999.

[76] J. Choi, D. Love, and P. Bidigare, "Downlink Training Techniques for FDD Massive MIMO Systems: Open-Loop and Closed-Loop Training With Memory," *IEEE Journal of Selected Topics in Signal Processing*, vol. 8, pp. 802–814, Oct. 2014.

[77] H. Burchardt, S. Sinanovic, Z. Bharucha, and H. Haas, "Distributed and Autonomous Resource and Power Allocation for Wireless Networks," *IEEE Transactions on Communications*, vol. 61, pp. 2758–2771, July 2013.

[78] X. Wu, M. Safari, and H. Harald, "3-State Fuzzy Logic Game on Resource ALlocation for Small Cell Networks," *IEEE PIMRC*, 2015.

[79] I. S. Feraud, M. M. Lara, and J. E. Naranjo, "A fuzzy logic model to estimate safe driving behavior based on traffic violation," in *2017 IEEE Second Ecuador Technical Chapters Meeting (ETCM)*, pp. 1–6, Oct 2017.

[80] Z. Shengzhe, W. Kai, and X. Wen, "Fuzzy Logic-based Control Strategy for a Battery/Supercapacitor Hybrid Energy Storage System in Electric Vehicles," in *Chinese Automation Congress (CAC)*, pp. 5598–5601, Oct 2017.

[81] F. Wang, Z. Wang, C. Qian, L. Dai, and Z. Yang, "Efficient Vertical Handover Scheme for Heterogeneous VLC-RF Systems," *IEEE/OSA Journal of Optical Communications and Networking*, vol. 7, pp. 1172–1180, Dec 2015.

[82] Q. Wang, D. Giustiniano, and M. Zuniga, "In Light and In Darkness, In Motion and In Stillness: A Reliable and Adaptive Receiver for the Internet of Lights," *IEEE Journal on Selected Areas in Communications*, vol. 36, pp. 149–161, Jan 2018.

[83] Y. Wang, D. Basnayaka, and H. Haas, "Dynamic Load Balancing for Hybrid LiFi and RF Indoor Networks," in *IEEE International Conference on Communication Workshop (ICCW), London, UK*, pp. 1422–1427, Jun. 2015.

[84] Y. Wang, X. Wu, and H. Haas, "Distributed Load Balancing for Internet of Things by Using Li-Fi and RF Hybrid Network," in *IEEE 26th Annual International Symposium on Personal, Indoor, and Mobile Radio Communications (PIMRC), HongKong, China*, pp. 1289–1294, Aug 2015.

[85] D. Niyato and E. Hossain, "Dynamics of Network Selection in Heterogeneous Wireless Networks: An Evolutionary Game Approach," *IEEE Transactions on Vehicular Technology*, vol. 58, pp. 2008–2017, May 2009.

[86] M. Bennis, S. Guruacharya, and D. Niyato, "Distributed Learning Strategies for Interference Mitigation in Femtocell Networks," in *IEEE Global Telecommunications Conference (GLOBECOM), Houston, USA*, pp. 1–5, Dec. 2011.

[87] P. Semasinghe, E. Hossain, and K. Zhu, "An Evolutionary Game for Distributed Resource Allocation in Self-Organizing Small Cells," *IEEE Transactions on Mobile Computing*, vol. 14, pp. 274–287, Feb. 2015.

[88] C. Leboucher, H. S. Shin, R. Chelouah, S. L. Menec, P. Siarry, M. Formoso, A. Tsourdos, and A. Kotenkoff, "An Enhanced Particle Swarm Optimisation Method Integrated With Evolutionary Game Theory," *IEEE Transactions on Games*, vol. PP, no. 99, pp. 1–1, 2018.

[89] L. Feng, Q. Yang, and K. S. Kwak, "Incentive-compatible packet forwarding in mobile social networks via evolutionary game theory," *IEEE Access*, vol. 5, pp. 13557–13569, 2017.

[90] S. Dimitrov and H. Haas, "Principles of LED Light Communications - Towards Networked LiFi," *Cambridge University Press*, Mar. 2015.

[91] S. Jivkova and M. Kavehrad, "Shadowing and Blockage in Indoor Optical Wireless Communications," in *IEEE Global Communications Conference (GLOBECOM), San Francisco, USA*, vol. 6, pp. 3269–3273, Dec. 2003.

[92] A. Blenk, A. Basta, and W. Kellerer, "HyperFlex: An SDN Virtualization Architecture with Flexible hypervisor Function Allocation," in *IFIP/IEEE International Symposium on Integrated Network Management (IM)*, pp. 397–405, May 2015.

[93] S. Khan, A. Gani, A. W. A. Wahab, A. Abdelaziz, K. Ko, M. K. Khan, and M. Guizani, "Software-Defined Network Forensics: Motivation, Potential Locations, Requirements, and Challenges," *IEEE Network*, vol. 30, pp. 6–13, Nov. 2016.

[94] R. Vilalta, R. Munoz, R. Casellas, R. Martinez, S. Peng, R. Nejabati, D. Simeonidou, N. Yoshikane, T. Tsuritani, I. Morita, V. Lopez, T. Szyrkowiec, and A. Autenrieth, "Multidomain Network Hypervisor for Abstraction and Control of Openflow- Enabled Multitenant Multitechnology Transport Networks [Invited]," *IEEE/OSA Journal of Optical Communications and Networking*, vol. 7, pp. B55–B61, Nov. 2015.

[95] M. S. F. Kader, M. M. Hossain, S. Ghose, and K. R. Zafreen, "Selection of Better Strategy for Self Organized Data Aggregation Techniques using Evolutionary Game Theory," in *2016 International Conference on Innovations in Science, Engineering and Technology (ICISET)*, pp. 1–4, Oct 2016.

[96] E. Biglieri, G. Caire, and G. Taricco, "Coding for the fading channel: a survey," *IOS Press*, 1999.

[97] 3GPP, "LTE – an end-to-end description of network architecture and elements," *3GPP LTE Encyclopedia*, 2009.

[98] Y. Wang, D. A. Basnayaka, X. Wu, and H. Haas, "Optimization of Load Balancing in Hybrid LiFi/RF Networks," *IEEE Transactions on Communications*, vol. 65, pp. 1708–1720, April 2017.

[99] Y. Wang, X. Wu, and H. Haas, "Fuzzy Logic Based Dynamic Handover Scheme for Indoor LiFi and RF Hybrid Network," in *2016 IEEE International Conference on Communications (ICC)*, pp. 1–6, May 2016.

[100] X. Zhiqiang, L. Jun, L. Zi, and Z. Yanping, "Queue-Theory-Based Service-Section Communication Bandwidth Calculation for Power Distribution and Utilization of Smart Grid," in *2015 8th International Conference on Intelligent Networks and Intelligent Systems (ICINIS)*, pp. 137–140, Nov 2015.

[101] J. Lian and M. Brandt-Pearce, "Multiuser MIMO Indoor Visible Light Communication System Using Spatial Multiplexing," *Journal of Lightwave Technology*, vol. 35, pp. 5024–5033, Dec 2017.

[102] L. Zeng, D. C. O'Brien, H. L. Minh, G. E. Faulkner, K. Lee, D. Jung, Y. Oh, and E. T. Won, "High Data Rate Multiple Input Multiple Output (MIMO) Optical Wireless Communications Using White LED Lighting," *IEEE Journal on Selected Areas in Communications*, vol. 27, pp. 1654–1662, December 2009.

[103] S. Jivkova, B. A. Hristov, and M. Kavehrad, "Power-Efficient Multispot-Diffuse Multiple-Input-Multiple-Output Approach to Broad-Band Optical Wireless Communications," *IEEE Transactions on Vehicular Technology*, vol. 53, pp. 882–889, May 2004.

[104] S. Hranilovic and F. R. Kschischang, "A Pixelated MIMO Wireless Optical Communication System," *IEEE Journal of Selected Topics in Quantum Electronics*, vol. 12, pp. 859–874, July 2006.

[105] M. Garfield, C. Liang, T. P. Kurzweg, and K. R. Dandekar, "MIMO Space-Time Coding for Diffuse Optical Communication," *Microwave and Optical Technology Letters*, vol. 48, no. 6, pp. 1108–1110, 2006.

[106] D. C. OBrien, "Indoor Optical Wireless Communications: Recent Developments and Future Challenges," *Free-Space Laser Communications IX*, pp. 6–12, 2009.

[107] Z. Chen and H. Haas, "Space Division Multiple Access in Visible Light Communications," in *IEEE International Conference on Communications (ICC)*, pp. 5115–5119, June 2015.

[108] K. Lee, I. D. Choi, and J. Y. Lee, "16-QAM Impedance Loading Board Design Supporting Single RF Beamspace MIMO System," in *IEEE International Symposium on Antennas and Propagation (APSURSI)*, pp. 327–328, June 2016.

[109] T. Komine and M. Nakagawa, "A Study of Shadowing on Indoor Visible Light Wireless Communication Utilizing Plural White LED Lightings," in *1st International Symposium onWireless Communication Systems, 2004.*, pp. 36–40, Sept 2004.

[110] Behlouli, P. Combeau, S. Sahugude, A. Julien-Vergonjanne, C. L. Bas, and L. Aveneau, "Impact of Physical and Geometrical Parameters on Visible Light Communication Links," in *2017 Advances in Wireless and Optical Communications (RTUWO)*, pp. 73–76, Nov 2017.

[111] Z. Dong, T. Shang, Y. Gao, and Q. Li, "Study on VLC Channel Modeling Under Random Shadowing," *IEEE Photonics Journal*, vol. 9, pp. 1–16, Dec 2017.

[112] T. Nishio, R. Nishioka, M. Morikura, and K. Yamamoto, "VRMAC: A Novel WLAN Medium Access Control Mechanism Using LEDs and A Camera," in *2013 IEEE Globecom Workshops (GC Wkshps)*, pp. 1121–1126, Dec 2013.

[113] Y. A. Chen, Y. T. Chang, Y. C. Tseng, and W. T. Chen, "A Framework for Simultaneous Message Broadcasting Using CDMA-Based Visible Light Communications," *IEEE Sensors Journal*, vol. 15, pp. 6819–6827, Dec 2015.

[114] Z. Wang, Y. Liu, Y. Lin, and S. Huang, "Full-Duplex MAC Protocol Based on Adaptive Contention Window for Visible Light Communication," *IEEE/OSA Journal of Optical Communications and Networking*, vol. 7, pp. 164–171, March 2015.

[115] B. Toma, H. M. Tsai, and M. Boban, "Simulating Vehicular Visible Light Communication: Physical Radio and MAC Modeling," in *2014 IEEE Vehicular Networking Conference (VNC)*, pp. 222–225, Dec 2014.

[116] B. Lin, X. Tang, Z. Ghassemlooy, Y. Li, S. Zhang, Y. Wu, and H. Li, "Interleaved Frequency Division Multiple Access for Uplink VLC," in *15th International Conference on Optical Communications and Networks (ICOCN)*, pp. 1–3, Sept 2016.

[117] M. Ismail, M. Z. Shakir, K. A. Qaraqe, and E. Serpedin, *Radio Frequency and Visible Light Communication Internetworking*, pp. 272–277. 2016.

[118] M. T. Alresheedi, A. T. Hussein, and J. M. H. Elmirghani, "Uplink Design in VLC Systems with IR Sources and Beam Steering," *IET Communications*, vol. 11, no. 3, pp. 311–317, 2017.

[119] R. Zhang, J. Wang, Z. Wang, Z. Xu, C. Zhao, and L. Hanzo, "Visible Light Communications in Heterogeneous Networks: Paving the Way for User-Centric Design," *IEEE Wireless Communications*, vol. 22, pp. 8–16, April 2015.